MAX-PLANCK-INSTITUT
FÜR METEOROLOGIE

IMPRS-ESM

International Max Planck Research School on Earth System Modelling

An Earth system modelling perspective on Arctic coastal erosion under climate change

David Marcolino Nielsen

Hamburg 2022

Berichte zur Erdsystemforschung **253**
Reports on Earth System Science **2022**

Hinweis

Die Berichte zur Erdsystemforschung werden vom Max-Planck-Institut für Meteorologie in Hamburg in unregelmäßiger Abfolge herausgegeben.

Sie enthalten wissenschaftliche und technische Beiträge, inklusive Dissertationen.

Die Beiträge geben nicht notwendigerweise die Auffassung des Instituts wieder.

Die "Berichte zur Erdsystemforschung" führen die vorherigen Reihen "Reports" und "Examensarbeiten" weiter.

Anschrift / Address

Max-Planck-Institut für Meteorologie
Bundesstrasse 53
20146 Hamburg
Deutschland

Tel./Phone: +49 (0)40 4 11 73 - 0
Fax: +49 (0)40 4 11 73 - 298

name.surname@mpimet.mpg.de
www.mpimet.mpg.de

Notice

The Reports on Earth System Science are published by the Max Planck Institute for Meteorology in Hamburg. They appear in irregular intervals.

They contain scientific and technical contributions, including PhD theses.

The Reports do not necessarily reflect the opinion of the Institute.

The "Reports on Earth System Science" continue the former "Reports" and "Examensarbeiten" of the Max Planck Institute.

Layout

Bettina Diallo and Norbert P. Noreiks
Communication

Copyright

An Earth system modelling perspective on Arctic coastal erosion under climate change

David Marcolino Nielsen

Hamburg 2021

David Marcolino Nielsen
aus São Paulo, Brasilien

Max-Planck-Institut für Meteorologie
The International Max Planck Research School on Earth System Modelling
(IMPRS-ESM)
Bundesstrasse 53
20146 Hamburg

Universität Hamburg
Geowissenschaften
Institut fuer Meereskunde
Bundesstr. 55
20146 Hamburg

Tag der Disputation: 14. Dezember 2021

Folgende Gutachter empfehlen die Annahme der Dissertation:
Dr. Mikhail Dobrynin
Prof. Dr. Johanna Baehr

Vorsitzender des Promotionsausschusses:
Prof. Dr. Hermann Held

Dekan der MIN-Fakultät:
Prof. Dr. Heinrich Graener

ISSN 1614-1199

For Maria

1936 –2020

The front cover photo was taken at the northeast coast of Muostakh Island, Laptev Sea, by the author on August 22nd 2019. This document was typeset using the `classicthesis` template developed by André Miede and Ivo Pletikosić available at: https://bitbucket.org/amiede/classicthesis/.

ABSTRACT

Arctic coastal erosion threatens coastal communities, damages infrastructure and releases organic carbon from permafrost, potentially increasing atmospheric greenhouse gas concentrations. However, no projections of Arctic coastal erosion exist so far. In this thesis, I take a novel approach, combining observations with ocean-wave and Earth system model (ESM) simulations to examine Arctic coastal erosion at present and under future climate change.

I close the gap between fine-scale coastal erosion and coarse-resolution ESMs in two complementary steps: connecting the temporal, and the spatial variability of erosion with mechanisms represented in ESMs. I show that the main modes of coastal erosion interannual variability, identified in observations from the Laptev Sea, respond to large-scale sea-ice and atmospheric variability, such as that modulated by the Arctic Oscillation, for example. About half of the spatial variability of long-term mean coastal erosion rates, at the pan-Arctic scale, is explained by a linear combination of ground-ice content, surface ocean wave and thawing degree-day exposure. I thus demonstrate, for the first time, that a semi-empirical description of coastal erosion at the pan-Arctic scale is possible, taking into account its main drivers at scales compatible with ESMs.

I present the first twenty-first century projections of Arctic coastal erosion, forcing my semi-empirical model with an ensemble of ESM simulations. Thereby, I make the first estimates of magnitude, timing and sensitivity of Arctic coastal erosion increase to climate change. I project the Arctic-mean coastal erosion rate to roughly double by 2100, and exceed its historical range of variability before the end of this century, even in a moderate-emission scenario. The sensitivity of Arctic coastal erosion to climate also increases, follwing the Arctic Amplification effect. Arctic coastal erosion could release about 2 PgC from permafrost by 2100, or by about 2.5 TgC $year^{-1}$ $^{o}C^{-1}$ in future global warming scenarios. Moreover, initial results from coupled ESM simulations, including erosion OC fluxes, suggest that the atmospheric CO_2 concentration increase in response to Arctic coastal erosion could be larger than the permafrost OC loss itself, due an amplifying effect resulting from changes in Arctic Ocean biogeochemistry.

In summary, this dissertation contributes to the understanding of Arctic coastal erosion within the Earth system under a changing climate. Here, I describe the mechanisms underlying Arctic coastal erosion at large scales, I make projections of Arctic coastal erosion under future climate scenarios, and discuss its evolution and possible impacts within the Earth system. Coastal erosion projections offer support for policy focused on coastal conservation and planning, while also sheds light on the uncertain future of the Arctic environment, especially at the land-sea interface. I show that Arctic coastal erosion is a relevant component of the Arctic carbon cycle, and should therefore be considered in future climate assessments.

ZUSAMMENFASSUNG

Die Küstenerosion in der Arktis bedroht die Küstengemeinden, beschädigt die Infrastruktur und setzt organischen Kohlenstoff aus dem Permafrost frei, was die Treibhausgaskonzentration in der Atmosphäre erhöhen könnte. Bislang existieren jedoch noch keine Prognosen zur arktischen Küstenerosion. In dieser Arbeit verfolge ich einen neuartigen Ansatz, indem ich Beobachtungen mit Erdsystemmodell- (ESM) und Ozeanwellensimulationen kombiniere, um die arktische Küstenerosion in der Gegenwart und unter zukünftigen Klimaänderungen zu untersuchen.

Ich schließe die Lücke zwischen der feinskaligen Küstenerosion und den grob aufgelösten ESMs in zwei sich ergänzenden Schritten: Ich verbinde die zeitliche und räumliche Variabilität der Erosion mit den in den ESMs dargestellten Mechanismen. Ich zeige, dass die wichtigsten Formen der mehrjährigen Variabilität der Küstenerosion, die mittels Beobachtungen aus der Laptewsee identifiziert wurden, auf großräumige Meereis- und atmosphärische Variabilität reagieren, die wiederum beispielsweise durch die arktische Oszillation moduliert werden. Etwa die Hälfte der räumlichen Variabilität langfristig gemittelter pan-arktischer Küstenerosionsraten wird durch eine lineare Kombination von Bodeneisgehalt, Oberflächenwellen des Ozeans und Tauwettergradtagen erklärt. Damit zeige ich erstmalig, dass eine semi-empirische Beschreibung der pan-arktischen Küstenerosion möglich ist, wobei die Haupttreiber sogar mit ESMs skalenkompatibel sind.

Ich präsentiere die ersten Projektionen der arktischen Küstenerosion für das einundzwanzigste Jahrhundert, indem ich mein semi-empirisches Modell mit einem Ensemble von ESM-Simulationen antreibe. Mit diesen erstelle ich die ersten Schätzungen über das Ausmaß, den Zeitpunkt und die Empfindlichkeit des Anstiegs der Klimawandel-bedingten arktischen Küstenerosion vorzunehmen. Diese Projektionen schätzen, dass sich die durchschnittliche Küstenerosionsrate in der Arktis bis zum Jahr 2100 etwa verdoppeln und ihre historische Schwankungsbreite noch vor Ende dieses Jahrhunderts überschreiten wird, selbst bei einem Szenario mit moderaten Emissionen. Die Empfindlichkeit der arktischen Küstenerosion gegenüber dem Klima nimmt ebenfalls zu, was auf die arktische Amplifikation zurückzuführen ist. Die arktische Küstenerosion könnte bis 2100 etwa 2 PgC aus dem Permafrost freisetzen, oder etwa 2,5 TgC Jahr^{-1} ^{o}C^{-1} in zukünftigen globalen Erwärmungsszenarien. Darüber hinaus deuten erste Ergebnisse aus gekoppelten ESM-Simulationen darauf hin, dass die arktische Küstenerosion zu einem größeren Anstieg der atmosphärischen CO_2-Konzentration führen könnte als der Permafrost-OC-Verlust, was auf einen Verstärkungseffekt zurückzuführen ist, der sich aus Veränderungen der Biogeochemie im Arktischen Ozeans ergibt.

Zusammenfassend leistet diese Dissertation einen Beitrag zum Verständnis der arktischen Küstenerosion innerhalb des Erdsystems unter einem sich ändernden Klima. Hier beschreibe ich die Mechanismen, die der arktischen Küstenerosion in großem Maßstab zugrunde liegen, mache Projektionen der arktischen Küstenerosion unter zukünftigen Klimaszenarien und diskutiere ihre Entwicklung und möglichen Auswirkungen innerhalb des Erdsystems. Küstenerosionsprognosen bieten Unterstützung für eine Politik, die sich auf den Schutz und die Planung der

Küsten konzentriert, und werfen gleichzeitig ein Licht auf die ungewisse Zukunft der arktischen Umwelt, insbesondere an der Schnittstelle zwischen Land und Meer. Ich habe gezeigt, dass die arktische Küstenerosion eine relevante Komponente des arktischen Kohlenstoffkreislaufs ist und daher bei zukünftigen Klimabewertungen berücksichtigt werden sollte.

PUBLICATIONS RELATED TO THIS DISSERTATION

Appendix A:

Nielsen, D. M., M. Dobrynin, J. Baehr, S. Razumov & M. Grigoriev (2020). "Coastal erosion variability at the southern Laptev Sea linked to winter sea ice and the Arctic Oscillation". *Geophysical Research Letters*, 47, e2019GL086876, https://doi.org/10.1029/2019GL086876

Appendix B:

Nielsen, D. M., P. Pieper, A. Barkhordarian, P. Overduin, T. Ilyina, V. Brovkin, J. Baehr & M. Dobrynin. "Projected increase of Arctic coastal erosion and its sensitivity to warming in the 21st Century" – *under review in Nature Climate Change*. Preprint available at: https://doi.org/10.21203/rs.3.rs-634673/v1

ACKNOWLEDGMENTS

Many people supported me during my PhD time in Hamburg, to whom I owe immense gratitude. In many ways, you helped me shape and enabled the completion of this work.

First, I would like to thank my supervisors for giving me this opportunity: it has been a thrilling and huge pleasure. I thank Mikhail Dobrynin, for bringing me into this exciting research topic, and allowing me enough freedom to explore, while also close and reliable support at the same time. I thank Johanna Baehr, for having me in her group, and for her incredible tact at guiding, which goes far beyond the scientific advice. It has been a true privilege, from which I can only hope to learn. I thank Victor Brovkin, for sharing some of his expertise and experience, and for including me in his group as well, which allowed me to see my work from a broader perspective. I also thank Lars Kutzbach, for being my Panel Chair during the last three and a half years, and for providing his critical view and thus helping me improve my work. I also thank all my co-authors, who contributed scientifically to the development of this work. I thank Katherine, Patrick, Zoé and Geet for the careful look over the unifying essay.

I am also grateful to the opportunity to join the Interantional Max Planck Research School on Earth System Modelling, which facilitated a truly multidisciplinary experience. I thank Antje Weitz, Cornelia Kampmann, and Michaela Born for being always so supportive. Warm thanks to Antje for being always so attentive.

I thank the inspirational and welcoming environment provided by the Climate Modelling group at Universität Hamburg. It has been great to be among you. In special, I thank Sebastian for the conversations during our long coffee breaks, Patrick for the exciting discussions and being always willing to help, Goratz for the warm company and support during the last year or so, and Vimal, Céline and Björn, who were also always there when I needed, even if virtually.

I thank the help provided from Tatiana Ilyina and her group, in especial by Fatemeh and Jöran for showing me the way around HAMOCC. I am excited to continue our work together.

I would also like to thank Iuliia Polkova and Norman Rueggen, who made it possible for me to join the expedition to Siberia in 2019. I owe thanks to Wolfram, Lutz and Zoé, who introduced me to the fascinating Lena Delta, and to everyone at the Samoylov research station in late summer 2019, for the sense of togetherness, despite being at the most remote spot on Earth I ever imagined I'd be. Thanks to Ivan and his friend, for the hospitality in the long Tiksi days. I am particularly grateful to Mikhail Grigoriev, for taking me on his boat to Muostakh, and the continuous monitoring effort, which enabled a good portion of this work to be done. I also thank my supervisors for supporting me on this endeavor.

I cannot properly express my gratitude to all the friends that participated in this journey. I thank Geet and Theresa for the unmeasured support, especially in the last couple of months. I am privileged to be among the IMPRS+ crew, and all the diversity and joy that it brings. I am thankful to Pin Hsin, Katherine, Leonie, Elliot, Diego, Laura, Thibaut, Arjun, Lennart, Moritz, George, Zoé, Theresa and Geet for

the friendship during this period. I thank my flatmates Katherine and Maurice, who were there next to me making this all much lighter, in their own particular ways.

Lastly, I would like to thank my parents and my family in São Paulo, for the unconditional support to my decisions. I also thank Pedro, for sharing this entire experience with me.

CONTENTS

Unifying Essay

Appendices

UNIFYING ESSAY

AN EARTH SYSTEM MODELLING PERSPECTIVE ON ARCTIC COASTAL EROSION UNDER CLIMATE CHANGE

1 INTRODUCTION

> "Polar ice can retreat markedly to the north at the end of our century and completely melt in the middle of next century."
>
> – Budyko (1972)

The first descriptions of climate feedbacks, often accompanied by dramatic climate projections (e.g. Budyko, 1969, 1972), propelled science to devote a substantial amount of effort to better understand, model, and assess the future evolution of the Earth's climate (e.g. IPCC, 2013). The work presented in this thesis is at least indirectly inspired by that approach. I set out to better understand, model, and make projections of Arctic coastal erosion under anthropogenic climate change until the end of this century. One of the key and novel aspects of the present work is my Earth system modelling perspective, which allows us to make such future assessments, nonexistent so far for Arctic coastal erosion.

1.1 *Arctic coastal erosion and its underlying mechanisms*

Leffingwell's pioneering expedition and early descriptions of Arctic coastal erosion

The earliest report on Arctic coastal erosion in the English language was probably made by Ernest de Koven Leffingwell in the early 1900s, in times when a good portion of scientific advances still consisted of exploring and describing nature with the bare eye. Leffingwell set off in 1906 on a privately-funded expedition with Danish explorer Ejnar Mikkelsen, with plans to investigate rumors on the existence of land north of Alaska. Despite the lack of success at finding new land, Leffingwell made the first detailed description of a large extent of the Alaskan coast after its initial recognition by Dease and Simpson (1838). Their ship, the Duchess of Bedford, was later locked on fast ice, destroyed, and the wood was used to build a cabin on Flaxman Island – a 6-kilometer long barrier island about 4 kilometers away from the continent. The small island served him as a seasonal shelter until 1914 for further descriptive work. During his time on Flaxman, Leffingwell described, almost naively to the modern reader's eyes, the process that forms the backbone of this thesis.

> "Ice is always seen underlying the soil. (...) Immediately over the beach, the plain ends in a steep mud cliff, which is broken by frequent gullies (... and) recedes under the action of the elements." – Leffingwell (1908)

The uniqueness of the Arctic coastal environment

The scenario portrayed by Leffingwell is common along the Arctic coast still nowadays: ice-rich erosive steep cliffs, often referred to as "coastal bluffs", contouring vast polygonal tundra plains (Fig.1a). The Arctic coast shows such peculiar characteristics because of the seasonal see-saw between frozen and unfrozen states, which make it somewhat special in comparison to its lower-latitude counterparts. Onshore, the

Arctic coast is dominated by permafrost – perennially frozen soil[1] – rich in ground ice and poorly consolidated sediments (Lantuit et al., 2012; Günther et al., 2015; Fuchs et al., 2018). Ground ice occurs as massive ice beds underlying the surface layers, as ice wedges (Fig.1a-b), and as pore ice in ice-bonded sediments (Hequette and Barnes, 1990). Between 50% and 90% of the permafrost volume is occupied by ground ice in Yedoma regions, also known as ice-complex deposits, which formed during the late Plesitocene up to about 12 thousand years ago and are extensive along the Siberian and Alaskan coasts (Strauss et al., 2013). Offshore, the Arctic coast is distinguished by the presence of sea ice. Sea ice normally wraps the Arctic coast during winter months, and retreats further north around summer. Only when sea ice retreats, can coastal erosion take place. During the sea-ice free, or open-water season (OWS), the coast is exposed to storms, and warm ocean waters and atmosphere, becoming vulnerable to erosion. The OWS duration is, therefore, of primary relevance to determine yearly amounts of Arctic coastal erosion (Overeem et al., 2011; Barnhart et al., 2014a). Within the OWS, erosion is controlled by a combination of local conditions.

The open-water season (OWS) as a pre-condition for erosion

> "Practically the only way such an island as this can be destroyed, is by wave-cutting at the sides and the consequent direct exposure of the ice to the sun. This is taking place very rapidly on the seaward side, as freshly fallen blocks of peat and ice show." – Leffingwell (1908)

Indeed, Arctic coastal erosion is the consequence of thermally and mechanically-driven mechanisms combined, which Aré (1988) described as follows. Sub-aerial permafrost thaw and ground-ice melt caused by positive surface air temperatures make the sediment subside, lose cohesion, and slump. Water from melting ground ice saturates the soil, flows in thaw streams towards the sea, and facilitates the slumping of the thawed material. This thermally-driven mechanism characterizes *thermo-denudation* (TD, Fig.1c). At the land-sea interface, ocean surface waves abrade coastal cliffs, while ocean currents transport the eroded sediment offshore. The mechanical effect from ocean waves characterizes *thermo-abrasion* (TA, Fig.1d). Positive sea temperatures also thaw the submarine permafrost, which grants the thermal component to TA. However, it is difficult to separate the thermal and mechanical effects, as they normally occur simultaneously (Aré, 1988). Therefore, TA is often interpreted as only the mechanical effect from wave abrasion, while the thermal effect from permafrost thaw is attributed to TD (e.g. Günther et al., 2015; Ogorodov et al., 2020; Baranskaya et al., 2021).

The two main controlling processes: thermo-denudation (TD) and thermo-abrasion (TA)

Sea level plays an important role in determining the effectiveness of TA. Higher water levels increase the contact area between land and sea, and therefore also cliff abrasion and submarine permafrost thaw. Sea level changes due to tides, however, are considered negligible in our case, as their amplitude in the Arctic region is minor compared to the rest of the globe (Fofonova et al., 2014). Tides might play an indirect role in driving ocean mixing, transporting heat towards the surface, and thus thinning and breaking sea ice, and eventually favouring the opening of

The role of storms in water level setup

1 Formally, *permafrost* is defined as "ground that remains at or below 0^{0}C for at least two consecutive years". Salinity in soil pore water may prevent it from actually freezing under negative temperatures, which characterizes *cryotic* soil – not necessarily frozen per se, but still permafrost. The "two consecutive years" implies that the cryotic state must persist during summer (Huissteden, 2020).

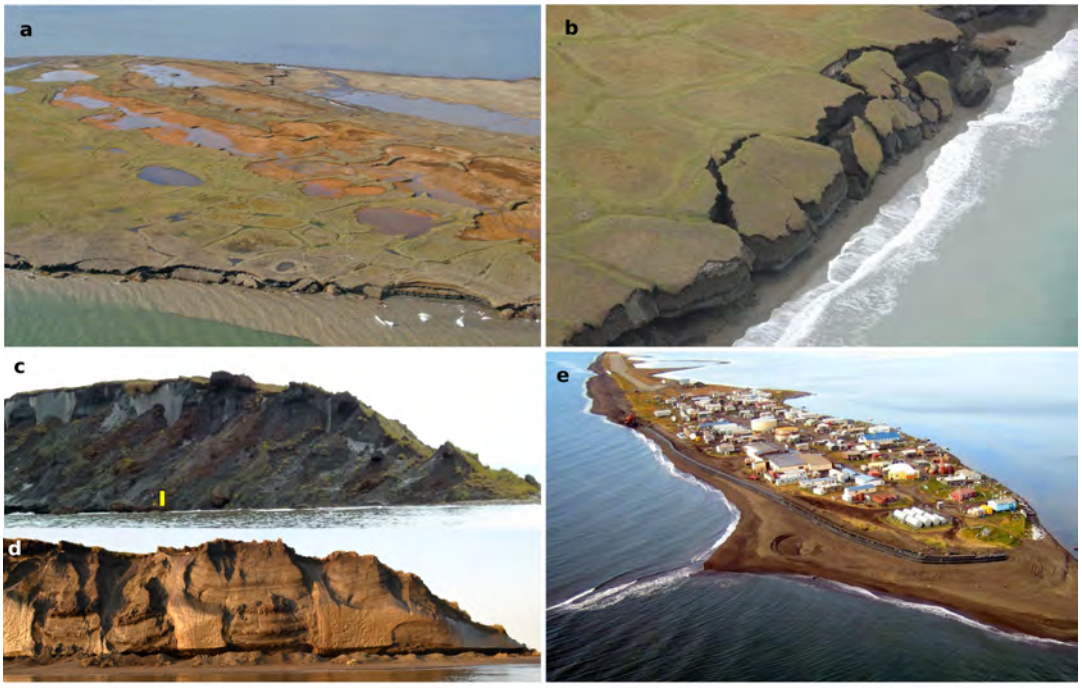

Figure .1: **a)** Oblique aerial image of Flaxman Island, Alaska, on 9 August 2006, modified from Gibbs and Richmond (2006). **b)** Collapsing blocks of permafrost at the Yukon Coast, Canada, modified from Nicole Couture's photo in Overduin et al. (2014). Frontal view of the northern cape of Muostakh Island, Laptev Sea, depicting the processes of **c)** thermo-denudation and **d)** thermo-abrasion. Modified from Günther et al. (2015). The yellow bar indicates a standing person for scale. **e)** The village of Kovalina, located on a barrier Island on the Alaskan Chukchi Sea, strongly affected by coastal erosion. Photo modified from Sakur (2013), available at: `https://www.bbc.com/news/magazine-23346370`. Ice-wedge polygons, typically 20 to 30 meters wide, are visible in both **(a)** and **(b)**. In **(a)**, one can see the formation and degradation of thermokarst lakes. The grey, and shiny light-brown cliff surfaces in **(c)** and **(d)**, respectively, indicate exposed bodies of massive ice. Ground ice makes up to more than 80% of Muostakh Island's volume (Günther et al., 2015).

polynyas and flaw leads (Holloway and Proshutinsky, 2007). Water level is, however, effectively setup by storms, which are therefore very relevant for coastal erosion (Jones et al., 2008). Single storm events during the open-water season contribute significantly to yearly erosion rates (Cunliffe et al., 2019). Barnhart et al. (2014b) used time-lapse images to verify that about 40% of erosion occurred during less than 5% of the open-water season at Drew Point, Alaska, in a case study.

The role of ice-wedges and block-failure events in increasing TA

The episodic character of erosion is also associated with TA and the local permafrost morphology. Wave abrasion opens notches at cliff bottoms, often several meters deep into the cliff, causing entire blocks of still frozen permafrost to break and fall into the water or onto the beach, when there is one, characterizing *block-failure* events (Fig.1b). As thermoerosional notches are deepened by undercutting waves (Fig.1d), and the tensile forces increase within the still-frozen hanging permafrost bluff, rupture planes often occur at the interface between ice wedges and sediment, where cohesion is less strong (Hoque and Pollard, 2009; Thomas et al., 2020). As a

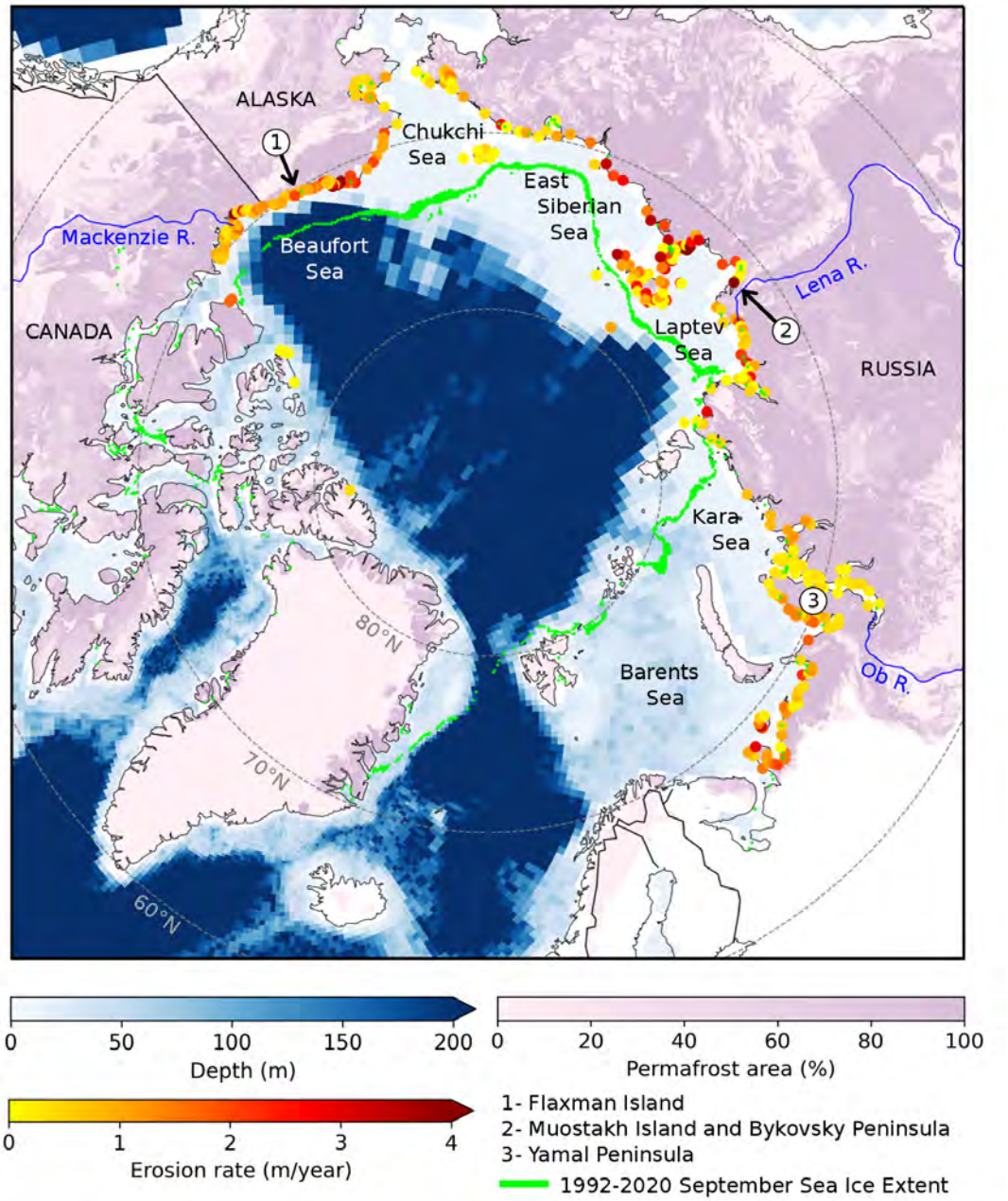

Figure .2: **The Arctic region.** Permafrost-affected soils coverage (Hugelius et al., 2013); upper ocean bathymetry, depicting the approximate extent of the continental shelf; 1992-2020 mean September sea-ice extent, defined as the contour of at least 15% sea-ice concentration (Kaleschke et al. (2001), obtained from the ICDC/CEN/Universität Hamburg at: `icdc.cen.uni-hamburg.de`); and long-term mean coastal erosion rates at coastal segments classified as erosive and with ground-ice content $> 0\%$ (Lantuit et al., 2012). Bathymetry data are displayed on the grid of the Max Planck Institute Earth System Model in its low-resolution configuration (MPI-ESM-LR), whose ocean component has a pole over Greenland and mean horizontal resolution of about 1.5 degrees (GR15).

consequence, episodic block-failure erosion is also dependent on local geomorphological properties, such as the presence and geometry of ice wedges, and pore-ice as a cohesive element in the ground.

Sea ice also plays an important role within the open-water season in decreasing the TA effect. The distance between the sea-ice margin and the coast determines the fetch for ocean waves to form, while sea-ice floes attenuate their propagation (Wadhams et al., 1988; Hošeková et al., 2020).

1.2 *On the socioeconomic relevance of Arctic coastal erosion*

Globally, coastal regions are especially vulnerable to climate change. They are the first to suffer the direct impact of sea-level rise, affecting millions of people worldwide (Nicholls and Cazenave, 2010; Rossi, 2019). As a consequence, people living in coastal areas have a more realistic perception of climate change, according to Milfont et al. (2014), and are more likely to contribute to cut down carbon emissions in comparison to populations living in the countryside. In the Arctic, coastal erosion aggravates the problem, to the point that entire villages are facing the imposing need for relocation, causing the migration of entire populations as actual *climate refugees* (Sakakibara, 2008; Mooney, 2015; Goode and Haner, 2016). On top of the economic damage, coastal communities fear not being able to preserve their culture after moving inland (Goode and Haner, 2016).

Arctic coastal erosion causes numerous socioeconomical losses. It damages modern and historical infrastructure, threatening traditional means of subsistence, such as fishing and hunting (Larsen et al., 2021). The chronic infrastructure damage also impedes the installation and maintenance of hydrocarbon industry facilities (Belova et al., 2018; Brady and Leichenko, 2020). In general, erosion substantially reduces the land-use potential of the Arctic coast, as large areas become uninhabitable. In Alaska, as of 2003, 86% of the native villages (i.e. 184 out of the 213) were affected by flooding or erosion (GAO, 2003). In a follow-up survey, 31 villages were classified as under “imminent threat" specifically from coastal erosion (GAO, 2009). Out of those, 12 native villages already decided to relocate. One example that has gained attention from the media is Kivalina (Fig.1e) (Sakur, 2013; Mooney, 2015; Goode and Haner, 2016; Thompson, 2017; Walker, 2021), a village of about 400 inhabitants on a barrier island on the West coast of Alaska towards the Chukchi Sea (Fig.2). Kivalina awaits the execution of its relocation by the U.S. Federal Government since 2006. The relocation cost for Kivalina alone was initially estimated at about 250 million US dollars (Hayes and Corporation, 2006). Considering the number of villages that already decided to relocate, disregarding the ones that may face this problem only in the future, one can estimate a pan-Arctic relocation cost on the order of billions of dollars, at least.

Coastal communities need to relocate due to Arctic coastal erosion, characterizing waves of climate refugees

As Arctic coastal erosion removes land, invaluable information is also lost. Archaeological sites have already been damaged, causing irreversible heritage data losses (Jensen, 2020; Nicu et al., 2021). Arctic coastal erosion also modifies historical natural coastal features (Jones et al., 2008; Larsen et al., 2021). Analyzing historical maps of the Alaskan coast, Jones et al. (2008) identified that coastal erosion removed entire capes and small islands, and connected thermokarst lakes with the sea, leading to the formation of new bays during the past two centuries. Out of seven coastal

features described by Dease and Simpson (1838), only two were still recognizable as of the work of Jones et al. (2008), and already threatened by erosion.

At this point, we may want to start asking questions about the future evolution of Arctic coastal erosion. In order to discuss its variability, we need first to define and, therefore, be able to quantify erosion, which is also central to the objective of this thesis.

1.3 *On the definitions of coast and coastal erosion*

On the etymology of 'shore' and 'coast'

The concept of coast, or shore, is closely related to erosion. The word *coast* derives from the old French *coste* (nowadays *côte*), with translates to rib[2], denoting the sides or flanks of a landmass (Oertel, 2005). The word *shore* evolved from the old German word *Schöre* (Oertel, 2005), which relates to the modern German words *Scheren*, meaning cutting or scissors, or *Scherung*, which translates to shear. One could interpret the first use of the word *Schöre*, on the one hand, as a reference to the area that cuts between land and sea or, on the other hand, as a reference to the shear between land and sea, hence erosion.

On the various definitions of coast

On the practical side, several definitions exist for *shore* and *coast*. Generally, both terms can be used interchangeably to refer to the area surrounding the land-sea interface, although *coast* may imply a larger scale than *shore* (Oertel, 2005). Aré (1988) used a rather broad definition of coast from Zenkovich (1962): "the zone between the edge of the shore scarp (cliff), on land, and the isobath to which waves locally transport sediment, in the sea". Barrell (1912) defined *shoreface* as the "relatively steep slope developed by breaking waves, which separates the sub-aerial plain above from the subaqueous below". Cowell et al. (2003) combined the previous definitions and made a conceptual zonation with respect to the shoreface position, defining three regions: the backshore, the upper and the lower shoreface. In this thesis, I take the definition of Lantuit et al. (2012), which modifies that of Cowell and distinguishes four regions: onshore, backshore, frontshore, and offshore (Fig.3). In this definition, the backshore elevation denotes the height of coastal cliffs, and the onshore zone starts at the clifftop towards inland. The frontshore and offshore zones correspond roughly to the definitions of nearshore *resuspension zone* and *deposition zone* of Jong et al. (2020), respectively. The resuspension zone is characterized by shallow waters and active mobilization of the eroded material by waves and currents, and sediment resuspension. The deposition zone is characterized by deeper waters and relatively long-term burial of the eroded material into the sediment, where resuspension is negligible. The extent and effectiveness of the nearshore resuspension and deposition is relevant to determine the residence time of the eroded material in the water column, and thus the remineralization of the organic matter therein (Bröder et al., 2018; Jong et al., 2020).

Coastal erosion is broadly defined as "a morphological change due to loss of material from a coastal system or subsystem" (Esteves, 2018), or as "the removal of sediment from the shore area to the ocean due to wave action" (Lantuit, 2008). In both definitions, there is loss of material, which causes the coast to retreat. In

2 The old French *coste* also developed to *costal* in modern English (in parallel to *coastal*), as an adjective to refer to the rib cage or the ribs themselves, most commonly used in a medical context (e.g. inter*costal* muscles).

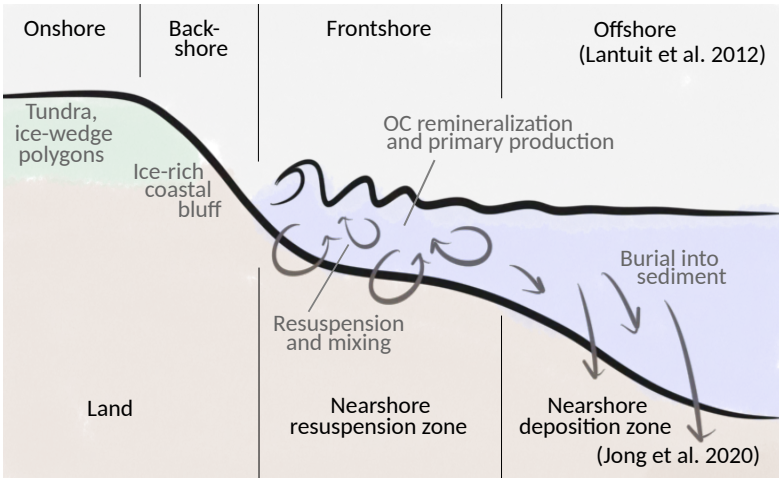

Figure .3: Schematic representation of a typical thermoerosive coastal section, adapted from the classifications presented in the ACD by Lantuit et al. (2012) and by Jong et al. (2020).

On the definitions of coastline and erosion rates

order to quantify coastal retreat, a reference needs to be established. Shoreline, or sheared line, refers precisely to the line between land and sea (Oertel, 2005). The shoreline retreat is thus the horizontal distance between two shoreline positions apart in time. This method naturally brings the question of shoreline placement. Arctic coastal erosion observations often place the shoreline at cliff tops, as cliffs are among the most common – and erosive – formations along the Arctic coast, and can be identified with remote sensing (Jones et al., 2009; Couture et al., 2018; Irrgang et al., 2018; Jones et al., 2018). In this dissertation, I use the term *coastal erosion rate*, or just *erosion rate*, expressed in meters per year, to refer to the yearly integrated shoreline retreat, as commonly used in the literature.

Leffingwell (1919) analyzed the first maps of the Alaskan coast made by explorers Dease and Simpson (1838) to make the first registered estimates of yearly erosion rates of "over a hundred feet" (∼30 m) at Drew Point, Alaskan Beaufort Sea coast (Fig.2). A century later, Jones et al. (2018) used satellite imagery and time-lapse photography to report rates of up to 22 m/year at the same place. Despite this apparent and misleading decrease over the course of one century, coastal erosion rates have increased in response to ongoing climate change.

1.4 *Connections and gaps between erosion and climate*

Observations show unanimous increase in Arctic coastal erosion rates

Observations show that erosion rates have increased throughout the Arctic in the past decades, often by a factor of two or more (e.g. Jones et al., 2009; Günther et al., 2015; Irrgang et al., 2018; Jones et al., 2018; Jones B. M., 2020; Ogorodov et al., 2020). The increase in erosion rates is explained by the simultaneous decrease in Arctic sea-ice cover (Overeem et al., 2011; Barnhart et al., 2014a; Notz and Stroeve, 2016; Comiso et al., 2017), and increase in surface air- (Serreze et al., 2009; Cohen et al., 2014) and permafrost temperatures (Biskaborn et al., 2019). The present-climate Arctic-mean coastal erosion rate is estimated at 0.5 m/year (Lantuit et al., 2012). Locally, erosion rates are as high as 20 m/year in Drew Point, Alaskan Beaufort Sea,

and on Muostakh Island, Laptev Sea (Jones et al., 2018; Grigoriev, 2019), for example (Fig.2). Günther et al. (2015) estimated that about 40% of Muostakh Island had been lost to coastal erosion and ground subsidence in the course of the previous 62 years. They expect Muostakh Island to disappear in the coming decade, echoing the early descriptions of Flaxman Island by Leffingwell (1908), but now in the context of anthropogenic climate change.

In the future, erosion rates are expected to increase even more

Arctic coastal erosion is expected to accelerate in the future. Arctic surface air temperature and sea-ice cover are projected to exceed their natural range of variability within the next century (Landrum and Holland, 2020). Arctic surface temperatures will continue increasing at least twice as fast as the global mean (Cai et al., 2018; Cai et al., 2021), and September Arctic sea-ice is projected to disappear within the next decades (Notz and SIMIP Community, 2020; Docquier and Koenigk, 2021). The OWS duration is projected to increase by 2 months per degree of global warming, reaching 6 months averaged along the marginal Arctic seas, in the most aggressive warming scenarios (Crawford et al., 2021). Despite clear evidence showing that Arctic coastal erosion might accelerate in comparison to the present-day climate, no dedicated projections have been made so far. Therefore, the timing, magnitude and sensitivity of Arctic coastal erosion to global warming remain unknown.

Arctic coastal erosion releases substantial amounts of permafrost organic carbon (OC)

There is a pressing need for comprehensive projections of Arctic coastal erosion, not only due to its socioeconomic impacts. Also of paramount relevance, is the permafrost organic carbon (OC) loss from Arctic coastal erosion in response to climate change (Vonk et al., 2012; Tanski et al., 2019; Tanski et al., 2021). It is estimated that about 10 Tg of permafrost OC is released due to Arctic coastal erosion every year, which is about as much as the OC flux all the Arctic rivers combined (Wegner et al., 2015). Because organic matter is well conserved in the permafrost since formation, it degrades relatively fast upon thaw, releasing CO_2 and methane to the surrounding Arctic Ocean and atmosphere (Vonk et al., 2014; Tanski et al., 2019). Although anthropogenic emissions are about three orders of magnitude larger (Friedlingstein et al., 2020), Arctic coastal erosion potentially adds to the atmospheric greenhouse gas concentration (Tanski et al., 2019; Tanski et al., 2021). In the ocean, the eroded material may sink and remain buried in the sediment (Couture et al., 2018; Jong et al., 2020), be transported offshore, remineralized and fuel primary production (Terhaar et al., 2021). The fate of the OC released by Arctic coastal erosion is currently under debate. A more detailed discussion on the fate of the eroded OC will follow in Section 4. Dedicated model simulations to estimate the OC flux from coastal erosion in response to climate change, as well as its degradation pathway after release, are still needed.

Historical modelling work on coastal erosion

Models for Arctic coastal erosion have substantially improved since the 1980s. The first models focused only on TA, or submarine erosion, using heat transfer formulations to represent the opening of notches at the inundated cliff bottoms (Kobayashi, 1985; Kobayashi et al., 1999). These models work on idealized domains of cliff and beach slope, and erosion is mainly driven by sea water conditions, such as sea temperature and water level. The submarine erosion models of Kobayashi have since been continuously applied to other model developments. Recently, Rolph et al. (2021) coupled Kobayashi's model with a dynamical storm-surge model, and obtained good agreement with observed decadal cumulative erosion at Drew Point, Alaska, and Mamontovy Khayata, Siberia. Hoque and Pollard (2009) added

a mechanical/torque component to Kobayashi's model, in order to simulate block-failure in a theoretical setup. Ravens et al. (2012) simulated block-failure erosion in a case study at Drew Point, Alaska, using a storm-surge model and Kobayashi's niche development formulation. Barnhart et al. (2014b), in a similar approach, added TD effects with a simple linear parameterization of subaerial erosion as proposed by Aré (1988), and tested three models for niche development and block degradation: that of Kobayashi (1985), and two iceberg-melt models (Russell-Head, 1980; White et al., 1980). Interestingly, they found Kobayashi's formulation to overestimate the overall erosion in comparison with observations. The iceberg model of White et al. (1980) performed best among the three, suggesting similarities in the governing physical processes.

Up to this point, Arctic coastal erosion models were one or two-dimensional. Thomas et al. (2020) presented an alternative with more sophisticated mechanics and thermodynamics, including elastic deformation, heat conduction, and pore water phase change, to simulate block failure in an idealized three-dimensional polygonal-tundra domain. Bull et al. (2020) presented a suite of coupled model components, including that of Thomas et al. (2020), and very high-resolution regional ocean circulation and surface wave models. The regional ocean model presented by Bull et al. (2020) had spatial resolution increasing to about 100 meters around the area of interest, at Drew Point, Alaska. The work of Bull et al. (2020) is certainly the most comprehensive so far in terms of the physical processes represented, and also likely the most accurate at reproducing realistic coastal erosion at the local scale. However, as of yet, it is computationally unfeasible to use their approach to make climate projections.

Hierarchy of high-resolution models for local application

There is indeed a movement towards high-resolution models while supercomputers become more powerful. Global atmospheric models have been improved to represent clouds well enough to pass a "Palmer-Turing test"[3] at the global scale (Stevens et al., 2019). However, such simulations are ultra-highly spatially resolved and can thus only be conducted for a limited number of days, even when making use high-performance computing centers. In order to be computationally feasible, long-term ensemble climate projections, such as those normally presented by the Intergovernmental Panel on Climate Change (IPCC, 2013), still require coupled ESMs to be fairly poorly resolved, in comparison to the atmospheric-only storm-resolving models. This limitation poses challenges for the representation of fine-scale processes, such as coastal erosion, in climate projections.

High resolution is not enough

The necessity of taking Arctic coastal erosion into account in climate projections is clear. It poses risks to coastal communities, causes infrastructure and socioeconomic damages, and releases organic carbon from permafrost to the surrounding ocean and atmosphere. However, there is a substantial *scale gap* between coastal erosion and the mechanisms represented by modern ESMs. Fritz et al. (2017) call for holistic approaches to address the multifaceted problem of the "collapsing Arctic coastlines". Turetsky et al. (2019) suggest that novel frameworks should be developed, to bridge the gap between abrupt permafrost thaw and climate projections. This is precisely what I set out to do. I take this suggestion, and examine Arctic coastal erosion from

The overarching goal of this thesis

3 The Palmer-Turing test, referred to as such by Stevens et al. (2019), is a simple visualization test presented by Palmer (2016), in which a graphic model output and a satellite image are compared. The test makes reference to Alan Turing's test to distinguish artificial intelligence from human intelligence by comparing answers given to the same questions.

an Earth system modelling point of view. I develop a novel modelling framework to fill the scale gap between Arctic coastal erosion and Earth system model simulations. Thereby, I aim at answering our overarching question:

How will Arctic coastal erosion change in the future with climate?

In the next two sections, I examine this question in detail. On my way to answer it, I develop a semi-empirical Arctic coastal erosion model compatible with ESMs and use it to future-climate simulations. I present the first twenty-first century projections of coastal erosion, and associated OC fluxes, at the pan-Arctic scale. Thereby, we are able to discuss how the sensitivity of Arctic coastal erosion increase to global warming changes with time in the future. But first, we need to verify whether coastal erosion rates respond to mechanisms represented in ESMs. By looking for this connection, I describe large-scale mechanisms, which work towards closing the scale gap between erosion and ESMs.

2 LARGE-SCALE DRIVERS OF ARCTIC COASTAL EROSION

My overarching goal is set: to assess the evolution of Arctic coastal erosion under future climate change. However, an obstacle emerges at the scale gap between erosion and the models that are actually used for climate projections. While coastal erosion has a spatial scale on the order of meters, state-of-the-art ESMs have spatial resolution on the order of tens or hundreds of kilometers. The small-scale coastal erosion variability needs to be embedded, or to respond, to the large-scale mechanisms represented in the ESMs, to allow us to make any statements on Arctic coastal erosion based on ESM data. In order to verify this link, one could look for empirical associations between Arctic coastal erosion and large-scale variables, and describe the underlying causal relationship with a plausible physical mechanism, or a chain of mechanisms. The mechanisms of Arctic coastal erosion itself are well understood already for some decades (Aré, 1988), and should stand as a starting point for this analysis. This prepares us for the first question I address in this thesis.

Q1: How can we link large-scale mechanisms, represented in Earth system models, with the spatial and temporal scales of Arctic coastal erosion variability?

I answer this question in two complementary steps. First, I link large-scale mechanisms represented in ESMs, such as the variability of sea-ice and atmospheric circulation, with erosion *temporal variability at the local scale* using in-situ observations from the Laptev Sea coast. Second, I use ESM grid-scale information on the thermal and mechanical drivers of erosion to explain its *spatial variability at the pan-Arctic scale*. I start investigating the large-scale drivers of Arctic coastal erosion, possibly counter-intuitively, by taking a closer look at point-observations from the Laptev Sea coast.

2.1 *A closer look at the Laptev Sea coast*

In-situ observations of Arctic coastal erosion rates are rare. They are normally made in large expeditions facilitated by international cooperation agreements (AWI, 2020).

Coastal erosion rate estimation is therefore more commonly done with satellite imagery (Farquharson et al., 2018; Irrgang et al., 2018), historical aerial photography (Lim et al., 2020), more recently with images made with drones (Cunliffe et al., 2019), or a combination of different methods (Lantuit et al., 2011; Günther et al., 2015; Jones et al., 2018). Usually, the coastline positioning data are identified on images, that are many years apart from each other. Erosion rates are thus often given as long-term mean estimates, with decadal or multidecadal temporal resolution. This limitation makes it challenging to empirically explore the temporal variability of erosion on shorter time scales.

Observations are scarce, thus statistics are not robust

However, rare exceptions do exist. Here, I make use of such an exception. In-situ measurements of coastal erosion rates at Muostakh Island and Bykovsky Peninsula, southern Laptev Sea (Fig.4), have been made by Dr. Mikhail Grigoriev, from the Melnikov Permafrost Institute in Yakutsk, Russia, almost every year since the early 1980s until present (Grigoriev, 2019). These data provide, therefore, an extraordinarily long time series of yearly temporal resolution. This allows us to address the first part of our first question, on the temporal variability of coastal erosion at the local scale. I identify[4] the main modes of coastal erosion variability in observations with a Principal Component Analysis (PCA), and by analyzing them in comparison with ERA-Interim reanalysis (Dee et al., 2011), I link coastal erosion variability with mechanisms represented at the scales of ESMs.

A unique dataset of in-situ observations

2.1.1 *The role of sea ice*

We have already seen how sea ice plays an important role in coastal erosion by determining the duration of the open-water season (OWS), which has been suggested as a first-order proxy for erosion (Overeem et al., 2011; Barnhart et al., 2014a). In the Laptev Sea, sea-ice melt starts normally between May and June, and sea-ice freeze-up normally starts between October and November, bounding the OWS (Nielsen et al., 2020). The variability in dates of sea-ice melt and freeze-up contains, thus, important information to explain coastal erosion variability.

Winter sea-ice anomalies in the Laptev sea serve as indicators for sea-ice melt onset dates. Krumpen et al. (2013) and Itkin and Krumpen (2017) have shown that sea-ice transport offshore, driven by surface winds during winter, is a precursor for early onsets of the OWS in the Laptev Sea. During winter, increasing sea-ice export, hence decreasing sea-ice cover and volume, associated with the opening of polynyas and flaw leads, increase ocean-atmosphere heat fluxes. Thin ice, newly-formed in these openings, is prone to melt earlier than thicker ice in the forthcoming melt season. In addition, younger and thinner ice allows for more solar shortwave radiation into the ocean, drawing a positive feedback to ice melt (Perovich et al., 2007). Therefore, such negative winter sea-ice anomalies anticipate the onset of the OWS and precondition negative sea-ice anomalies during summer in the Laptev Sea (Krumpen et al., 2013; Itkin and Krumpen, 2017).

Winter sea ice as a precursor for OWS duration...

I indeed find the signature of winter sea ice as a precursor to OWS duration in coastal erosion observations. Winter (February-March-April, FMA) sea-ice coverage anomalies averaged over the Laptev Sea correspond to the first principal component

4 See Appendix A: Nielsen, D. M., M. Dobrynin, J. Baehr, S. Razumov & M. Grigoriev (2020). "Coastal erosion variability at the southern Laptev Sea linked to winter sea ice and the Arctic Oscillation". *Geophysical Research Letters*, 47, e2019GL086876, https://doi.org/10.1029/2019GL086876

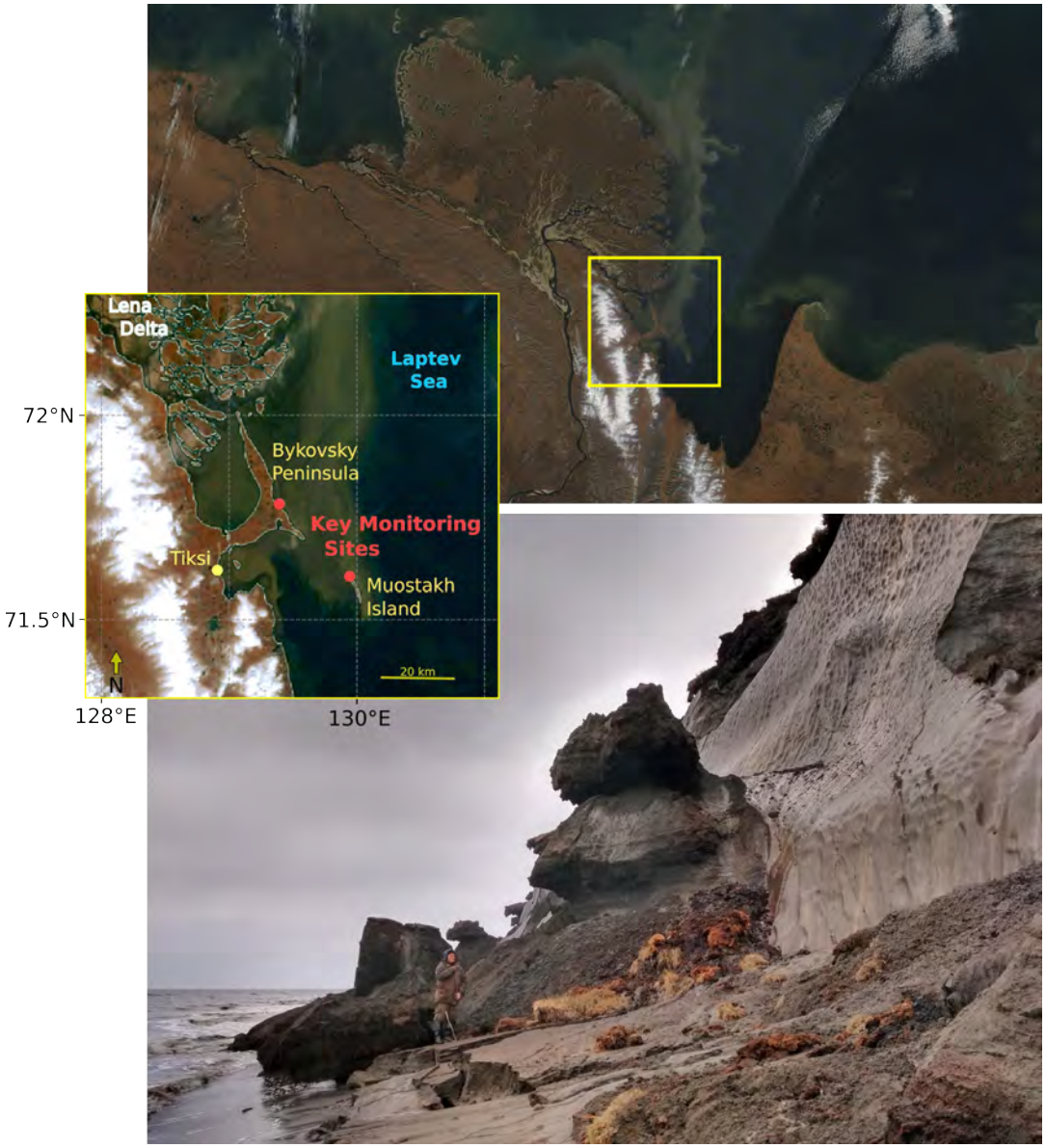

Figure .4: The location of the southern Laptev Sea key monitoring sites within the Lena River delta region, shown at the top [corrected reflectance (true color) image from Terra/MODIS, obtained from NASA Worldview at https://worldview.earthdata.nasa.gov]. The inset shows the specific monitoring points at Bykovsky Peninsula and Muostakh Island, adapted from (Nielsen et al., 2020). The bottom picture shows a cliff on the northeast coast of Muostakh, taken by the author on the 22nd of August, 2019. Blocks of unconsolidated sediment are visible equilibrating on top of each other at the beach, surrounded by thaw mud, and being washed away by the sea. The distinguished patterned light-brown surface on the cliff wall is an exposed body of massive ice, likely late-Pleistocene aged (Yedoma). The person standing on the lower-left corner of the photo is Dr. Mikhail Grigoriev, who has been monitoring coastal erosion rates almost every year during summer at least since 1982 at the key monitoring sites.

(PC1) from erosion ($r = -0.68$, $p < 0.01$, see Appendix A for details). Such a relationship is also found between PC1 and the OWS duration. I suggest, therefore, that winter sea-ice anomalies work as a precursor for coastal erosion in the Laptev Sea, as it helps modulate the duration of the OWS. Moreover, I identify that PC1 from erosion and winter Laptev sea-ice concentration anomalies present predominant low-frequency variability (period of ∼20 years). By analyzing the variability of winter sea ice spatially, we note that this low-frequency mode is not exclusive in the Laptev Sea, but is also predominant over the East Siberian and Chuckchi Seas. Therefore, I propose that the first mode of coastal erosion variability, identified in observations, responds to large-scale drivers of the climate system, expressed as winter sea-ice anomalies identified over the Laptev Sea.

...and therefore also for coastal erosion

A number of drivers has been proposed to explain the source of low-frequency variability of Arctic sea-ice. One good candidate driver is the Atlantic Multidecadal Variability (AMV, Kerr, 2000).[5] The low-frequency imprint of the AMV on climate has been shown by a number of studies. The AMV modulates precipitation (Enfield et al., 2001; Knight et al., 2006; Zhang and Delworth, 2006; Ting et al., 2011; Madrigal-González et al., 2017), surface temperature (Pohlmann et al., 2006; Zhang and Delworth, 2007; Steinman et al., 2015), Atlantic hurricane frequency (Knight et al., 2006; Zhang and Delworth, 2006), and terrestrial and marine ecosystems (Edwards et al., 2013; Rivero-Calle et al., 2015; Madrigal-González et al., 2017; Koul et al., 2021). Of relevance to this thesis, is the AMV modulation of Arctic sea ice. On the one hand, it has been long known that Arctic sea ice responds to large-scale atmospheric circulation patterns (Colony and Thorndike, 1984; Deser et al., 2000). Positive AMV conditions, in particular, are associated with a pattern of low sea-level pressure anomalies and cyclonic surface atmospheric circulation, that favour sea-ice export from the Kara, Laptev and East Siberian seas into the central Arctic Ocean (Castruccio et al., 2019). AMV-driven cyclonic circulation anomalies are also associated with increasing cloud longwave radiation, and consequently positive surface temperature anomalies and sea-ice loss in the Laptev and East Siberian seas (Castruccio et al., 2019). On the other hand, ocean heat fluxes may also play a role. With a long climate simulation (i.e. 3,600 years) and simple multiple linear regression models, Zhang (2015) showed that each the Atlantic and Pacific ocean heat fluxes into the Arctic exaplain, individually, about one quarter of the multidecadal variability of September Arctic sea-ice anomalies.

Potential sources of low-frequency sea-ice variability

While PC1 in erosion data shows decadal-scale variability, which I linked to low-frequency winter sea-ice variability, the second principal component (PC2) shows higher-frequency variability (period of ∼4 years), and is linked with the Arctic Oscillation (AO) during winter and summer.

2.1.2 *The role of the Arctic Oscillation*

The AO is the first mode of atmospheric mass variability in the Northern Hemisphere, derived from the first empirical orthogonal function (EOF) of geopotential heights (identified in many levels, also in sea level pressure) north of 20^{o}N (Thompson and

5 The AMV has initially been referred to as Atlantic Multidecadal Oscillation (AMO), although there is limited data to identify its oscillatory behaviour in observations. It has been shown, with model simulations, that the periodicity of the AMV is not internally driven, but rather externally forced by volcanic activity (Otterå et al., 2010; Mann et al., 2020, 2021).

Wallace, 1998). The AO has a distinct zonally symmetric pattern associated with the stratospheric polar vortex (Baldwin and Dunkerton, 1999). In general, the AO has significant effects on surface weather, especially on the intensity and frequency of storms (Baldwin and Dunkerton, 1999; Thompson and Wallace, 2001), and also on Arctic sea-ice (Wang and Ikeda, 2000). Over the Laptev Sea, in particular, the AO has an impact on sea ice both during winter and summer, although via different mechanisms.

Winter AO

During winter, the positive AO drives surface winds blowing from the southwest over Laptev Sea, pushing sea ice away from the coast and into the Arctic Ocean (Rigor et al., 2002). The AO-related winter sea-ice export from the Laptev Sea, driven by surface winds, leads to the opening of flaw leads and polynyas, which freeze and replace thick ice by new, thinner ice (Rigor et al., 2002). Once again, thinner ice allows for more efficient heat fluxes from ocean to atmosphere, and is more likely to melt faster than older and thicker ice, anticipating the onset and thus prolonging the subsequent OWS (Krumpen et al., 2013; Itkin and Krumpen, 2017). Thus while PC1 is associated with winter sea-ice anomalies with low-frequency variability, PC2 and the winter AO present higher-frequency variability (period of $\sim$4 years). Therefore, the winter AO is linked with erosion variability through high-frequency modulation of OWS duration, through sea-ice surface-wind transport.

Summer AO

During summer (June-July-August, JJA), the negative AO is associated with positive surface air temperature anomalies over its polar center of action, including the Arctic Ocean and Greenland. Ding et al. (2017) described how negative AO-like summer anticyclonic circulation drives surface warming by adiabatic descent, which is then reinforced by surface moistening, increasing low-cloud coverage and diffuse downward longwave radiation. As a consequence, the negative summer AO-related circulation leads to summer negative sea-ice anomalies (Ding et al., 2017). Therefore, negative summer AO conditions may contribute to erosion via TD, through surface warming, and TA, through decreasing sea-ice cover and hence increasing the impact of ocean waves. Moreover, Ogi et al. (2016) showed that positive winter AO conditions, combined with negative summer AO conditions, drive negative September Arctic sea-ice cover anomalies. I also find that strong erosion rates often follow a switch in sign from positive winter AO to negative summer AO, and vice-versa. Taking only extreme-erosion years, significant negative correlations emerge between the winter and summer AO indices. Therefore, and although the direct correlation between PC2 and the summer AO index is weaker than that of the winter AO, I identify the combined effect of both in erosion observations, along with the associated physical mechanisms.

2.1.3 *Implications and limitations for 'closing the gap'*

Regional dependency

These results are valid for the Laptev Sea, in specific for the monitoring sites at Muostakh and Bykovsky, and cannot be directly generalized to the pan-Arctic scale. One reason is that the large-scale drivers proposed here could play different roles in other regions. For example, Zhang et al. (2003) proposed that positive AO conditions would lead to negative sea-ice anomalies in the eastern Arctic, and positive sea-ice anomalies in the western Arctic, and vice-versa. Therefore, generalizations should be made with caution. Nonetheless, this fact does not invalidate the general link I proposed between fine-scale coastal erosion and large-scale drivers. The example of

Zhang et al. (2003) shows that these same large-scale drivers may play a different role in controlling coastal erosion in other regions in the Arctic.

The current generation of ESMs is able to represent general characteristics of both Arctic sea ice and the AO, although biases with respect to observations do exist. Such comparative analyses have been performed with the latest three ensembles of the Coupled Model Intercomparison Project phases 3, 5 and 6 (CMIP3, CMIP5 and CMIP6, respectively). Arctic-mean biases in the seasonal cycle and decadal trends of sea ice have improved (Davy and Outten, 2020), although the spatial pattern of trends is still not well simulated (Shu et al., 2020). Sea-ice persistence in monthly variability is generally overestimated (Davy and Outten, 2020). Notz and SIMIP Community (2020) reported an improvement in terms of sea-ice sensitivity to anthropogenic CO_2 emissions, although most models would be unable to represent a simultaneous plausible evolution of sea-ice area and global warming. With respect to the AO, most models are in general able to represent its spatial pattern and frequency spectrum, despite of biases in location and intensity of its centers of action (Gong et al., 2016). In fact, the MPI-ESM performed best among a 26-model ensemble from CMIP5 at representing both the temporal variability and spatial structure of the AO (Jin-Qing et al., 2013).

Biases in modern ESMs

Here, I have shown that the first two main modes of coastal erosion temporal variability, identified in observations at the southern Laptev Sea, are linked with mechanisms defined at scales relatively larger than those typically used to characterize erosion. Temporal variability of erosion does not only respond to very local conditions (e.g. storm events) and geomorphological properties (e.g. ground-ice content, polygonal block and coastal geometry). Taking winter Laptev sea-ice anomalies, and the summer and winter AO indices as explanatory variables in linear regression models, we are able to explain a large fraction of the interannual variability of coastal erosion rates in observations ($r = 0.54 - 0.76$). This is the first step towards our final goal: to investigate the future evolution of Arctic coastal erosion in the context of anthropogenic climate change, for which we ought to take an Earth system modelling perspective.

2.2 *An ESM-compatible pan-Arctic coastal erosion model*

In the previous section, I have looked at the *temporal* variability of erosion at two monitoring sites at the southern Laptev Sea coast. This was a first step forward towards the overarching goal of this thesis. We need now to broaden our spatial coverage to be able to draw more general conclusions on the relationship between Arctic coastal erosion and climate change. Next, I examine the *spatial* variability of coastal erosion at the pan-Arctic scale.

Temporal vs. spatial variability

I take an empirical approach to explain the spatial variability of erosion. I use the Arctic Coastal Dynamics (ACD) database (Lantuit et al., 2012) as my observational reference for coastal data, and ERA20C reanalysis (Poli et al., 2016) as my reference for TA and TD. The ACD is the most up-to-date compilation of coastal erosion observations and observations-based estimates at the pan-Arctic scale, distributed along 1314 coastal segments. For each coastal segment, the ACD brings information on long-term mean erosion rates (time invariant), ground-ice and organic carbon content, coastal segment dimensions and landform classification. ERA20C is used

because it covers the time span from the ACD. I harmonize the data by attributing ERA20C grid cells to ACD individual coastal segments (Fig.5a) in order to examine empirical relationships between coastal erosion rates and their drivers.

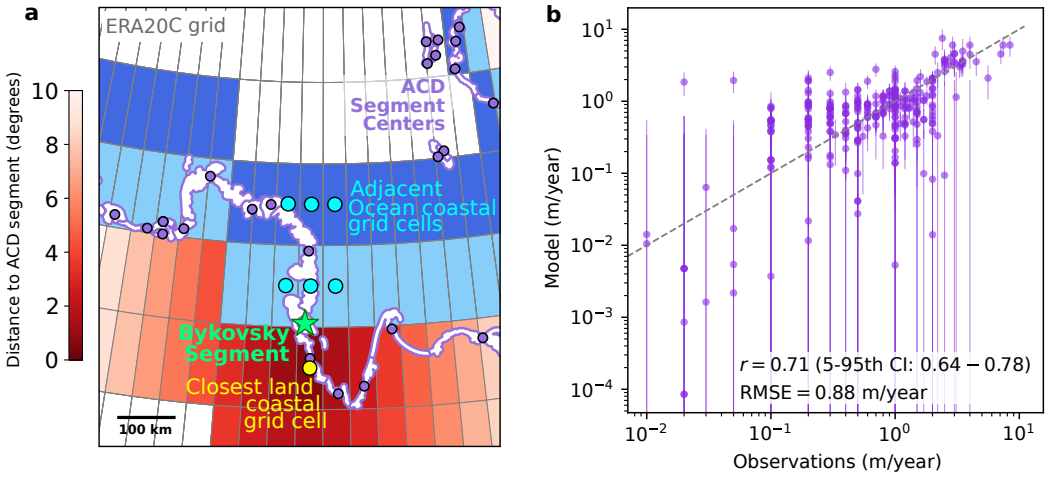

Figure .5: **a)** Example of the data harmonization strategy applied between the Arctic Coastal Dynamics (ACD) database and ERA20C reanalysis for the Bykovsky coastal segment in the ACD. Purple circles mark the center of the ACD coastal segments. The green star marks the center of the Bykosvky segment, which is linked to the closest coastal land grid cell from ERA20C, marked in yellow. Distances between ERA20C grid cells and the Bykosvky segment are shown in red tones. The attributed coastal ocean grid cells, marked in light blue, are those adjascent to it the attributed land coastal cell. I take two "rows" of ocean coastal grid cells, highlighted by the different tones of blue. **b)** Scatter plot between observed and modelled long-term mean erosion rates. Each dot is a coastal segment from the ACD. Vertical lines represent two standard deviations of uncertainties from our erosion model. The 1:1 line is shown in dashed grey. Only ACD segments classified as erosive and with excess ground ice are considered in the model.

Our model accounts for about half of the spatial variability of erosion

With a rather simple linear model, I am able to explain about half of the observed spatial variability at the pan-Arctic scale ($r = 0.71$, $R^2 = 0.50$, $n = 306$, Fig.5). Previous studies have suggested spatial empirical relationships between erosion and its environmental drivers individually, at regional levels, or with a smaller number of data. Hequette and Barnes (1990) found that ground-ice content and ocean-wave energy are good linear estimators for coastal erosion rates, and reported significant predictive power for their combined effect ($r \simeq 0.55 - 0.74$) at a relatively small number of coastal stretches ($n = 11 - 14$) at the Beaufort Sea coast. At the pan-Arctic scale, Lantuit et al. (2012) reported a moderate correlation ($r = 0.48$, $n = 608$) between erosion rates and ground-ice content. However, they did not explore the role of thawing temperatures or waves – to account for TD and TA, respectively – in driving the spatial variability of erosion. In our model, spatial variability of erosion is explained by thawing air temperature and wave exposure, combined with groud-ice content. Threfore, my results show progress in comparison to previous studies, not only in terms of correlation strength. We thereby highlight the importance of the combined effect of coastal erosion drivers in controlling the spatial variability of erosion.

Having explored the temporal and spatial variability of erosion, we are ready to take a step forward towards the conception of a semi-empirical coastal erosion model for the pan-Arctic scale. I take the linear relationship derived from observations as the model's spatial component, which provides us with dynamic spatial variability of erosion. Only ground ice, from observations, is assumed constant. The temporal component in the erosion model is represented by a linear combination of the Arctic-mean thermal and mechanical drivers, to account for the role of TD and TA, respectively, which provides us with the signal from climate change. Absence of coastal sea ice is a pre-condition for erosion. My erosion model is compatible with the scale and processes represented in modern ESMs, it accounts for the main drivers of Arctic coastal erosion, and explains a large fraction of its spatial variability. In the next section, I force my erosion model with the latest twenty-first century climate projections to investigate the future evolution of Arctic coastal erosion.

A semi-empirical model for Arctic coastal erosion

3 Arctic coastal erosion under future climate change

One main concern regarding the erosion of the Arctic coast, is the consequent organic carbon (OC) loss from permafrost. The degradation of OC-rich permafrost eroded material could release greenhouse gases to the ocean and atmosphere, affecting climate and the marine environment. Here, I use my semi-empirical erosion model to investigate the response of Arctic coastal erosion, and the associated permafrost OC loss, to climate change in twenty-first century scenarios.

3.1 *Abrupt thaw and the permafrost-carbon feedbck*

About one quarter of the land surface in the Northern Hemisphere is underlain by permafrost (Huissteden, 2020), which is estimated to store about twice as much carbon as the atmosphere (Tarnocai et al., 2009; Hugelius et al., 2013; Friedlingstein et al., 2020). With ongoing climate change, the degradation of the organic matter exposed due to permafrost thaw releases greenhouse gases at amounts enough to increase surface warming, characterizing the *permafrost-carbon feedback* (Schaefer et al., 2014; Schuur et al., 2015). However, this feedback mechanism is associated with large uncertainties, even in terms of its sign, due to a number of climate-biogeosphere interactions.

The permafrost-carbon feedback is associated with large uncertainties

The permafrost region could represent either a net ecosystem carbon sink or source, which is particularly uncertain with future climate change. Under moderate-warming scenarios permafrost could, counter-intuitively, represent a net carbon sink, due to increasing net primary production (NPP) enhanced by longer and more efficient plant-growing seasons in temperature-limited high latitudes, compensating for permafrost-carbon emissions (Schuur et al., 2009; McGuire et al., 2018). Only under more aggressive warming scenarios would permafrost become a net source. In addition, the sign of the permafrost-carbon net balance does not only depend on temperature, but also on the CO_2 concentration itself, as it also plays a role in NPP through CO_2 fertilization (Kleinen and Brovkin, 2018). Furthermore, soil drying upon warming accelerates bacterial activity and organic matter decomposition, which would in principle increase greenhouse gas emissions, and thus contribute positively to the feedback. However, soil drying suppresses methane emissions in specific, not

CO_2 emissions. Therefore, soil hydrology also adds to the uncertainty related to the sign of the permafrost-region feedback. Despite the uncertainties, the representation of permafrost has improved in the most recent ESM generations in terms of *gradual* thaw, such as active-layer dynamics (e.g. McGuire et al., 2018; Burke et al., 2020). However, *abrupt* permafrost thaw is not yet represented in the current generation of ESMs (Turetsky et al., 2019, 2020).

Abrupt thaw could be key piece of the puzzle

Abrupt permafrost thaw, or sudden permafrost collapse, comprises thermokarst, the erosion of hill slopes inland, riverbanks and coastal cliffs – all of which have not yet been considered in climate projections so far (Turetsky et al., 2019, 2020). Abrupt permafrost thaw contributes positively to the permafrost-carbon feedback, and could completely offset the effect of the increasing uptake by primary production in intermediate-emission scenarios (Turetsky et al., 2020). Future greenhouse gas emissions from permafrost could thus be underestimated by up to 40% (Turetsky et al., 2020). Arctic coastal erosion can account for a large portion of this amount. Abrupt permafrost thaw is listed as one of the "10 top new highlights in climate science", to which priority should be given in future research (Pihl et al., 2021). It has been proposed that novel, holistic and multidisciplinary approaches should be developed to enable the representation of abrupt permafrost thaw in ESM simulations, in order to improve climate projections (Fritz et al., 2017; Turetsky et al., 2019).

There is, therefore, a pressing need for improved projections of Arctic coastal erosion. In addition to its socioeconomic relevance, the associated OC release contributes to the uncertain permafrost-carbon feedback. Moreover, key climatic variables, such as Arctic-mean surface air temperature and sea ice cover, are projected to exceed their natural range of variability within the next decades (Landrum and Holland, 2020). Therefore, Arctic coastal erosion and the associated permafrost OC loss are expected to increase in the future. However, the magnitude, timing and sensitivity of Arctic coastal erosion to global warming are still unknown, which frames our second research question.

Q2: How will Arctic coastal erosion change with climate until the end of this century? And how large would the associated organic carbon loss from permafrost be?

CMIP6-based ensemble projections

With my semi-empirical model in hands, we are able to simulate the evolution of Arctic coastal erosion and its associated organic carbon loss from permafrost. I force our erosion model with a 10-member ensemble of historical and future scenario simulations performed with the Max Planck Institute Earth System Model (MPI-ESM, Mauritsen et al., 2019) for the Coupled Model Intercomparison Project phase 6 (CMIP6, O'Neill et al., 2016). With this ensemble, I also force the Wave Model (WAM, The WAMDI Group, 1988) to generate ocean surface waves. MPI-ESM and WAM simulations provide us with the thermal and mechanical drivers of erosion for our model, respectively. I use ground-ice content from the ACD (Lantuit et al., 2012), which we assume to be constant over time. Sea-ice information is also obtained from MPI-ESM, since open-water is a condition for erosion to take place. I translate our erosion rates into OC projections by combining them with ACD data (i.e. organic-carbon and ground-ice content, and coastal segment dimensions). I present the first twenty-first century projections of coastal erosion at the pan-Arctic scale.

I project[6] the Arctic-mean coastal erosion rate to roughly double from 0.9 m/year during the historical period (1850-1950) to between 2.0±0.7 and 2.6±0.8 m/year by the end of the twenty-first century (2081-2100) under CMIP6 moderate and high-emission scenarios, i.e. shared socioeconomic pathways (SSP) SSP2-4.5 and SSP5-8.5, respectively. I find that, even in the intermediate scenario of climate change, the Arctic-mean erosion is projected to very likely (at least 90% probability) emerge from its historical range by mid twenty-first century, increasing consistently and significantly to values unseen before in the past century. Analogously, I project the pan-Arctic organic carbon loss from permafrost, due to coastal erosion, to also roughly double from about 6.9 TgC/year during the historical period to between 13.1 and 17.2 TgC/year by the end of the century, following the intermediate and high-emission scenarios, respectively. In total for the period 1900-200, I estimate cumulative permafrost OC losses due to Arctic coastal erosion at 1.9 PgC (1.3-2.5 PgC, Fig.6). Long-term cumulative OC-loss estimates do not differ substantially between scenarios because yearly OC fluxes start diverging only after the second half of the 21st Century.

The first 21st-century projections of Arctic coastal erosion

My results help constrain previous estimates of OC losses from abrupt permafrost thaw. Turetsky et al. (2020) estimated cumulative permafrost OC losses from abrupt thaw in the same period at between 8.9 ± 2.3 PgC and 18.1 ± 4.8 PgC following intermediate and high-emissions scenarios, respectively. However, their OC loss projections have limitations that impede a direct comparison with my results. First, their definition of abrupt thaw is broader than only coastal erosion. Turetsky et al. (2020) included inland abrupt-thaw processes, such as hill-slope erosion and thermokarst lake formation and degradation. Moreover, they did not distinguish between inland hill-slope erosion and coastal erosion, assuming a historical pan-Arctic erosion mean rate significantly larger (i.e. 6.5 m/year) than that of coastal erosion alone (i.e. 0.9 m/year, this study). Second, Turetsky et al. (2020) assumed erosion rates to increase linearly over time, following the mean rate of increase from gradual permafrost thaw. Third, they forcefully created diverging scenario projections by changing abrupt-thaw rates in the intermediate-emission scenario, so that a 50% difference in cumulative OC loss was obtained with respect to the aggressive-emission scenario by 2300. Here, I use a semi-empirical model to dynamically simulate changes in both the spatial and temporal variability of Arctic coastal erosion, responding to dynamical changes in its main thermal and mechanical drivers. Therefore, I improve the representation of one specific form of abrupt permafrost thaw, and thereby take a first step to help constrain the uncertainties in the estimates made by Turetsky et al. (2020).

Previous abrupt-thaw projections

Arctic coastal erosion could represent a major fraction of net changes in the permafrost-region carbon by the end of the century. However, large uncertainties in the permafrost-region carbon response to climate change make it difficult to put my results into perspective. For example, McGuire et al. (2018) showed contrasting results from an ensemble of models representing dynamic permafrost and vegetation.

6 See Appendix B: Nielsen, D.M., Pieper, P., Barkhordarian, A., Overduin, P., Ilyina, T., Brovkin, V., Baehr, J. & Dobrynin, M. "Projected increase of Arctic coastal erosion and its sensitivity to warming in the 21st Century" – *under review in Nature Climate Change*. Preprint available at: https://doi.org/10.21203/rs.3.rs-634673/v1

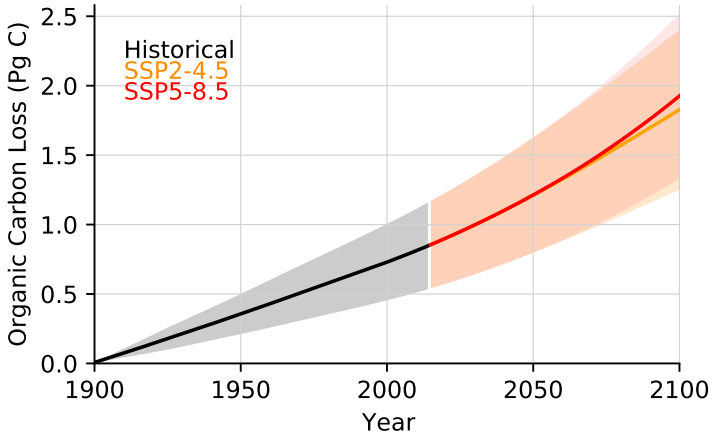

Figure .6: Cumulative permafrost organic carbon (OC) loss due to Arctic coastal erosion. The accumulating period starts in 1900 for consistency with Turetsky et al. (2020).

Coastal erosion is a relevant component of the permafrost-carbon feedback

On the one hand, in an intermediate-emission scenario, the permafrost region could represent either a source or a sink of about 70 PgC by 2300 depending on the model, and most of the changes would occur before 2100. On the other hand, in an aggressive-emission scenario, the permafrost region would represent a net source of between 74 and 652 PgC by 2300 in all models, and the most pronounced changes would occur after 2100 (McGuire et al., 2018). Qualitatively similar results were presented by Kleinen and Brovkin (2018) using MPI-ESM. They simulated net cumulative changes in the permafrost region carbon of between +7 (land uptake) and -11 (loss) PgC by 2100 following an intermediate and a high-emission scenario, respectively. Comparing my estimates with the results of Kleinen and Brovkin (2018), Arctic coastal erosion could thus account for between about 17% and 26% of the net changes by 2100, either contributing to a net loss, or counter-acting a net uptake. Noteworthy, these relatively large fractions are compared to cumulative *net* changes in the permafrost-region carbon balance. The net changes are between one and two orders of magnitude smaller than its components, i.e. soil heterotrophic respiration and primary production, which act to nearly cancel each other. Both soil respiration and primary production respond linearly to global mean surface air temperatures (SAT) in the simulations of Kleinen and Brovkin (2018).

Erosion sensitivity to climate follows the Arctic Amplification

Arctic coastal erosion also responds linearly to global-mean SAT, which characterizes its sensitivity to climate change. The sensitivity of erosion to climate follows the pattern of Arctic Amplification (AA, Serreze et al., 2009) after its onset in the mid 1970s. The AA is quantified as the sensitivity of the Arctic-mean SAT to the global-mean SAT. At the AA onset, erosion sensitivity increases from values non-significantly different from zero to about 0.4-0.5 m $year^{-1}$ $^{o}C^{-1}$ during the second half of this century. In terms of OC loss, the erosion sensitivity is estimated at about 2.3-2.8 TgC $year^{-1}$ $^{o}C^{-1}$ The increase in sensitivity follows the AA because, from the 1970s onward, the correlation between erosion and Arctic-mean SAT increases driven by the increasing trends. Once both the thermal and mechanical drivers of erosion respond to Arctic-mean SAT, AA causes Arctic coastal erosion to accelerate in the future in response to global warming.

My Arctic coastal erosion and OC loss projections are associated with relatively large uncertainties. The largest fraction of uncertainties originates from the empirical estimation of the erosion model coefficients. The fraction of erosion-model uncertainties increases with time in simulations: from about 76% during the historical period to up to 97% by the end of the century. The remaining and smaller fraction of uncertainty stems from the ensemble spread. In addition, the erosion model assumes linear additive contributions from the thermal and mechanical drivers of coastal erosion. Synergistic, or amplifying effects, could however take place. This highligts the need for further work at improving coastal erosion modelling at the pan-Arctic scale.

Our projections of coastal erosion rates should inform policy makers with a focus on socioeconomic planning and the sustainable future of Arctic coastal communities. In addition, our projections of OC loss from permafrost lay out the path for future work to investigate the impact of coastal erosion on the changing Arctic Ocean, specifically on its role as a carbon sink of global relevance. Some of this work is already ongoing, as presented next.

4 AN APPLICATION IN ARCTIC OCEAN BIOGEOCHEMISTRY MODELLING

The permafrost-carbon feedback is often mentioned as a point of concern associated with Arctic coastal erosion (e.g. Vonk et al., 2013; Turetsky et al., 2019), which assumes a consequent increase in atmospheric greenhouse gas concentrations. Although recent work has shown that the erosion of specific coastal landform types does release CO_2 directly to the atmosphere (Tanski et al., 2019; Tanski et al., 2021), there are still large uncertainties regarding the degradation pathway of the organic matter released by erosion in the ocean. In fact, it is not clear how much Arctic coastal erosion actually contributes to an increase in atmospheric greenhouse gas concentrations. There are mechanisms, that could buffer or even counteract the effect of Arctic coastal erosion, which should not be taken for granted. Two examples are: 1) The eroded material can directly sink and be buried in the ocean sediment for millennia, having little or no influence on the atmosphe; and 2) The eroded material can fuel marine primary production, which in turn decreases the oceanic concentration of CO_2, enhancing atmospheric uptake, and thus actually decreasing atmospheric greenhouse gas concentrations. The latter mechanisms draws an even negative feedback from Arctic coastal erosion to global warming. Therefore, large uncertainties regarding the fate of the OC released by coastal erosion in the ocean still remain. In this section, I take the first steps towards closing this gap with an Earth system modelling setup. I investigate the degradation of the permafrost OC released in the ocean by coastal erosion at the pan-Arctic scale using a comprehensive ESM, including the representation of ocean biogeochemistry. I aim at answering the question posed by Wheeling (2019):

The fate of the OC released by coastal erosion is uncertain

4.1 *'Where does the carbon go when the permafrost coast erode?'*

Here, I discuss the mechanisms relevant to determine the fate of the OC released by erosion in the ocean, in parallel to illustrating preliminary modelling results. I use MPI-ESM with a modified version of the Hamburg ocean carbon cycle model

(HAMOCC, Ilyina et al., 2013), in which OC fluxes from Arctic coastal erosion are included. I prescribe a constant pre-industrial OC flux of 6.7 TgC/year from Arctic coastal erosion, estimated in the previous section (Nielsen et al., 2021). Yearly fluxes are distributed on daily resolution to allow for a realistic seasonal cycle, based on positive air temperatures and ocean surface waves (i.e. the thermal and mechanical drivers of erosion). Our simulations are initialized and reproduce the dynamics of a pre-industrial control simulation performed with MPI-ESM for the CMIP6 exercise, and conducted for 350 years. We examine the the last 50 years of simulations, when a new steady state in the upper Arctic Ocean is achieved. In order to encompass the uncertainties surrounding the degradation pathway of the OC released by erosion, six simulations are performed. The simulations differ in terms of two important organic matter characteristics, namely C/N ratios and POC-DOC fractions. By making combinations of different C/N and POC-DOC scenarios, we investigate the role of primary production, and the residence time of organic matter in the water column, which ultimately control the fate of the OC released by coastal erosion.

Description of the modelling strategy

The residence time of the eroded material in the water column is important to determine the time scale of remineralization. When the eroded material sinks and is buried in the ocean-bottom sediment, remineralization occurs at long (i.e. millennial) time scales (Vonk et al., 2012; Bröder et al., 2018). The fraction of the eroded material that settles in the sediment in uncertain. It has been estimated that between 13% and 65% of the OC released by erosion is buried in the sediment (Hilton et al., 2015; Couture et al., 2018; Grotheer et al., 2020). The sinking velocity of the eroded material is proportional to its size, conventionally referred to as being either *particulate* or *dissolved*. While particulate OC (POC)[7] sinks relatively fast into the sediment (3.5–5.0 m/day in a simplified HAMOCC configuration, in accordance to Martin et al., 1987; Kriest and Oschlies, 2008), dissolved OC (DOC) stays longer in suspension in the water column (represented as a passive tracer in HAMOCC), allowing for more effective remineralization. After settling in the sediment, the exchange of material between water column and sediment still takes place due to resuspension.

POC sinks into the sediment, where remineralization is slow

In the Arctic Ocean, resuspension is primarily driven by ocean surface waves and storms, by increasing bottom shear stress (Lavelle et al., 1984; Wegner et al., 2013; Klein et al., 2019). Resuspension prolongs the time of residence of the terrigenous OC in the water column (Jong et al., 2020). The transport of sediment by resuspension, as it is forced by surface conditions, decreases with increasing depth, and is thus limited to the nearshore resuspension zone. The extent of the nearshore resuspension zone is expected to be relatively large on the Siberian shelf, as it covers kilometers at depths of less than 20 meters (Fig.2). Therefore, resuspension plays an important role in increasing remineralization of OC from Arctic coastal erosion. However, the effect of ocean surface waves and storms on producing resuspension is not represented in MPI-ESM, which causes the residence time of the eroded material in the water column to be reduced. Although the OC flux from coastal erosion into the Arctic Ocean is mostly in the particulate form (Sánchez-García et al., 2011; Tanski et al., 2016), we include part of the OC as DOC to allow for longer residence times. A POC-DOC fractioning of the OC released by erosion is meant to compensate for the

Resuspension and the POC-DOC fraction scenarios

7 For the sake of simplicity, here we use *organic carbon* to refer to *organic matter*, although the latter would also include other elements than carbon, such as oxygen, nitrogen, and phosphorus.

effect of a quasi-permanent sedimental burial, and thus allowing for more time for remineralization. The OC input is then given as either 90% POC and 10% DOC, or 10% POC and 10% POC. These two extreme POC-DOC fraction scenarios encompass a wide range of possibilities, and thus also allows us to examine the sensitivity of the simulated changes to differing residence times and remineralization rates.

Another governing factor to determine the fate of the organic matter released by erosion is its nutrient content, as it controls the pace of primary production. Coastal erosion is estimated to fuel about one-fifth of the Arctic marine primary production (assuming a direct OC release into the ocean, Terhaar et al., 2021). In turn, primary production consumes DIC and thus increases the Ocean's capacity to take up atmospheric CO_2. However, primary production in the Arctic Ocean is limited by the availability of nutrients, in specific nitrate (Vancoppenolle et al., 2013). The remineralization of OC releases CO_2 and inorganic nutrient compounds, such as nitrate and phosphate. Thus, the larger the nutrient load in the OM released by erosion, the more it allows for primary production, as it is remineralized.

Primary production is limited by nutrient availability

The carbon-nutrient (or carbon-nitrogen) ratio (C/N) of marine organic matter ranges typically about 7 or 8 (precisely 6.625 in HAMOCC, Redfield, 1934; Takahashi et al., 1985). Permafrost C/N values are substantially larger than those in organic matter from the ocean. For example, Couture et al. (2018) reported C/N values of 15.1±3.7 (mean ± standard deviation) from 50 samples taken within 282 km along the Yukon coast, Canada (Fig.2), with minimum and maximum values ranging between 11.3 and 25.9. Fuchs et al. (2020) and Wetterich et al. (2020) reported C/N values of 12.7±3.5 from the Lena River delta region in Siberia. Here, I use three values of C/N to represent the organic matter from coastal erosion: 10, 14 and 18, comprehending the range reported in the literature (Schirrmeister et al., 2011; Couture et al., 2018; Fuchs et al., 2018; Jongejans et al., 2018; Fuchs et al., 2019, 2020; Wetterich et al., 2020; Bristol et al., 2021; Tanski et al., 2021). Once the fixed C/N value of the marine organic matter in HAMOCC is lower than that of permafrost, the excess carbon is given to the model as dissolved inorganic carbon (DIC), which assumes a fraction of instantaneous remineralization. This assumption is backed-up by recent field experiments, that show that OC from erosion is 'rapidly' lost to CO_2 upon thaw (Tanski et al., 2019; Tanski et al., 2021). As of yet, I examine the effect of OC release from coastal erosion on air-sea CO_2 fluxes in the Arctic Ocean.

Coastal permafrost C/N ratio scenarios

The Arctic Ocean acts as an important sink of atmospheric CO_2. It is estimated to account for up to $\sim$ 14% of the world's Ocean CO_2 uptake, although it covers less than 4% of the world's Ocean area, and remains partially covered by sea ice year-round (Bates and Mathis, 2009). The CO_2 uptake in the Arctic Ocean is among the largest in the globe per unit area (Laruelle et al., 2014). The Arctic Ocean is such an efficient CO_2 sink for two main reasons. First, the solubility of gases is higher at low water temperatures (Henry and Banks, 1803). Second, primary production during the summer months consumes DIC and thus increases the air-sea CO_2-concentration gradient (Bates and Mathis, 2009). Observations-based assessments have estimated the Arctic Ocean's (north of 66^{o}N) CO_2 uptake at 66 – 199 TgC/year (Bates and Mathis, 2009) and 50 – 310 TgC/year (Yasunaka et al., 2018), although large uncertainty ranges remain. Dedicated modelling studies have estimated the Arctic Ocean's CO_2 uptake at 59 TgC/year (Manizza et al., 2011), and more recently at 139–167 TgC/year (Manizza et al., 2019) for the present-day climate, which lie well

The Arctic Ocean is an important CO_2 sink

within the observational range. Manizza et al. (2019) reported a decrease in the Arctic Ocean's sink capacity in recent decades, despite the also decreasing sea-ice cover. The sign of future trends is uncertain, as competing mechanisms come into play (Vancoppenolle et al., 2013; Manizza et al., 2019; Woosley and Millero, 2020). Here, we focus on the Arctic Ocean's CO_2 sink capacity during pre-industrial conditions.

4.2 *Coastal erosion decreases the Arctic Ocean's CO_2 sink capacity*

Preliminary modelling results

The Arctic Ocean takes up about 67 (64–71) TgC/year of atmospheric CO_2 in our simulations when the OC flux from Arctic coastal erosion is included (Fig.7a). Between parentheses is the maximum range in our 6-member ensemble. Our simulated mean value is about 10 TgC/year lower than the reference, where coastal erosion fluxes are not included (Fig.7b). Therefore, Arctic coastal erosion yields a 13% (8–17%) reduction of the annual-mean Arctic Ocean CO_2 uptake in our simulations (Fig.7c). The proportional difference is larger if one excludes the regions of direct Atlantic influence from this analysis (i.e. the Baffin Bay, the Greenland, Norwegian and Barents Seas), where the uptake is substantially larger mainly due to perennially low sea-ice cover, and the erosion input is relatively small. Considering this smaller inner-Arctic domain, the Ocean uptake of CO_2 decreases by about 31% (18–41%) from 34 TgC/year in the reference run to 23 (20–28) TgC/year when the OC flux from coastal erosion is included. The decrease in the Arctic Ocean's CO_2 uptake is robust in all of our six simulations.

The amplifying effect of ocean alkalinity

The magnitude of the simulated decrease in Arctic Ocean's CO_2 sink capacity ($\sim$ 10 TgC/year) is about 1.5 times larger than the OC flux from coastal erosion itself ($\sim$ 7 TgC/year). The reason for this result is twofold. First, the remineralization of organic matter released by erosion increases surface DIC, which acts to decrease the CO_2 imbalance between ocean and atmosphere. Second, OC remineralization also decreases alkalinity, which in turn decreases the ocean capacity to retain CO_2. Although primary production does increase in all of our scenarios, which acts to decrease DIC and increase alkalinity, the effect of DIC increase through remineralization of the high-C/N organic matter, and the associated alkalinity decrease, takes over. During the entire simulation period, and in all scenarios, DIC is consistently larger, and alkalinity is consistently lower, when coastal erosion is represented, in comparison to the reference. In summary, our results suggest that Arctic coastal erosion acts to drive ocean CO_2 outgassing, regardless of C/N ratios, effectiveness sediment burial and remineralization rates – the latter two indirectly assessed through the different POC-DOC fractions. The simulated changes are, however, not spatially uniform.

Siberian shelf: from net sink to net source of CO_2

The largest changes are simulated over the eastern Arctic shelf, in the Laptev and East Siberian Seas, where OC fluxes from coastal erosion are relatively large (Fig.7c,d). Coastal erosion turns a large portion of this region from a net sink into a net source of CO_2 (Fig.7a,b). This switch in flux sign is robust across all of our six simulations. According to previous modelling studies, riverine fluxes of organic and inorganic carbon and nutrients could turn the Beaufort and Laptev Sea regions from net sinks into net sources of CO_2 as well, both in present-climate (Terhaar et al., 2019) and in pre-industrial (Lacroix et al., 2020) conditions. The latter was also based on MPI-ESM simulations, modified to include riverine carbon and nutrient fluxes. These results are in accordance with observations, where a heterotrophic (i.e. net

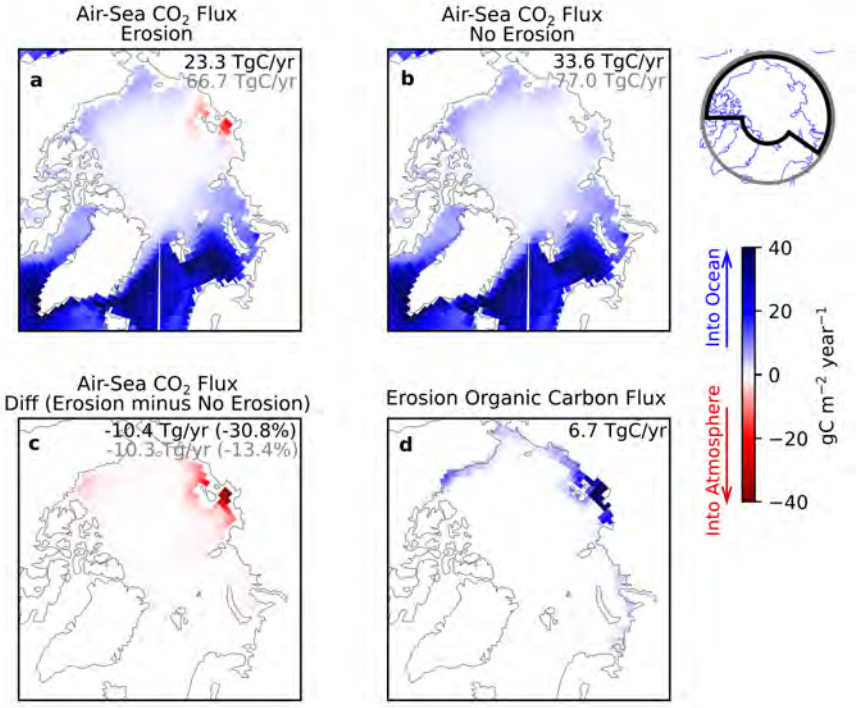

Figure .7: Air-sea CO_2 fluxes, expressed in mass of carbon, in the simulations including Arctic coastal erosion (ensemble mean) **(a)**, in the CMIP6 reference **(b)**, and the difference between the two **(c)**. Long-term annual means are calculated from the last 50 years of simulations. The version of MPI-ESM was used so that simulations are identical to the CMIP6 reference, except for the Arctic coastal erosion input. Since we are using the one-way coupling configuration (i.e. HAMOCC does not influence atmosphere neither ocean), the ocean dynamics in our simulations is still identical to the reference. The pre-industrial OC flux from coastal erosion is displayed in **(d)**. Pan-Arctic totals are displayed on the upper-right corners of each panel for the entire Arctic circle (grey), and excluding regions of Atlantic influence (black), where coastal erosion is negligible. The two integrating domains are illustrated in the map on the upper-right panel. Positive values (blue) represent downward fluxes, from the atmosphere into the ocean.

sink) state of the East Siberian and Laptev Seas has also been verified (Anderson et al., 2009). Recent expeditions suggested autotrophic (i.e. net source) conditions for the East Siberian Sea (Humborg et al., 2017). However, the latter was conducted within summer months, where indeed a CO_2 uptake is expected. The year-round net metabolic state of the Siberian shelf is determined by a fine balance between a number of mechanisms.

Mechanisms of air-sea CO_2 exchange in the Laptev Sea

In an elucidating sensitivity study, Wåhlström et al. (2013) showed that the Laptev Sea outgasses in spring and autumn, while takes up CO_2 during summer. On the one hand, during spring, riverine DIC and DOC loads causes a CO_2 accumulation before sea-ice melts to allow for the air-sea exchange. During autumn, increasing storms and decreasing riverine discharge cause the ocean stratification to virtually disappear in shallow regions, and the surface becomes supersaturated in CO_2 with respect to the atmosphere. On the other hand, during summer, low-sea ice area and high solar incidence and water temperatures steeply enhance primary production,

which consumes CO_2 making the surface ocean undersaturated with respect to the atmosphere. In addition, the residence time of OC in the Siberian shelf is relatively long, estimated at 1-2 years (Sharples et al., 2017), which allows for more time for remineralization, and thus increasing the overall impact of erosion fluxes. Under present-climate conditions, the sign of the year-round net flux in the Laptev Sea would be, therefore, determined by the combination of the duration of the open water season, riverine loads of carbon and nutrients, wind speeds and storms driving vertical mixing, primary production and its controlling factors, such as light availability and water temperature (Wåhlström et al., 2013). Among these factors, Arctic coastal erosion acts to drive a net CO_2 flux ocean to atmosphere.

Our preliminary results suggest that Arctic coastal erosion indeed contributes to increase atmospheric CO_2 concentrations, due to a decrease in the Arctic Ocean's CO_2 sink capacity. The magnitude of the decrease in the ocean CO_2 sink capacity is about 1.5 times larger than the permafrost OC loss due to coastal erosion itself. This amplification stems from the effect of decreasing ocean alkalinity, which results from the OC remineralization, in addition to the effect of increasing DIC. These results, of still ongoing work, reflect only pre-industrial conditions as of yet. Historical and future-scenario simulations should be conducted to investigate the sensitivity of these results to changes due to climate change. For example, decreasing sea-ice cover and increasing surface temperatures could increase primary production, acting to increase the ocean sink capacity. In addition, this modelling analysis assumes that all the permafrost OC loss due to erosion is released into the Arctic Ocean directly. However, Tanski et al. (2021) recently showed that a large fraction of the eroded OC is degraded still onshore, if the transport towards the sea is slow, such as in retrogressive thaw slumps and in TD-dominated high-cliff coastlines. A direct OC release to the sea would take place at block-failure and low-cliff TA-dominated coasts (Tanski et al., 2021). Thus, if the OC from erosion is released directly into the atmosphere as CO_2, the amplifying effect resulting from decreasing ocean alkalinity could be smaller.

Limitations and future work

Here I have taken the first steps towards tracing the fate of the OC released by Arctic coastal erosion using a comprehensive ESM. Our preliminary results indicate a robust decrease in the Arctic Ocean's CO_2 sink capacity during pre-industrial conditions, obtained in all simulations conducted with a wide range of C/N and POC-DOC scenarios. Thereby, these results shed light on the yet still uncertain sign of the Arctic coastal erosion effect on air-sea CO_2 exchange.

5 SUMMARY AND CONCLUSIONS

In this section, we objectively go through the research questions I posed in this thesis, directly followed by the answers I provided to them. In the final section, we discuss whether the gaps posed initially were actually closed in the course of this thesis, within a broader context, and look out to suggest future work that could be done to fill the remaining gaps.

We set out to better understand, model, and make projections of Arctic coastal erosion under the the context of the ongoing anthropogenic climate change. I took an Earth system modelling perspective to be able to reach this goal. The need for this perspective made us spend a good effort at closing the scale gap between erosion, identified at scales on the order of meters, and ESMs, which have spatial resolution on the order of tens or hundreds of kilometers. Although our primary goal was clearly stated, closing the scale gap was our underlying quest. This sets the two research questions I posed in this thesis:

Q1: How can we link large-scale mechanisms, represented in Earth system models, with the spatial and temporal variability of Arctic coastal erosion?

In Section 2, I provided answers to this question in two complementary steps. First, I looked at the temporal variability of coastal erosion locally, using point-observations from the Laptev Sea (Grigoriev, 2019). Then, I examined the spatial variability of erosion at the pan-Arctic scale, using long-term erosion rates estimates from the ACD (Lantuit et al., 2012). In terms of the temporal variability of erosion, I verified that:

- The two first main modes of coastal erosion variability, identified in yearly in-situ observations from the southern Laptev Sea coast, at Bykovsky Peninsula and Muostakh Island, are linked with mechanisms represented in ESMs, at scales larger than those typically considered for erosion.
- The first main mode of coastal erosion variability is linked with low-frequency (period $\sim$20 years) winter sea-ice cover anomalies averaged over the Laptev Sea. The predominant low-frequency variability in sea-ice over the Laptev Sea preconditions early onsets, and hence prolongs the following open-water season. The longer the open-water season, the more coastal erosion, to a first-order approximation.
- The second main mode of coastal erosion variability is linked with higher-frequency variability (period $\sim$4 years) in the Arctic Oscillation (AO) during winter and summer. On the one hand, positive winter AO conditions drive a large-scale circulation pattern associated with negative sea-ice anomalies in the Laptev Sea, dragged by surface winds, thus also anticipating the onset of the open-water season. On the other hand, negative summer AO conditions drive a large-scale circulation pattern associated with surface warming and sea-ice loss. Therefore, the winter AO contributes to coastal erosion in the Laptev Sea by prolonging the open-water season, while the summer AO contributes to TD by increasing permafrost thaw, and to TA by decreasing the wave-attenuation effect of sea ice, and increasing the fetch for ocean surface waves.
- The local temporal variability of coastal erosion rates, measured at the Laptev Sea, does not only respond to local environmental conditions and geomorphological properties, but also to mechanisms represented at scales compatible with and represented in ESMs, such as the AO and Laptev-Sea wide low-frequency winter sea-ice variability.

Considering the Earth system modelling perspective, not only do we need the local temporal variability of erosion to be compatible with the scale and mechanisms represented in ESMs. We also need to represent the spatial variability of erosion at the pan-Arctic scale. In this respect, I verified that:

- About half of the spatial variability in long-term coastal erosion mean rates is explained by ground-ice content, combined with the mechanical and thermal drivers of erosion, i.e. ocean-surface wave and thawing temperature exposure. This result stands as the first successful empirically-derived description of the spatial variability of coastal erosion , as a function of its main drivers, at the pan-Arctic scale.

The answers to the first question allowed us to present a semi-empirical coastal erosion model at the pan-Arctic scale, compatible with the scales and mechanisms represented in ESMs. With this model in hands, I was able to asses the evolution of Arctic coastal erosion under future climate change scenarios, and thus address the second question of this thesis.

Q2: How will Arctic coastal erosion change with climate until the end of this century? And how large would the associated organic carbon loss from permafrost be?

I answered this question in Section 3 by forcing our coastal erosion model with a 10-member ensemble of future climate and surface ocean wave simulations performed with the MPI-ESM for the CMIP6 exercise and the wave model WAM, respectively. I analyzed the historical period (starting in 1850 until present) and twenty-first century projections (until 2100) following the shared socioeconomic pathways SSP2-4.5 and SSP5-8.5, which correspond to future moderate and high-emission scenarios, respectively.

- The Arctic-mean coastal erosion rate is projected to increase from about 0.9 ± 0.4 m/year during the historical period to between 2.0 ± 0.7 m/year and 2.6 ± 0.8 m/year by the end of the twenty-first Century under moderate and high-emission scenarios, respectively. The associated organic carbon (OC) loss from permafrost is projected to increase from about 6.9 ± 5.4 TgC/year in the historical period to between 13.1 ± 6.7 TgC/year and 17.2 ± 8.2 TgC/year by the end of the century in the future scenarios. These projections translate to an increase in the permafrost OC loss due to Arctic coastal erosion by a factor of between 1.9 and 2.5 by the end of this century in comparison to the historical period.

- The 1900-2100 cumulative permafrost-OC loss due to Arctic coastal erosion is estimated at between 1.3 and 2.5 PgC. These estimates are comparable with projected cumulative net changes in the permafrost-region carbon pool, although the latter are still very uncertain and model-dependent.

- The Arctic coastal erosion mean rate is projected to exceed its historical range of variability before the end of the century in both scenarios. Considering the uncertainties in projections, which stem from ensemble spread and the

estimation of the erosion-model empirical coefficients, the Arctic-mean coastal erosion rate is projected to likely exceed (at least 66% probability) its historical range of variability by 2023, and very likely (at least 90% probability) by 2049.

- Simulated changes in Arctic coastal erosion linearly follow changes in global-mean surface air temperature (SAT). For one degree in global SAT increase, the Arctic-mean coastal erosion rate increases by about 0.4-0.5 m/year, or about 2.3-2.8 TgC/year in terms of permafrost OC loss.

- The sensitivity of Arctic coastal erosion to climate significantly increases between the historical period and the twenty-first Century. The increase in erosion sensitivity follows the evolution of the Arctic Amplification (AA) after its onset in the 1970s and afterwards. The correspondence between erosion sensitivity and the AA results from the increasing correlation between global- and Arctic-mean SAT, and the linear response of the coastal erosion drivers to the Arctic-mean SAT.

Our permafrost OC loss estimates allowed us to take one step further towards the quantification of effective contribution of Arctic coastal erosion to changes in atmospheric greenhouse gas concentrations, and thus to the permafrost-carbon feedback. I quoted the question posed by Wheeling (2019): "Where does the carbon go when the permafrost coast erode?". I am careful not to frame it here as one of the core research questions of this thesis, as we are still not able to fully answer it. Nevertheless, in Section 4, I conducted dedicated ESM simulations to investigate the fate of the OC released by Arctic coastal erosion during pre-industrial climate conditions, and described initial results:

- Arctic coastal erosion decreases the Arctic Ocean's CO_2 sink capacity. In pre-industrial climate conditions, the Arctic Ocean annual CO_2 uptake decreased by about 13% in response to coastal erosion OC input. Considering the inner-Arctic domain, which excludes the regions of Atlantic influence (e.g. Barents Sea), the Ocean CO_2 uptake is decreased by 31%.

- The simulated magnitude of the Arctic Ocean's loss in CO_2 uptake due to coastal erosion is about 50% larger than the OC input from coastal erosion itself, in terms of mass of the OC released. The remineralization of OC from erosion produces DIC, decreasing the ocean CO_2 sink capacity up to the same amount as the carbon input. In addition, OC remineralization decreases ocean alkalinity, which decreases the ocean capacity to retain CO_2, resulting in this apparent amplifying effect.

- The largest simulated changes in air-sea CO_2 fluxes take place in the Laptev and East Siberian shelves, which partially shift from net carbon sinks to net carbon sources of CO_2. The spatial distribution of CO_2 fluxes is comparable to osbervations and previous modelling work representing riverine loads of carbon and nutrients on the Arctic shelves.

- These results are robust across a wide range of sensitivity scenarios of organic matter composition, in terms of nutrients loads and particulate/dissolved fractions. In summary, the simulations suggest that Arctic coastal erosion

indeed acts to increase atmospheric CO_2 concentrations, thus contributing positively to the permafrost-carbon feedback. Moreover, the contribution from coastal erosion would be larger than the OC loss from permafrost itself, due to the amplification effect from decreasing ocean alkalinity, resulting from the organic matter remineralization.

5.2 *Have we closed the gap?*

> "Why spend much effort and resources resolving that which cannot be predicted, if one can predict the statistics of that which cannot be resolved?"
>
> – Emanuel (2020)

The first research gap described in this thesis stands between the fine scale of Arctic coastal erosion and the resolution and mechanisms represented in ESMs. To quote Turetsky et al. (2019): "Detailed process models of these dynamics could be impractical to run directly within Earth-system models. Frameworks must be developed to understand and quantify the effect of these fine-scale processes at the global level." The development of such a framework is at the core of this thesis. Emanuel (2020) warned that, with the increasing capacity of supercomputers, climate research often falls into the trap of "computing too much" and overlooking process understanding. One could see room for this concern here too. Although this thesis did evolve around a task on modelling and computing, on the way to tackle it, we also learned about the mechanisms underlying Arctic coastal erosion from an unusual perspective.

Methods vs. process understanding

The individual links in the chain of mechanisms connecting coastal erosion and ESMs were already known before my work on this thesis. For example: sea-ice motion is driven by large-scale atmospheric variability (Colony and Thorndike, 1984), such as that represented by the Arctic Oscillation (AO, Thompson and Wallace, 1998), which favors sea-ice export from the Laptev Sea during winter (Rigor et al., 2002). Winter sea-ice export antecipates the onset of the open-water season (OWS, Krumpen et al., 2013; Itkin and Krumpen, 2017), whose duration, in turn, is a first-order proxy for coastal erosion interannual variability (Overeem et al., 2011). Such apparently linear chains of mechanisms are in fact immerse in a genealogical network of scientific advance. Therefore, 'closing the gap' or 'developing a framework' are not necessarily mere technical or intermediate methodological steps. They often consist, to a large extent, of investigative work that brings pre-existing and disconnected knowledge together, allowing for process understanding and, consequently, the eventual layout of new research ideas.

Room for improved predictions

One example emerges from the link between the OWS duration and the AO in the Laptev Sea, which could be explored to improve coastal erosion predictions. Schirojan (2021) found mild, however significant, prediction skill of OWS duration in the Laptev Sea up to four years in advance, using a decadal prediction system based on the MPI-ESM (Brune and Baehr, 2020). One could take advantage of the lagged link between the winter AO and the early onset of the melt season during

spring/summer to make improved OWS predictions, based on a selection of ensemble members with a subsampling method (Dobrynin et al., 2018). Improvements in OWS predictions in the Laptev Sea would be relevant not only for coastal erosion, but could also contribute to the planning of fishing activities and shipping routes, for example.

The other major gap composing this thesis concerns the future evolution of Arctic coastal erosion. Looking back at the historical development of Arctic coastal erosion models, since the work of Kobayashi (1985), this is the first time an ESM was used for such projections. The use of an ESM enabled us to embed coastal erosion in centennial-scale standardized future climate change scenarios, making my results comparable with previous work on the future of the permafrost-region carbon (e.g. Kleinen and Brovkin, 2018; McGuire et al., 2018). This was allowed by the successful development of the semi-empirical modelling approach, with which the physical drivers of erosion are combined to represent the statistics of coastal erosion at the pan-Arctic scale in a computationally cheap way. Here, I used a 10-member ensemble of ESM simulations to force a surface-ocean wave model. Both climate and wave simulations were used to force the erosion model. This is a natural first step towards the implementation of a parameterization scheme, in which erosion rates and OC fluxes are calculated online in a fully coupled ESM equipped with the representation of waves.

Towards an online parameterization

The empirical approach taken here relied heavily on the availability of coastal erosion rate observations. The in-situ measurements diligently made for decades at Muostakh Island and Bykosvky Peninsula by Grigoriev (2019), as well as the compilation and standardization of data at the pan-Arctic scale in the ACD (Lantuit et al., 2012), were fundamental to the development of this work. However, we are still limited to draw empirical conclusions on the temporal variability of coastal erosion at the pan-Arctic scale, for which I made informed assumptions and scenario/sensitivity tests. Consequently, the erosion projections presented in this thesis are followed by relatively large uncertainties. Most of them resulting from the empirical estimation of the erosion-model coefficients. By using an empirical approach, only with more observations would these uncertainties decrease in magnitude. The use of Synthetic Aperture Radar (SAR) data is a promising alternative to enable more frequent and spatially wide monitoring of coastal retreat rates in the Arctic (Bartsch et al., 2020).

On the importance of observations

Arctic oastal erosion is a relevant and, conversely, relatively certain component of the future Arctic carbon cycle, in comparison to other of its components. While the sign of the net change in the permafrost-region carbon depends on the climate scenario we follow, ranging between -11 PgC (net loss) and +7 PgC (net gain) by 2100 (Kleinen and Brovkin, 2018), Arctic coastal erosion contributes to a net carbon loss, estimated at about -2 PgC by 2100 (Nielsen et al., 2021), increasing linearly with global warming (at a rate of 2.3-2.8 TgC year^{-1} ^{o}C^{-1}, Nielsen et al., 2021). Moreover, assuming a direct flux into the ocean, initial modelling results suggested that the consequent increase in atmospheric CO_2 concentrations could be amplified by up to 50% due to changes in alkalinity with respect to this amount, under pre-industrial conditions. Further work will be carried to investigate the response of the Arctic Ocean biogeochemistry, in specific, to my OC flux projections.

The relevance of coastal erosion to the Arctic carbon cycle

In summary, this thesis examined Arctic coastal erosion in the Earth system under climate change. This thesis 1) contributed to the understanding of the large-scale mechanisms underlying Arctic coastal erosion, 2) presented projections of its evolution in twenty-first century scenarios, and 3) discussed its possible impacts on the Arctic carbon cycle, from an Earth system modelling point of view.

APPENDICES

COASTAL EROSION VARIABILITY AT THE SOUTHERN LAPTEV SEA LINKED TO WINTER SEA ICE AND THE ARCTIC OSCILLATION

The work in this appendix has been published as:

Nielsen, D. M., M. Dobrynin, J. Baehr, S. Razumov & M. Grigoriev (2020). "Coastal erosion variability at the southern Laptev Sea linked to winter sea ice and the Arctic Oscillation". *Geophysical Research Letters*, 47, e2019GL086876, https://doi.org/10.1029/2019GL086876

Coastal erosion variability at the southern Laptev Sea linked to winter sea ice and the Arctic Oscillation

David Marcolino Nielsen[1,2], Mikhail Dobrynin[1,3], Johanna Baehr[1], Sergey Razumov[4] and Mikhail Grigoriev[4]

[1]Institute of Oceanography, Center for Earth System Research and Sustainability (CEN), Universität Hamburg, Hamburg, Germany

[2]International Max Planck Research School on Earth System Modelling, Max Planck Institute for Meteorology, Hamburg, Germany

[3]Deutscher Wetterdienst (DWD), Hamburg, Germany

[4]Melnikov Permafrost Institute, Siberian Branch of the Russian Academy of Science, Yakutsk, Russia

Received: 28 December 2019 / Accepted: 14 February 2020 / Published online: 18 February 2019

ABSTRACT

Arctic coastal erosion experiences pronounced effects from ongoing climate change. The Laptev Sea figures among the Arctic regions with the most severe erosion rates. Here, we use unprecedentedly long records of almost 30 years of annual in-situ coastal erosion rate measurements from Bykovsky Peninsula and Muostakh Island to separate the main modes of variability, which we attribute to large-scale drivers. The first (lower-frequency) and second (higher-frequency) modes are associated with winter sea-ice cover in the Laptev Sea and with the Arctic Oscillation, respectively, which together account for $85.1 \pm 24.1\%$ of the total observed variance. Arctic coastal erosion has so far been neglected in Earth system models (ESMs). The proposed mechanisms set favorable conditions for coastal erosion at large scales (synoptic to planetary scales), compatible with those represented in modern ESMs.

A.1 INTRODUCTION

The Arctic has been experiencing pronounced effects of climate change: increasing surface (Serreze et al., 2009) and permafrost temperatures (Biskaborn et al., 2019) and decreasing sea-ice extent (Notz and Stroeve, 2016). Consequently, the Arctic coasts are now being longer than previously exposed to the action of warm air and ocean waves, leading to thermal and mechanical erosional processes. At the Laptev Sea, eastern Siberian Arctic, the historical mean coastal erosion rate is estimated at 0.7 m $year^{-1}$, somewhat larger than the pan-Arctic mean of 0.5 m $year^{-1}$ (Lantuit et al., 2012), with specific locations showing annual retreats of >20 m (Günther et al., 2015), and figuring among the most rapidly eroding sites in the Arctic. Irrgang et al. (2018) presented similar mean rates of 0.7 m $year^{-1}$ with significant time variability for the Yukon coast, Canada.

The erosion of permafrost coasts release substantial amounts of organic carbon (OC) to the marginal Arctic seas, estimated at 14±4 Tg $year^{-1}$, comparable to the pan-Arctic OC flux from riverine discharge of 40±4 Tg $year^{-1}$ (Wegner et al., 2015). Vonk et al. (2012) estimated the OC flux from the East Siberian Arctic Shelf (comprehending part of the Laptev and East Siberian Seas) at 44±10 Tg $year^{-1}$, from which 11±4 Tg $year^{-1}$ would be resulting from coastal erosion. Günther et al. (2013) estimated a significantly smaller carbon flux of 0.66±0.05 Tg $year^{-1}$ from the Laptev Sea coast, using a combination of remote sensing data and in-situ measurements. Moreover, the organic matter from thawed permafrost was found to be highly biologically reactive (Vonk et al., 2014). Couture et al. (2018) estimated that only 13% of the eroded OC is sequestered in the near-shore sediment at the Beaufort Sea. In a incubation experiment, Tanski et al. (2019) recently showed that the direct release of atmospheric CO_2 from coastal erosion has been underestimated. Given the projected rapid decrease in Arctic sea-ice extent (Barnhart et al., 2016), intensification of surface wind and waves (Dobrynin et al., 2012; Dobrynin et al., 2015) and permafrost thaw (Schuur et al., 2009; Schaefer et al., 2014), the degradation of ice-rich thermo-abrasive Arctic coasts will likely increase in the future, leading to the recycling of larger amounts of permafrost carbon into CO_2 and, thus, increasing the atmospheric carbon-climate feedback. However, comprehensive modelling studies considering the role of coastal erosion on climate are still needed (Fritz et al., 2017).

Arctic coastal erosion is primarily limited by the presence of sea ice. Overeem et al. (2011) suggested that the duration of the open-water season (OWS), i.e. the time of year when the coast is sea-ice free, is a good first-order estimator for coastal erosion, given that both quantities have increased at similar rates between 1979-2002 and 2002-2007 (1.5 and 1.6-fold, respectively). Barnhart et al. (2014a) presented a circum-Arctic analysis of OWS duration, and concluded it has larger relevance in explaining coastal vulnerability, in comparison with setup and wave heights. Both studies used sea-ice concentration (SIC) data from nearshore grid cells to derive OWS duration, and disposed of long-term means of coastal erosion rates. The variability of Arctic coastal erosion also responds to environmental conditions within the OWS, such as positive air surface temperatures (Günther et al., 2015) and the frequency and intensity of storms (Jones et al., 2009). Cunliffe et al. (2019) recently showed that single storm events may be relevant for total annual shoreline changes.

The Arctic Oscillation (AO) is the dominant mode of sea-level pressure variability in the Northern Hemisphere (Thompson and Wallace, 1998) and plays an important role on weather, including the frequency and intensity of storms (Thompson and Wallace, 2001) and Arctic SIC anomalies (Wang and Ikeda, 2000). During winter, its positive phase (AO+) favours positive surface air temperature (SAT) anomalies over the Eurasian continent (Thompson and Wallace, 2000). At the Laptev Sea, the winter AO+ is associated with surface winds blowing from southeast, its continental margin, transporting sea ice away from the coast and into the central Arctic Ocean, thus contributing to the opening of polynyas and formation of new thin ice, increased heat fluxes from ocean to atmosphere and local surface warming (Rigor et al., 2002). Krumpen et al. (2013) and Itkin and Krumpen (2017) showed that late-winter sea-ice export from the Laptev Sea, thus the formation of thin ice, is correlated with negative SIC anomalies in the forthcoming summer and may as well contribute to earlier onsets of the melt season.

Previous studies have focused on process-based approaches to address the issue of Arctic coastal erosion by, for example, modelling block-failure events [e.g. Hoque and Pollard (2009), Ravens et al. (2012), and Barnhart et al. (2014b)]. Although physically meaningful, the high spatial resolution needed in that setup (order of meters) is not compatible with the scale of the still relatively coarse-resolution state-of-the-art Earth system models (ESMs, order of hundreds of kilometers). Here, we aim at exploring the predominant large-scale drivers of coastal erosion observed at the southern Laptev Sea, by encompassing information from large areas (synoptic to planetary scales), thus responding more directly to dynamic and thermodynamic mechanisms of the climate system, which are inherently better represented in modern ESMs than small scale ones.

A.2 DATA AND METHODS

The search for statistically robust relationships between external drivers and coastal erosion variability is often hampered by the lack of long and well-resolved observations (Lantuit et al., 2011). Although in the last decade, the availability of high resolution satellite imagery has advanced the use of remotely-sensed shoreline-change mapping (Jones et al., 2018). Here, we analyze unprecedentedly long in-situ observations of coastal erosion rates from Bykovsky Peninsula and Muostakh Island at its North Cape (hereafter, Muostakh-N) and at its Northeast coast (Muostakh-NE), southern Laptev Sea (Fig. A.1-a,b). Measurements have been yearly made by the end of August since 1982 until present (Grigoriev, 2019). Some gaps in observations occur between 1983 and 1996 in different years for each site. Since 1982, a total of 28 years of data are available for Bykovsky and Muostakh-NE, and 29 years for Muostakh-N. Since the observations are spatially limited, generalizations to the scale of the Laptev Sea must be made with caution (see Section 4 for a detailed discussion). For more detailed descriptions of the key monitoring sites, we refer the reader to Lantuit et al. (2011) on Bykovsky Peninsula and Günther et al. (2015) and Overduin et al. (2016) on Muostakh Island. The main modes of variability of coastal erosion observations are separated with a Principal Component Analysis (PCA).

The Arctic Oscillation (AO) is defined as the first Empirical Orthogonal Function (EOF), of SLP north of 20^{o}N (Thompson and Wallace, 1998). The AO index is

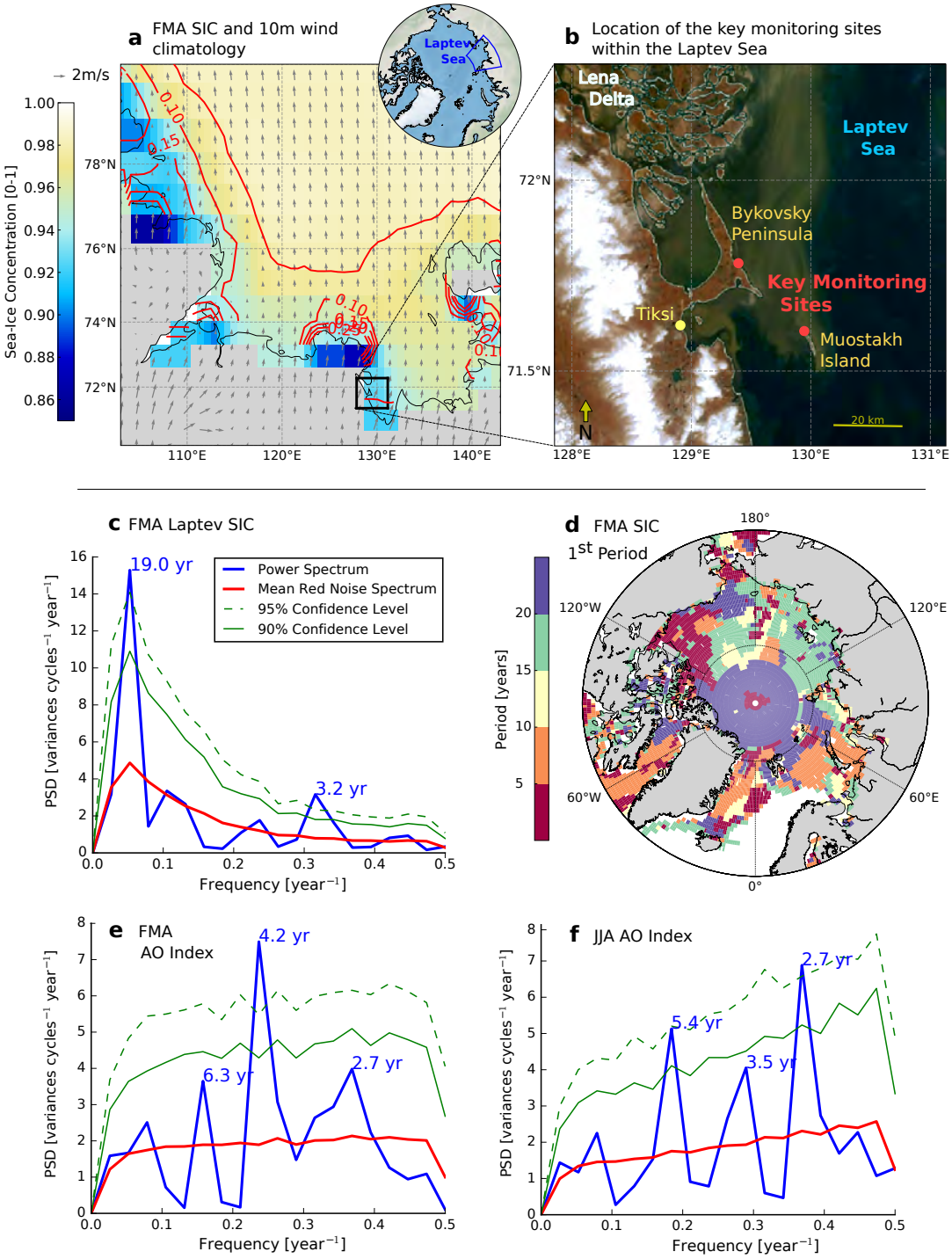

Figure A.1: **Variability of winter Laptev Sea ice and the Arctic Oscillation.** Climatology of sea-ice concentration (SIC) and 10-meter winds in the Laptev Sea **(a)**. Red contours show SIC 2σ in 0.05% intervals. Location of the long-term key-monitoring sites **(b)**. The background satellite image (September 9^{th}, 2009) was obtained from NASA Worldview application (`https://worldview.earthdata.nasa.gov`) and had contrast enhanced. Power spectral density (PSD) of FMA SIC averaged over the Laptev Sea (FMA LSIC) **(c)**, and of FMA **(e)** and JJA AO indices **(f)**. The green full and dashed lines indicate the 90% and 95% confidence levels, respectively. In **(d)** we show a map of predominant periodicity [years], corresponding to the maxima of PSD in FMA SIC per grid cell. Note that the frequencies are obtained from the 39-year long period (1980-2018) from ERA-Interim. Even though peaks in PSD are significant at the 95% level, calculated with a formal probabilistic method (See Supplementary Material), the exact periods should be taken with caution due to the frequency discretization.

the principal component (PC), associated with the first EOF. We calculate the AO in seasonal means, and focus on the Arctic winter (February-March-April, FMA) when sea-ice reaches its maximum concentration in the Laptev Sea, and in summer (June-July-August, JJA), before the field measurements.

From ERA-Interim Reanalysis (Dee et al., 2011), we obtain data on sea-ice concentration, SIC [%], for the calculation of seasonal means and OWS duration, sea-level pressure, SLP [hPa], for the calculation of the AO indices, and a list of dynamics and thermodynamics variables to explore the underlying physical mechanisms (see Supplementary Information). These data are disposed in a Gaussian grid of $\sim 0.7^o$ horizontal resolution, from 1979 to 2018. Daily SIC data are averaged over the Laptev Sea (100^oE-140^oE, 70^oN-82^oN, Fig. 1a) to create Laptev SIC (LSIC) time series. From daily LSIC, we use a threshold of 15% open ice (85% sea-ice cover) to determine the start date of the melting period, the end date of the recovery period, and the duration of the open water season (see Supporting Material for details).

We define especially strong and weak erosion rates, those larger than half a standard deviation above or below their mean ($> |0.5\sigma|$, "extreme"). Analogously, we define close-to-neutral conditions those when coastal erosion rates were smaller than half a standard deviation around their mean ($< |0.5\sigma|$, "neutral"). In order to focus on the interannual variability, long-term linear trends are removed from all time series, and anomalies were calculated with respect to the 1979-2018 period. More details on the statistical methods and metrics are available in the Supporting Material.

A.3 Large-scale main modes of coastal erosion variability

A.3.1 *Laptev Sea ice and the lower-frequency mode*

Winter (February-March-April, FMA) sea-ice concentration (SIC) presents predominantly low-frequency variability over much of the eastern marginal Arctic seas. The Laptev SIC (LSIC) varies in the decadal time scale, with a peak period of $\sim$19 years (Fig. A.1c), similarly to its neighbouring seas. Spatially, most of the Laptev, East Siberian and Chuckchi Seas FMA SIC shows frequency with maximum power spectral density (PSD) values corresponding to periods longer than 15 years (Fig. A.1d), as well as in parts of the East Kara Sea, especially in non-coastal grid cells, suggesting independence from land processes. In the Barents and Beaufort Seas, variability of FMA SIC is relatively higher, with peak periods shorter than 10 and 5 years, respectively.

The predominant low-frequency variability of FMA LSIC is likely due to oceanic mechanisms. Zhang (2015) showed that Atlantic and Pacific heat transport have maximum significant correlations with September Arctic sea-ice extent with a 2-year lag. The Atlantic Multidecadal Variability (AMV), in its positive phase (AMV+), is associated with a negative SLP anomaly over the Kara, Laptev and East Siberian Seas, driving a cyclonic circulation and consequent export of sea ice into the Arctic Ocean during winter (Castruccio et al., 2019). The AMV+ is also significantly correlated with positive anomalies of cloud longwave radiative forcing at the surface, consequent positive SAT anomalies, and negative anomalies of ice strength during winter over much of the East Siberian and Laptev Seas (Castruccio et al., 2019). Although here

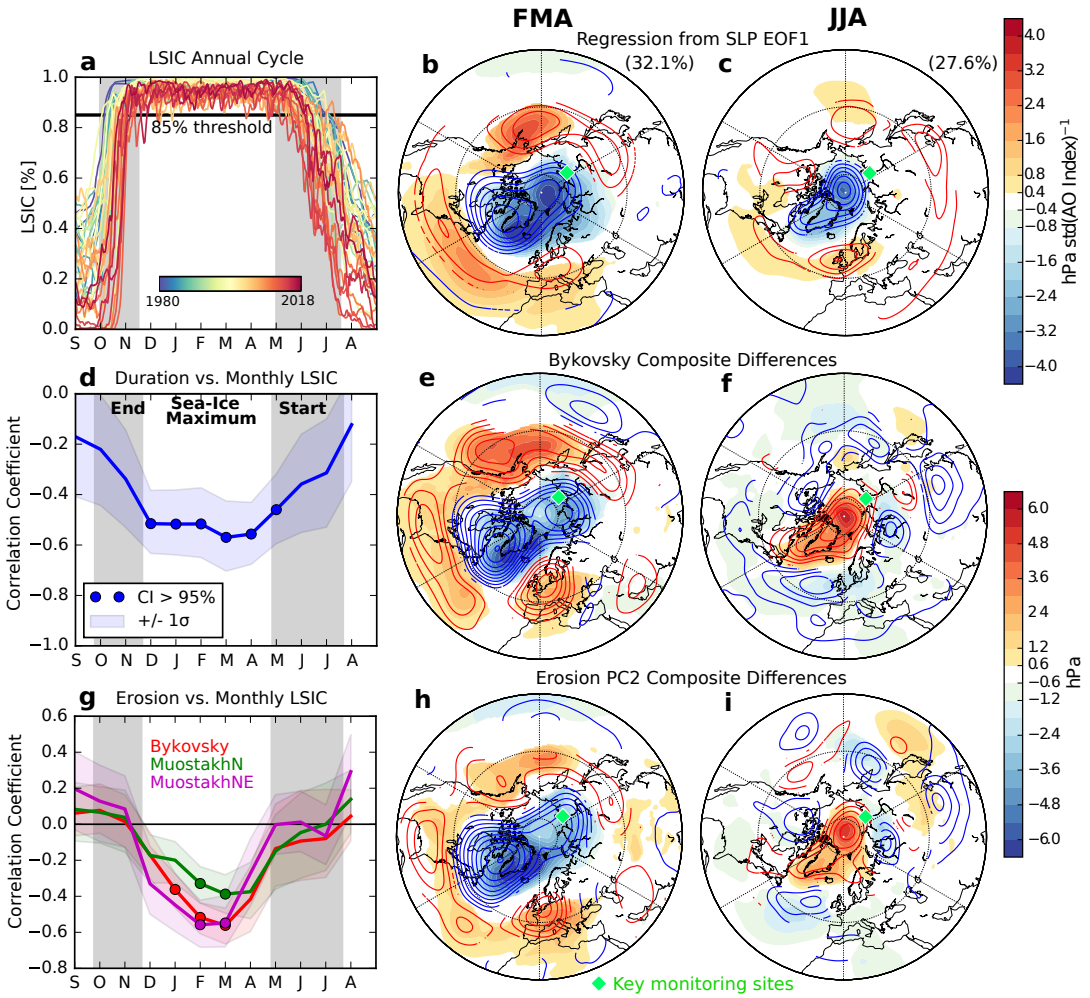

Figure A.2: **Large-scale drivers: Laptev Sea Ice Cover and the Arctic Oscillation.** Left: The annual cycle of daily Laptev Sea Ice Concentration (LSIC) **(a)**. Correlation coefficients between monthly LSIC anomalies and the duration of the OWS **(d)**, and between monthly LSIC anomalies and the observed coastal erosion rates **(g)**. Shadings illustrate a 1σ envelope of bootstrapped correlations; filled circles highlight significant correlations at the 95% level. The mean periods of melt onset and end of freeze-up are highlighted with grey bars. Middle and right: The Arctic Oscillation (AO) patterns expressed as regression coefficients between SLP (shadings) and Z200 (contours) anomalies and the AO index in FMA **(b)** and JJA **(c)**. Units are changes in SLP [hPa] and Z200 [m] per standard deviation of the AO index. Coefficients are only shown where the the 95% confidence level is exceeded ($p < 0.05$). Composites differences of SLP (shading, hPa) and Z200 (contours, m) in FMA and JJA selecting years with respect to Bykovsky time series **(e, f)** and PC2 from coastal erosion observations **(h, i)**. Values are only shown when the strong and weak composite means present opposite signs. Z200 contours are drawn at 50-meter intervals.

noted, the study of the low-frequency variability source of winter LSIC is beyond the scope of this letter.

Negative winter LSIC anomalies are associated with longer OWS ($r = -0.57$ in March, $p < 0.05$, Fig. A.2a,d) and with larger coastal erosion rates ($r < -0.50$, $p < 0.05$, Fig. A.2g). Moreover, positive FMA LSIC anomalies are more strongly associated with late onset dates of OWS ($r = 0.50$, $p < 0.01$), than with early demise dates of previous year's OWS ($r = -0.33$, $p \simeq 0.21$). Indeed, late-winter sea-ice export from the Laptev Sea persists into negative summer SIC anomalies (Krumpen et al., 2013), which anticipates the onset of the melting period (Itkin and Krumpen, 2017). Thus, negative FMA LSIC anomalies contribute to lengthen the OWS, which has been suggested to be the first-order driver of Arctic coastal erosion (Overeem et al., 2011; Barnhart et al., 2014a).

The first principal component (PC1), derived from coastal erosion observations, accounts for $56.5 \pm 16.0\%$ of the total variance and seems to be associated with FMA LSIC anomalies (Fig. A.3a). PC1 shows minimum values around 1997 and 2016, and maximum values between 2005 and 2010, in agreement with the FMA LSIC time series and its decadal variability. The correlation coefficient between PC1 and FMA LSIC is $r = -0.68$, and $r = -0.69$ if a 10-year cutoff low-pass filter is applied to the latter (both $p < 0.01$). All three time series of coastal erosion agree in contributing to PC1 with positive loading coefficients (Fig. S1). Applying a low-pass filter to PC1 as well, a linear relationship with FMA LSIC and the OWS duration appears even stronger (up to $r = -0.89$, Fig. S2). Therefore, we propose that PC1 represents the low-frequency variability in FMA LISC, which modulates the duration of the OWS.

A.3.2 *The Arctic Oscillation and the higher-frequency mode*

In parallel, coastal erosion seems to be associated with the Arctic Oscillation (AO) in both winter and summer, with opposite polarities. The differences between the strong and weak erosion composites of SLP show spatial patterns strikingly similar to the AO in its positive phase (AO+) in FMA (Fig. A.2b,e), and in its negative phase (AO−) in JJA (Fig. A.2c,f). Not only is the general annular mode visible in the composite means of SLP and Z200, but also is the meridional shift of the node latitude between winter and summer (Ogi et al., 2004), suggesting an association between coastal erosion and the AO with its equivalent barotropic signature, in accordance with (Thompson and Wallace, 1998).

The second principal component (PC2) from coastal erosion observations accounts for $28.6 \pm 8.1\%$ of the total variance and varies in quasi-unison with the AO indices, especially after 2010 (Fig. A.3c). Correlation coefficients are $r = 0.46$ ($p < 0.05$) with the FMA AO and $r = -0.33$ ($p = 0.25$) with the JJA AO. Bykovsky and Muostakh-N present large PC2 loadings with opposite signs, in accordance with the anti-correlation found between the FMA and JJA AO in years of especially strong and weak erosion rates, explored in the next section. To support the PC2-AO linkage, we propose the following mechanisms.

The FMA AO is associated with southern surface winds, which advect sea-ice away from the coast of the Laptev and East Siberian Seas, increasing the production of new thin ice, the opening of polynyas and flaw leads, thus increasing heat fluxes from the ocean to the atmosphere, and resulting in local surface warming (Rigor

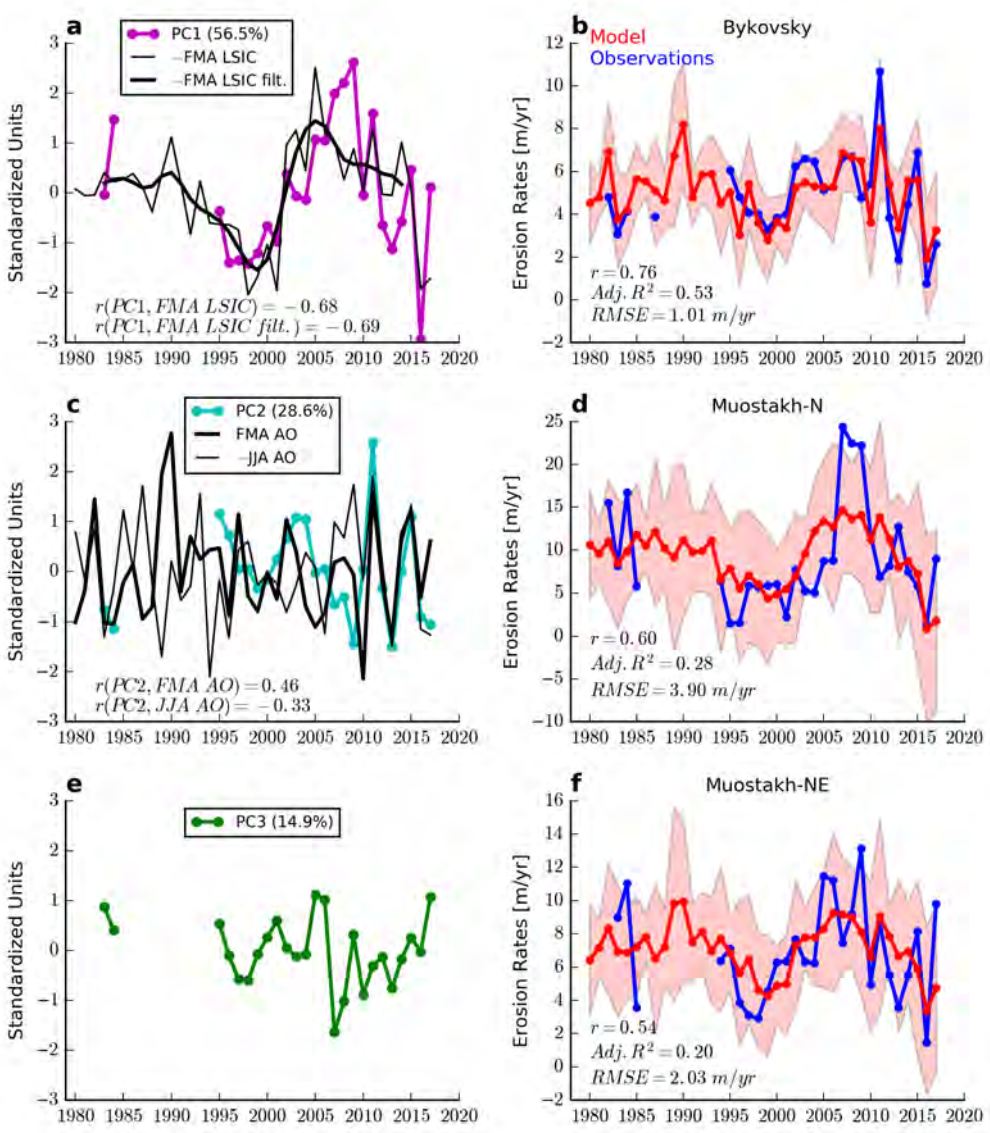

Figure A.3: **PCA and MLR models for coastal erosion.** Left: **(a)** PC1 (purple) and winter Laptev sea-ice concentration anomalies (FMA LSIC, thin black) and the latter with a low-pass filter (thick black), **(c)** PC2 (light blue) and FMA (thick black) and JJA (thin black) AO indices, **(e)** PC3 (green). Right: full MLR models (red), taking the FMA LSIC, FMA AO and JJA AO as explanatory variables, and observed coastal erosion rates at Bykovsky **(b)**, Muostakh-N **(d)** and Muostakh-NE **(f)**. Red shadings highlight the 1σ range of model results.

et al., 2002). We also identify this pattern in regressions using the FMA AO index and in our PC2 erosion composite difference (Fig. S3 a,b).

The JJA AO− is associated with positive surface temperature anomalies in the Laptev Sea. Ding et al. (2017) showed that anticyclonic circulation anomalies with barotropic structure over Greenland the Arctic Ocean (the JJA AO polar center of action, Fig. 2c) increase low-level cloudiness by warming and moistening the lower troposphere, which is then translated in increasing incoming longwave radiation. They further suggest that this mechanism is dominated by circulation changes, reinforcing the role of the AO. We verify this mechanism in PC2 composite differences (Fig. S4c-h). We find significant correlations between the JJA AO index and surface downward longwave radiation over the Laptev Sea. Indeed, significant regression coefficients seem bounded by the coastline, suggesting that the Laptev Sea plays an important role as a source of moisture to this end. However, total integrated water-column content does not show such significant relationships, despite of a pattern of predominant positive anomalies. The signal is made more clear in low-cloud cover anomalies, suggesting that moisture is mainly increased in the lower troposphere. Therefore, a negative JJA AO condition would, in a large scale, create favorable conditions for thermally-driven coastal erosion by increasing surface warming. The JJA AO− is also associated with negative summertime Arctic SIC anomalies, driven by negative SLP anomalies over the polar cap and an associated anticyclonic circulation (Ogi et al., 2008; Wernli and Papritz, 2018). In fact, Ogi et al. (2016) showed that both winter and summer AO indices are good predictors for September SIC anomalies. Negative SIC during summer, and consequent larger fetch for wind waves, would also increase the vulnerability of Arctic coasts to the action of waves.

While PC1 and FMA LSIC show variability in decadal time scales, the AO shows relatively higher-frequency variability with predominant periods between ∼2.7 and ∼4.2 years, for both winter and summer indices (Fig. A.1e,f). Therefore, we suggest that PC2 represents the higher-frequency imprint of the AO onto the coastal erosion observations. We do not attribute the third PC to any climatic driver; it probably represents the signature of local properties, not responding directly to the FMA LSIC and AO effects (Fig. A.3e). The first two modes account together for $85.1 \pm 24.1\%$ of the total variance and can be associated with mechanisms (see summary in Figure S6) identifiable at scales larger than those typically considered for Arctic coastal erosion.

A.4 Quantifying the role of the large-scale drivers at each site

We employ Multiple Linear Regression (MLR) models to estimate the relative role of FMA LSIC and the AO indices at explaining the variance of observed coastal erosion rates at each individual site. To emphasize the different frequencies between drivers, a low-pass Lanczos filter with a cutoff-period of 10 years is applied to FMA LSIC, allowing decadal to longer-scale variability.

The role of each explanatory variable varies considerably between sites. The FMA LSIC alone explains 21%, 30% and 22% of the observed variance of coastal erosion at Bykovsky, Muostakh-N and Muostakh-NE, respectively. The AO indices explain at most 17% (FMA) and 27% (JJA) of the variance at Bykovsky. The proportion of explained variance increases, but does not double, when both AO indices are used as

covariates, suggesting some degree of colliearity. Taking the *full model*, i.e. combining FMA LSIC and both FMA and JJA AO indices, 53% (Bykovsky), 28% (Muostakh-N) and 20% (Muostakh-NE) of the variance is explained. MLR experiments are also done separately taking only years of extreme and neutral erosion rates. The goodness-of-fit of models increases in 77% of the experiments in the extreme case, and decreases in 72% of the experiments in the neutral case. Thus, the proposed drivers are generally better able to explain coastal erosion in years of extreme values, than during years when coastal erosion rates are closer to their mean state. Therefore, the MLR models do not only capture the low, but also the high values of erosion rates, suggesting that the proposed drivers are associated with the anomalies at both ends of the observed range. For Bykovsky, the proportion of explained variance reaches 87% for the full model with extreme years ($r = 0.95$). The single-variable FMA LSIC model performs best in the extreme cases and explains 53% of the variance for Muostakh-N ($r = 0.75$) and 32% Muostakh-NE ($r = 0.60$). The dominant role of the low-frequency FMA LSIC variability is visible in the three modelled time series (Fig. A.3b,d,f).

The differences in magnitude in MLR coefficients (Table S1) stem from the different observed variance among the three time series. The standard deviations are 2.0, 3.0 and 6.2 m/year for Bykosvky, Muostakh-N and Muostakh-NE, respectively. The maximum rate observed at Muostakh-N reaches 25 m/year in 2007, while in Bykovsky the maximum value observed is 11 m/year in 2012, for example. These extreme years coincide in time with years of relatively low FMA LSIC and high and low peaks in FMA and JJA AO indices, respectively

Strong erosion rates often follow a switch in the AO sign from AO+ in FMA to AO− in JJA, and vice-versa. The correlation betweeen FMA and JJA AO indices is weak for the period 1980-2018, if all years are taken ($r = -0.16,\ p \simeq 0.35$). Selecting years of extreme erosion rates, negative and significant correlations between the FMA and JJA AO indices emerge: $r = -0.72$ ($p < 0.05$) for Bykovsky, $r = -0.59$ ($p < 0.05$) for Muostakh-N, and $r = -0.56$ ($p < 0.01$) for Muostakh-NE (Fig. S3). This negative lag-correlation goes against the preferred maintenance of the AO sign between winter and summer (Ogi et al., 2004). Determining the sign of extreme erosion rates, solely based on the information of switches of the AO sign between winter and summer, yields accuracy rates of 70% for Bykovsky, 67% for Muostakh-N and 33% for Muostakh-NE. Breaking down by sign of rate anomalies, true positive rates (sensitivity) are 80%, 75% and 25%, while true negative rates (specificity) are 60%, 60% and 38% for Bykovsky, Muostakh-N and Muostakh-NE, respectively. Therefore, the linkage from the switch in sign between winter and summer AO to coastal erosion rates is more clearly noticeable at Bykovsky and Muostakh-N, than at Muostakh-NE.

Differences in results observed between Bykovsky and Muostakh may be due to local differences in geomorphological properties, which determine the prevailing erosion mechanism at each site. Thermo-denudation (TD) is identified as subaerial erosion primarily driven by temperature changes, hence ground-ice melt, permafrost thaw, and the consequent ground destabilization. Thermo-abrasion (TA) is characterized by the action of the kinetic energy of waves at undercutting coastal cliffs, leading to formation of notches at the land-sea interface, and subsequent rupture and fall of entire coastal blocks onto the shallow surf zone, which are then removed by ocean currents and waves. In TA-dominated coasts, a shoreline change is only apparent

at the event of a block rupture, which may suddenly result after several months of mechanical abrasion of the cliff base by waves. Therefore, the TA component may add a delay to the shoreline position in response to external drivers. Although the relative role of TD and TA often show high variability within small areas, Günther et al. (2015) showed that both processes were similarly important to total coastal erosion rates at Muostakh on average, and at Muostakh Cape specifically, in the period between 2010 and 2013. Lantuit et al. (2011) showed that different backshore landforms at Bykovsky are significantly associated with erosion rates. They described larger means and variability at coastal stretches affected by alases and retrogressive thaw slumps, which is the case of our key-monitoring site at Bykovsky, at the southeastern portion of the Peninsula, facing the Laptev Sea to Northeast. In this specific coastal segment, TD may play a more important role than TA in determining the total coastal erosion mean annual rates.

Both monitoring sites present ice-rich morphology and are thus prone to thermally-driven erosion. The volumetric ground-ice content has been estimated at 79% for Bykovsky Peninsula by (Fuchs et al., 2018) and at 87% for Muostakh Island by (Günther et al., 2015). From the ACD database (Lantuit et al., 2012), the ground-ice content is estimated at 60% at both locations, larger than both the Laptev Sea and Arctic coast means of ∼23% and ∼13%, respectively (Figure S5). Each of the two sites may also experience locally different weather conditions. Therefore, differences in response to the proposed drivers are also expected among sites.

Not only does coastal erosion respond to climate change, but also do sea ice and the AO. Pavlidis et al. (2007) estimated a 1.5-2.5 fold increase of Arctic coasal erosion rates by 2100, especially pronounced in areas where the largest changes in sea-ice are expected. Barnhart et al. (2016) showed that the duration of the ice-free season at the Laptev Sea coast is projected to leave the normal range of variability by the end of the 21^{st} century. Cai et al. (2018) showed a projected positive trend in the summer AO index between 2030 and 2100. Both studies followed a high-emission scenario (RCP 8.5, IPCC (2013)). Therefore, the relative role of the here depicted main modes of coastal erosion variability may change in the future with climate.

A.5 CONCLUSION

We identify the main modes of coastal erosion variability in the Laptev Sea based on almost 30 years of coastal erosion in-situ observations from Bykovsky Peninsula and Muostakh Island. The first mode accounts for 56.5±16.0% of the total variance and seems to respond to decadal-scale changes in winter sea-ice concentration (SIC), predominant over much of the eastern marginal Arctic Seas, including the Laptev and East Siberian Seas. The second and higher-frequency mode accounts for 28.6±8.1% of the total variance and can be associated with the Arctic Oscillation (AO) during winter and summer. Together, the first two modes explain 85.1±24.1% of the total variance, thus most of the observed variability may rely on large-scale drivers.

SIC averaged over the Laptev Sea during winter (FMA) is an indicator for sea-ice melt start and end of freeze-up dates, and hence modulates the duration of the OWS between two summer measurements. This is the first-order driver of coastal erosion variabililty at Bykovsky and Muostakh. The FMA AO likely contributes to coastal

erosion by anticipating the onset of the melt season. Negative JJA AO conditions are associated with decreasing summer SIC anomalies, allowing increased fetch and wave activity, and with increasing surface warming, contributing to ground-ice melting. Therefore, the JJA AO would play a role on increasing Arctic coastal erosion by setting up large-scale conditions favourable to both thermo-abrasion and thermo-denudation. We also show that extreme erosion years follow a switch in sign from AO+ in FMA to AO− in JJA and vice-versa. Taking only these years, significant negative correlations between the FMA AO and JJA AO indices emerge, indicating a combined effect of two. We suggest that differences in the contribution of the proposed drivers between sites are attributed to local characteristics, such as ground-ice content, backshore material and prevailing coastal erosion mechanism.

Our findings stand as an initial step towards bridging Arctic coastal erosion and large-scale climate variability. This is appealing because modern ESMs cannot physically represent coastal erosion at its small scale, but do represent synoptic- to planetary-scale mechanisms, such as pressure and wind changes, to which our proposed drivers directly respond. Also, the large-scale first-order drivers of coastal erosion may be common to other regions in the Arctic. Thereby, we recommend that Arctic coastal erosion start being considered in historical and future climate projections.

ACKNOWLEDGEMENTS

This work is supported by the NUNATARYUK project, which has received funding from the European Union's Horizon 2020 research and innovation programme under grant 773421. M. Grigoriev and S. Razumov were supported by the Russian Foundation for Basic Research (RFBR) grants 18-05-70091 and 18-45-140057. The authors thank Lars Kutzbach, Victor Brovkin and the Climate Modelling group at Universität Hamburg for their support, and the Editor and the two anonymous reviewers for their valuable contributions. ERA-Interim data are available from ECMWF's website at: www.ecmwf.int/en/forecasts/datasets. Coastal erosion data are available from PANGAEA at: https://doi.pangaea.de/10.1594/PANGAEA.905519.

A.6 SUPPLEMENTARY INFORMATION

A.6.1 *Statistical Methods and Metrics*

The variables used to explore the proposed physical mechanisms, obtained from ERA-Interim reanalysis (Dee et al., 2011): geopotential height at 200hPa, Z200 [m], 10-meter wind components [m/s], surface air temperature, SAT [^{o}C], surface thermal radiation downward, STRD [W/m^2], total-column water, TCW [kg/m^2], and low-cloud cover, LCC [%].

The composite analysis is calculated with monhtly ERA-Interim variables, by taking field means over years of especially strong and weak erosion rates, separately. We define strong and weak erosion rates, those higher than 0.5 and lower than -0.5 standard deviations around the mean, respectively. In order to focus on the interannual variability, long-term linear trends are removed from all time series.

The main modes of variability of coastal erosion are depicted with a Principal Component Analysis (PCA). To do so, we take the 27 coinciding years of data from the three coastal erosion sites. Eigenvalues and eigenvectors are calculated on the correlation matrix of the centered and standardized time series. Uncertainties of eigenvalues are calculated following the rule of thumb of North et al. (1982).

The role of each large-scale driver in explaining the variance of the observed coastal erosion rates is quantified with Multiple Linear Regression (MLR) model experiments. The statistical significance of the MLR coefficients is assessed with a bootstrapping methodology. This consists of building 10,000 data series by random sampling with replacement, and then examining the distribution of the generated statistics. Significance levels of simple linear correlations are also calculated with bootstrapping. We use alpha values ($1 - p$) of 86%, 95% and 99% in two-tailed tests from the generated distributions.

Periodograms, or estimations of power spectral density (PSD), of time series are calculated over the ERA-Interim period (1979-2018) using a fast Fourier transform algorithm. Confidence levels for periodograms are estimated from the distribution of 10,000 spectra of generated red noise time series. In order to focus at low-frequency variability modes, we often use a low-pass Lanczos filter, which is made clear throughout the text when applied.

From daily LSIC, the dates of onset and demise of the open-water season are identified. The LSIC time series is smoothed with a 31-day running mean, so it only crosses the threshold once per year in each direction. The time of year between these two dates is here defined as the open-water season. Since erosion rates are always measured in the middle of summer of year n, we calculate the contributing duration of the open-water season by combining the first half (until August 31st) of the open-water season of year n with the second half of the open-water season (from September 1st onward) of year $n - 1$. In other words: the time of year between September 1st of year $n - 1$ and August 31st of year n when LSIC$<$85%. Start and end dates lie on average ($\mu \pm \sigma$) on days 154$\pm$18 (around the 1st of June) and 297$\pm$15 (around the 24th of October), respectively.

For the calculation of the AO indices, we use standard EOF routines, where SLP values are weighted to account for grid-cell size changes as a function of latitude.

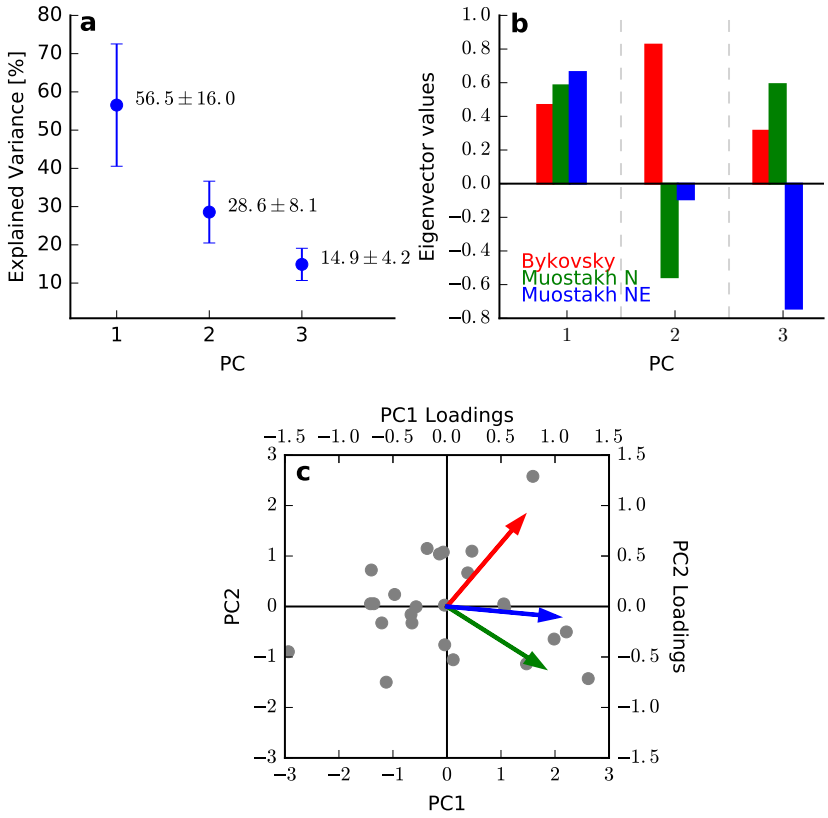

Figure A.4: **PCA on Coastal Erosion Rates.**: a, Proportion of explained variance of each PC. Error bars are calculated following North et al. (1982). b, Eigenvector values (weights) for each time series of erosion rates, to compose each PC. c, Biplot, showing the observations in the PC1-PC2 space, and the projection of the original variables' loadings on this plane.

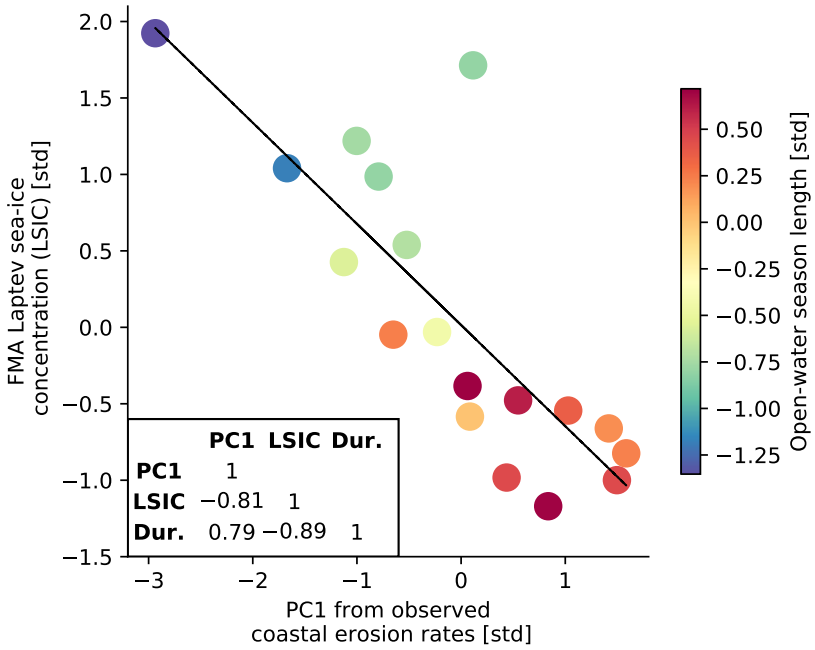

Figure A.5: **Linear relationship between PC1, LSIC and Duration of the open-water season**. All time series are detrended, standardized, and have a 10-year cutoff low-pass Lanczos filter applied. The inset table shows correlation coefficients, all significant at a 99% level.

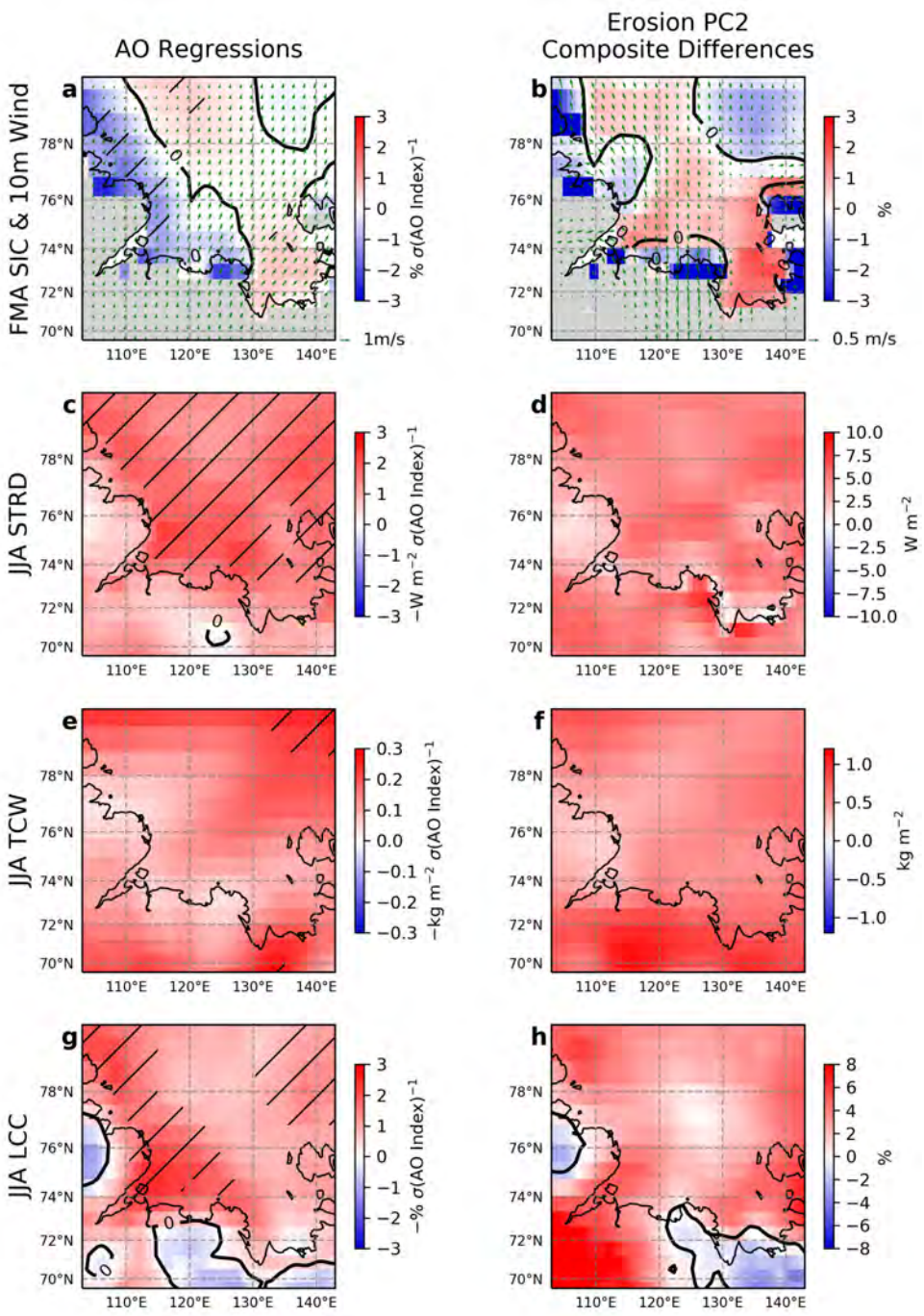

Figure A.6: **AO-related anomalies.** Regression coefficients (left column) and differences between high and low PC2 composites (right column) for FMA sea-ice concentration (SIC) and 10-meter winds (**a, b**), JJA surface thermal radiation downward (STRD, **c, d**), JJA total column water (TCW, **e, f**) and low-cloud cover (LCC, **g, h**). Regression units are per standard deviation of the FMA or JJA AO index. Hatching indicate regression p-values of 0.1. Regression coefficients for JJA are inverted, i.e. $\times(-1)$.

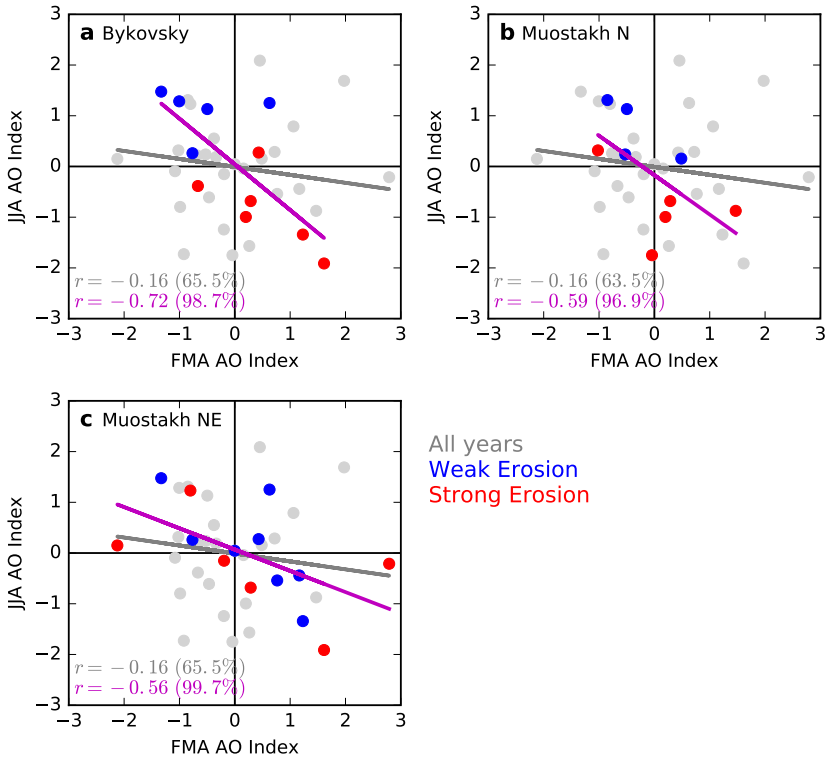

Figure A.7: **Anti-correlation between FMA AO and JJA AO.** Scatter plots between AO indices in FMA and JJA. Years when erosion rates were especially strong (red, erosion$> 0.5\sigma$) and weak (blue, erosion$< -0.5\sigma$) are highlighted, taking observations from Bykovsky (a), Muostakh-N (b) and Muostakh-NE (c). The weak correlation between the FMA and JJA AO indices obtained when all years are taken ($r = -0.16$, best fitted line in grey) increases to $r = -0.72$ ($p < 0.05$) for Bykovsky, $r = -059$ ($p < 0.05$) for Muostakh-N, and $r = -0.56$ ($p < 0.01$) for Muostakh-NE (best fit lines in magenta) if only strong and weak erosion years are taken.

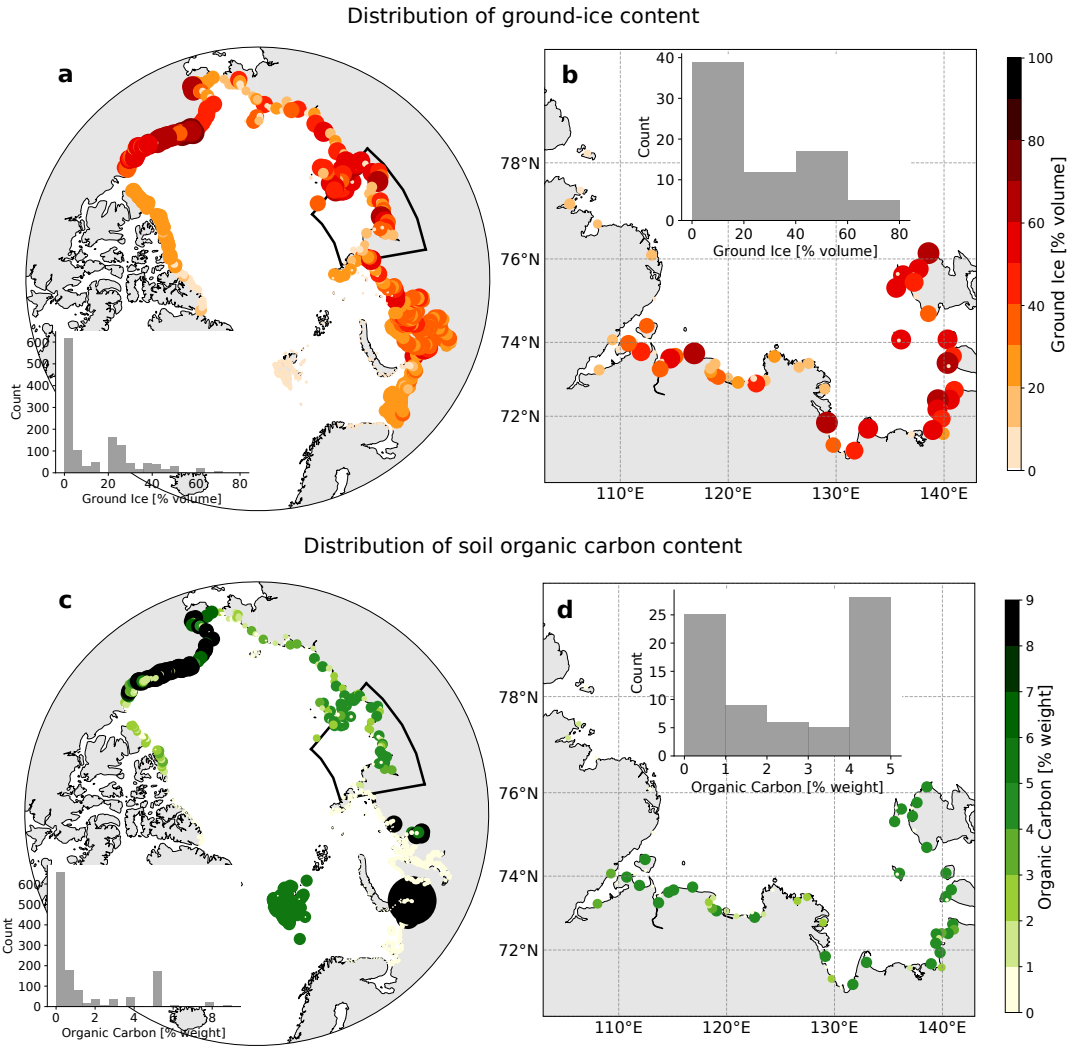

Figure A.8: **Organic carbon and ground-ice content distributions.** Ground-ice [% volume] and organic carbon [% weight] of all ACD coastal segments **(a, c)** and within the Laptev Sea coast **(b, d)**, respectively. ACD data was obtained from Lantuit2012.

Large-scale drivers	Proposed Mechanism	Observed Evidence
FMA LSIC	- The duration of the open-water season (OWS) is the first-order driver of Arctic coastal erosion (Overeem et al. 2011; Barnhart et al. 2014). - Late-winter (FMA) negative sea-ice anomalies in the Laptev Sea are associated with also negative anomalies during summer and an early onset of the melting season (Krumpen et al. 2013; Itkin and Krumpen 2017), therefore, a proxy for the lengthening of the OWS, and to increased coastal erosion. - Arctic sea ice responds to Atlantic and Pacific heat transport, presenting significant decadal-scale variability (Day et al. 2012, Zhang et al. 2015). - Therefore, we propose that decadal-scale variations in FMA SIC modulate the OWS duration and appear as the first PC from coastal erosion observations.	- Our frequency analysis show that FMA sea-ice concentrations has predominant variability in the 15-20 years range over most of the Laptev and East Siberian Seas (Fig. 1-c,d). - FMA LSIC shows significant correlations with the duration of the OWS (Fig. 2d) and with observed coastal erosion rates (Fig. 2g). In specific, FMA LSIC is significantly correlated with onset dates of the OWS ($r=0.50$, $p<0.01$). - The correlation between PC1 and FMA LSIC is also significant ($r=-0.68$, Fig. 3a), especially if a low-pass filter is applied ($r=-0.81$, Fig. S2). As well as the correlation between PC1 and the OWS durations ($r=0.79$, Fig. S2). - In MLR models, when FMA LSIC is tested against the variability of coastal erosion at each site, it explains alone between 21% and 30% of the total variance.
FMA AO	- The winter AO+ is associated with strengthened surface winds blowing from the continent on to the Laptev Sea, removing sea ice from the nearshore zone, opening coastal leads and polynyas, leading to the formation of new thin sea ice, increasing turbulent ocean-atmosphere heat fluxes and thus causing local surface warming (Rigor et al. 2002). - Late-winter (FMA) negative sea-ice anomalies in the Laptev Sea are associated with also negative anomalies during summer and an early onset of the melting season (Krumpen et al. 2013; Itkin and Krumpen 2017), therefore, a proxy for the lengthening of the OWS, and to increased coastal erosion. - The duration of the open-water season (OWS) is the first-order driver of Arctic coastal erosion (Overeem et al. 2011; Barnhart et al. 2014). - Therefore, we propose that winter AO+ contributes to increased coastal erosion in the Laptev Sea, by higher-frequency modulation of the OWS duration.	- The SLP and Z200 composite differences from PC2 and the spatial distribution of AO regressions on SLP and Z200 show similar spatial patterns (Fig. 2-b,c,e,f). - The FMA and JJA AO indices show significant correlations with PC2 (Fig. 3c). Although correlations are often mild, one should have in mind that we are comparing very localized erosion measurements with a climatic mode of variability of planetary scale. - The FMA AO Index regressed on 10-meter winds and SIC anomalies and the composite difference of the same variables made with PC2 show similar spatial patterns over the Laptev Sea (Fig. S2a,b), supporting the early-onset and longer OWS hypothesis, and in agreement with patterns shown by Rigor et al. (2002). - The JJA AO index regressed on surface longwave downward radiation, total column water and low-level could cover are statistically significant and qualitatively agree with composite differences calculated from our PC2 (Fig. S2c-h) and with the mechanism proposed by Ding et al. (2017). - When selecting years of extreme erosion, significant correlations emerge between the FMA and JJA AO indices (Fig. S4), suggesting that the AO in both seasons play a role at coastal erosion, which is more easily detectable when the signal is stronger than the noise and erosion rates assume values substantially different from their mean state.
JJA AO	- Positive sea-level pressure anomalies over the Arctic Ocean and Greenland, associated with anomalous surface anticyclonic atmospheric circulation, result in adiabatic descent and surface warming, thus increasing lower tropospheric moisture, low-level cloudiness and downward longwave radiation (Ding et al. 2017). This set of atmospheric dynamics and thermodynamics characteristics warm the lower atmosphere over the AO polar center of action and consequently favor, in a large scale, coastal erosion by thermo-denudation. - The same mechanism also plays a role at decreasing sea-ice concentration anomalies during summer (Ding et al. 2017), which would increase the coastal fetch, and thus increase the coastal vulnerability to erosion by thermal-abrasion (Overeem et al. 2011; Barnhart et al. 2014).	

Figure A.9: **Summary of proposed physical mechanisms.** Proposed mechanisms and observed evidences, which support the associations between the main modes of observed coastal erosion variability and the suggested large-scale drivers.

Table A.1: **MLR model results.** Correlation coefficient between modelled and observed erosion rates, r, adjusted coefficient of determination, $Adj.R^2$, and regression coefficients, β_n [m year^{-1} σ^{-1}], for combinations of explanatory variables. Numbers between parentheses bring results of MLR ajusted taking only years of especially strong and weak erosion. *Italic*, **bold** and ***italic bold*** numbers are statistically significant at the 86%, 95% and 99% levels, respectively. Results are presented taking the entire time series (All), selecting years of especially strong or weak erosion rates ($> |0.5\sigma|$), and neutral years ($< |0.5\sigma|$).

	r			Adj. R^2			ß$_1$			ß$_2$			ß$_3$		
Explanatory variables	All	$> \|0.5\sigma\|$	$< \|0.5\sigma\|$	All	$> \|0.5\sigma\|$	$< \|0.5\sigma\|$	All	$> \|0.5\sigma\|$	$< \|0.5\sigma\|$	All	$> \|0.5\sigma\|$	$< \|0.5\sigma\|$	All	$> \|0.5\sigma\|$	$< \|0.5\sigma\|$
Bykosvky															
FMA LSIC	0.49	0.56	0.70	*0.21*	*0.26*	*0.44*	**-1.09**	***-1.54***	***-0.49***						
FMA AO	0.45	0.72	0.31	*0.17*	**0.49**	0.00	**0.92**	***2.18***	*-0.16*						
JJA AO	0.55	**0.84**	0.38	*0.27*	***0.67***	0.06	**-1.06**	***-2.10***	*0.21*						
FMA AO+JJA AO	0.60	**0.88**	0.42	*0.31*	***0.74***	0.00	*0.55*	*1.06*	-0.10	*-0.84*	***-1.58***	0.17			
FMA AO+FMA LSIC	**0.75**	***0.92***	0.70	***0.52***	***0.83***	*0.38*	**1.18**	***2.20***	-0.03	***-1.36***	***-1.57***	***-0.48***			
FMA AO+JJA AO+FMA LSIC	**0.76**	***0.95***	0.80	***0.53***	***0.87***	**0.51**	**0.99**	***1.61***	0.07	*-0.36*	***-0.82***	*0.23*	***-1.19***	***-1.16***	***-0.52***
Muostakh-N															
FMA LSIC	0.57	0.75	0.43	**0.30**	***0.53***	0.11	***-4.21***	**-7.45**	*-0.78*						
FMA AO	0.10	0.09	0.56	***-0.04***	***-0.06***	0.25	-0.04	0.86	**-0.87**						
JJA AO	0.33	0.44	0.08	*0.08*	0.14	**-0.09**	*-2.01*	*-3.71*	0.13						
FMA AO+JJA AO	0.37	0.49	0.57	0.07	0.12	0.17	*-1.14*	-2.45	**-0.89**	**-2.43**	**-4.92**	-0.10			
FMA AO+FMA LSIC	0.58	0.76	0.61	**0.29**	**0.51**	0.24	0.75	1.04	*-0.72*	***-4.37***	***-7.48***	-0.48			
FMA AO+JJA AO+FMA LSIC	0.60	0.76	0.61	**0.28**	**0.49**	0.14	0.19	0.10	*-0.71*	*-1.06*	-1.38	0.03	***-3.90***	***-6.81***	-0.49
Muostakh-NE															
FMA LSIC	0.50	0.60	0.16	*0.22*	*0.32*	*-0.08*	**-1.69**	-2.35	0.19						
FMA AO	0.09	0.08	0.55	**-0.03**	***-0.06***	0.23	0.28	0.33	0.77						
JJA AO	0.16	0.17	0.22	-0.01	-0.04	-0.06	-0.46	-0.58	-0.20						
FMA AO+JJA AO	0.16	0.17	0.59	-0.05	*-0.12*	0.18	0.10	-0.03	0.76	-0.43	-0.60	-0.19			
FMA AO+FMA LSIC	0.54	0.63	0.55	*0.23*	*0.31*	0.13	*0.69*	0.80	0.78	***-1.86***	-2.49	-0.03			
FMA AO+JJA AO+FMA LSIC	0.54	0.66	0.59	*0.20*	*0.30*	0.06	*0.83*	1.41	0.76	0.26	0.86	-0.19	***-1.97***	***-2.94***	0.01

PROJECTED INCREASE OF ARCTIC COASTAL EROSION AND ITS SENSITIVITY TO WARMING IN THE 21ST CENTURY

The work in this appendix is under review for publication in *Nature Climate Change*, as of the date of this thesis' submission, and is available as:

Nielsen, D.M., Pieper, P., Barkhordarian, A., Overduin, P., Ilyina, T., Brovkin, V., Baehr, J. & Dobrynin, M. "Projected increase of Arctic coastal erosion and its sensitivity to warming in the 21st Century" – *under review*. Preprint available at: https://doi.org/10.21203/rs.3.rs-634673/v1

Projected increase of Arctic coastal erosion and its sensitivity to warming in the 21st Century

David Marcolino Nielsen[1,2], Patrick Pieper[1], Armineh Barkhordarian[1], Paul Overduin[3], Tatiana Ilyina[4], Victor Brovkin[4], Johanna Baehr[1] and Mikhail Dobrynin[5]

[1]Institute of Oceanography, Center for Earth System Research and Sustainability (CEN), Universität Hamburg, Hamburg, Germany

[2]International Max Planck Research School on Earth System Modelling, Max Planck Institute for Meteorology, Hamburg, Germany

[3]Alfred Wegener Institute Helmholtz Centre for Polar and Marine Research, Potsdam, Germany

[4]Max Planck Institute for Meteorology, Hamburg, Germany

[5]Deutscher Wetterdienst (DWD), Hamburg, Germany

Submitted on 7 June 2021

ABSTRACT

Arctic coastal erosion damages infrastructure, threatens coastal communities, and releases organic carbon from permafrost. However, the magnitude, timing and sensitivity of coastal erosion increase to global warming remain unknown. Here, we project the Arctic-mean erosion rate to roughly double by 2100 and very likely exceed its historical range of variability by mid-21st century. The sensitivity of erosion to warming also doubles, reaching 0.4-0.5 m $year^{-1}$ $^{o}C^{-1}$ and 2.3-2.8 TgC $year^{-1}$ $^{o}C^{-1}$ by the end of the century under moderate and high-emission scenarios. Our first 21st-century pan-Arctic coastal erosion rate projections should inform policy makers on coastal conservation and socioeconomic planning. Our organic carbon flux projections also lay out the path for future work to investigate the impact of Arctic coastal erosion on the changing Arctic Ocean, on its role as a global carbon sink, and on the permafrost-carbon feedback.

Arctic coast erosion is caused by a combination of thermal and mechanical drivers. Permafrost thaw and ground-ice melt lead to soil decohesion and slumping, while surface ocean waves mechanically abrade the coast (Aré, 1988). Sea-ice loss expands the fetch for waves (Overeem et al., 2011; Casas-Prat and Wang, 2020b), and prolongs the open-water season, increasing the vulnerability of the Arctic coast to erosion (Barnhart et al., 2014a; Barnhart et al., 2016). In the past decades, coastal retreat rates have increased throughout the Arctic, often by a factor of two or more (Jones et al., 2009; Günther et al., 2015; Irrgang et al., 2018; Jones et al., 2018; Jones B. M., 2020). The historical acceleration of erosion in the Arctic is linked with the observed decreasing sea-ice cover (Overeem et al., 2011; Barnhart et al., 2014a; Stroeve and Notz, 2018), increasing air surface (Serreze et al., 2009; Cohen et al., 2014) and permafrost temperatures (Biskaborn et al., 2019). In the future, erosion rates are expected to continue increasing. Arctic surface air temperature is projected to exceed its natural range of variability within the next decades (Landrum and Holland, 2020). Arctic sea ice decline has already exceeded natural variability (Landrum and Holland, 2020), and summer ice-free conditions are projected by mid-21st century (Notz and SIMIP Community, 2020). New regimes of surface waves are projected in the Arctic Ocean and along the coast (Dobrynin et al., 2012; Dobrynin et al., 2015; Casas-Prat and Wang, 2020a). Consequently, Arctic coastal erosion rates are expected to increase in the coming decades. However, the extent of this increase is still unknown, as no projections of Arctic coastal erosion rates are available. To fill this gap, we present the first 21st-century projections of coastal erosion at the pan-Arctic scale.

The thawing of permafrost globally releases organic carbon (OC) and increases atmospheric and oceanic greenhouse gas concentrations, feeding back to further warming (Vonk et al., 2012; Schaefer et al., 2014; Schuur et al., 2015; Tanski et al., 2019). Arctic coastal erosion alone releases about as much OC as all the Arctic rivers combined (Vonk et al., 2012; Wegner et al., 2015), fueling about one-fifth of Arctic marine primary production (Terhaar et al., 2021). Despite consistent improvements in the representation of permafrost dynamics (Koven et al., 2013; Burke et al., 2020), the current generation of Earth system models (ESMs) does not account for abrupt permafrost thaw, which may cause projections of OC losses to be largely underestimated (Turetsky et al., 2020; Pihl et al., 2021). Arctic coastal erosion is one form of abrupt permafrost thaw (Tanski et al., 2019) and a relevant component of the Arctic carbon cycle (Vonk et al., 2012; Fritz et al., 2017). Nonetheless, it has not been considered in climate projections so far. The scale mismatch between Arctic coastal erosion and modern ESMs requires the development of holistic models, that account for the key large-scale processes to bridge this gap (Fritz et al., 2017; Turetsky et al., 2019; Nielsen et al., 2020).

In this study, we present a novel approach to represent Arctic coastal erosion at the scales of modern ESMs. We develop a semi-empirical Arctic coastal erosion model combining observations from the Arctic Coastal Dynamics (ACD) database (Lantuit et al., 2012), climate reanalyses, ESM and ocean surface wave simulations. Our model considers the main thermal and mechanical drivers of erosion as dynamical variables, represented by yearly-accumulated positive temperatures and significant

wave heights, and constant ground-ice content from observations. Our approach allows us to make 21st-century projections of coastal erosion at the pan-Arctic scale. We quantify the magnitude, timing and sensitivity of Arctic coastal erosion and its associated OC loss in the context of climate change.

B.2 EMERGENCE OF ARCTIC COASTAL EROSION

We project the Arctic-mean coastal erosion rate to increase from 0.9±0.4 m/year during the historical period (1850-1950) to between 2.0±0.7 and 2.6±0.8 m/year by the end of the 21st Century (2081-2100), in the context of anthropogenic climate change, according to the socio-economic pathway (SSP) scenarios SSP2-4.5 and SSP5-8.5, respectively (Fig. B.1a). This translates to an increase of the Arctic-mean coastal erosion rate by a factor of about between 2.2 and 2.9 by the end of the century with respect to the historical period. The SSP2-4.5 and SSP5-8.5 scenarios describe medium and high radiative forcings due to greenhouse gas emissions (O'Neill et al., 2016), respectively, and include the pathway of the current cumulative CO_2 emissions (Schwalm et al., 2020). In both scenarios, our projections show that the Arctic-mean erosion exceeds its historical range of variability before the end of the century (Fig. B.1b).

We find it likely (≥66% probability) that the Arctic-mean erosion exceeds its historical range by around 2023, and very likely (≥90% probability) by 2049 (Fig. B.1b), considering the largest distributions of uncertainties in our projections (i.e. ensemble spread and erosion model uncertainties). The emergence of the Arctic-mean erosion rate would very likely have happened by around 2010,if we take only the ensemble spread to define the historical range. Significant differences in projections between the two scenarios are only noticeable in the second half of the century, after a complete emergence from the historical range. Our erosion time-of-emergence estimates reflect those of its drivers, which take place around mid-21st Century (Fig. B.1c,d), in accordance with previous studies (Landrum and Holland, 2020; Notz and SIMIP Community, 2020).

Arctic coastal erosion is typically caused by a combination of thermo-denudation (TD) and thermo-abrasion (TA) Aré, 1988, which act together to thaw permafrost, melt ground ice, abrade and transport coastal material off shore. We take yearly-accumulated daily positive temperatures and significant wave heights to represent TD and TA: hereafter, the *thermal* and *mechanical* drivers of erosion, respectively. As various landform types compose the Arctic coast, the relative contribution of the thermal and mechanical drivers differs at the local scale. Erosion is predominantly thermally driven at retrogressive thaw slumps, observed at the Bykovsky Peninsula, Laptev Sea (Lantuit et al., 2011), and in the Mackenzie Delta region – Beaufort Sea (Lantuit and Pollard, 2008; Lantz and Kokelj, 2008), for example (Fig. B.2a), as the sediment transport from ocean waves play a secondary role in coastal retreat in such formations. Erosion is also predominantly thermally driven in enclosed bays and in coastal segments protected by spits and barrier islands, where the fetch for ocean waves is limited (Baranskaya et al., 2021), although barrier island themselves are often susceptible to wave abrasion (Farquharson et al., 2018). In contrast, erosion of ice-rich cliffs, which occur extensively along the Beaufort and Laptev Sea coast for example (Jones et al., 2009; Günther et al., 2015; Jones et al., 2018), requires

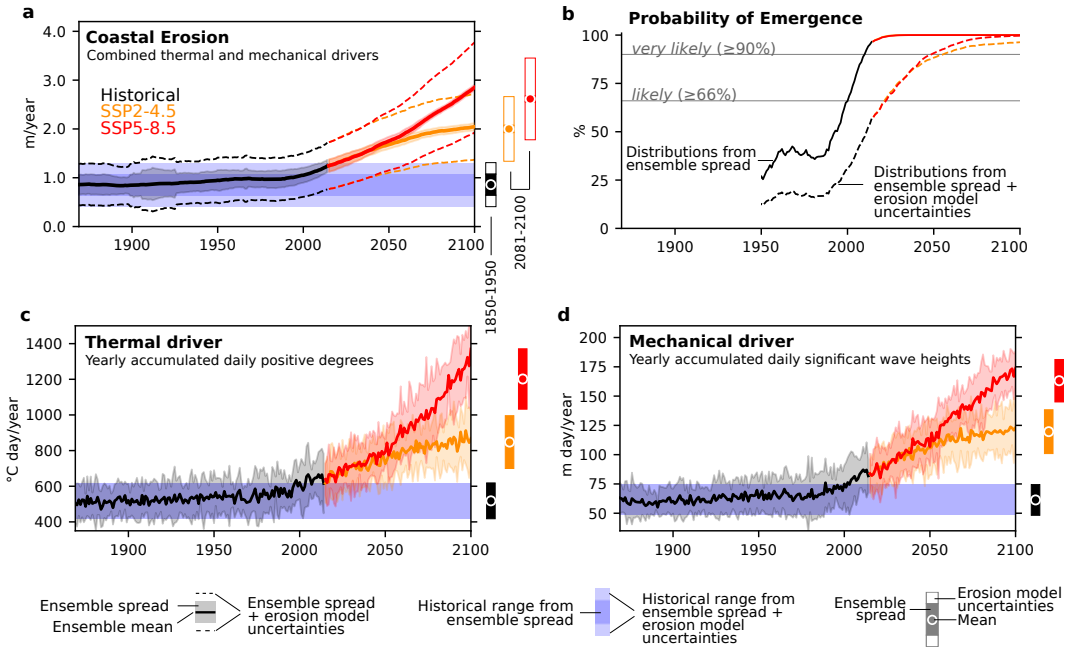

Figure B.1: **Arctic coastal erosion projections. a)** Time evolution of the Arctic-mean coastal erosion rate, expressed as the combined effect of its thermal and mechanical drivers. **b)** Yearly probabilities that the Arctic-mean coastal erosion rate leaves the historical range of variability, calculated from distributions of ensemble spread and erosion model uncertainties (see Methods). In both scenarios, it is very likely (>90% probability) that the Arctic-mean erosion emerges from its historical range by mid 21st century, although the exact time of emergence is sensitive to our erosion model uncertainties. The thermal **(c)** and mechanical **(d)** drivers of erosion, expressed as yearly-accumulated daily positive degrees and significant wave heights, respectively. The erosion time series depict long-term means and therefore show little interannual variability in comparison to its drivers.

the mechanical action from ocean waves to open notches at the land-sea interface, causing the subsequent failure of often still frozen large blocks of permafrost. In some locations, the relative contribution of the thermal and mechanical drivers is more balanced than described above. At Muostakh Island in the Laptev Sea, for example, thermo-denudation and abrasion are estimated to contribute similarly to maintain erosion rates of up to 25 m/year (Günther et al., 2015). In our erosion model, we initially assume equal contributions from the thermal and mechanical drivers at the pan-Arctic scale during the observational period. This assumes that deviations occur comparably in both directions. We also make extreme 10-90% and 90-10% scenarios of relative thermal-mechanical contributions to test the sensitivity of our results to that assumption (see Methods and Table S1). Attributing 90% of mechanical contribution yields about 15-20%s larger Arctic-mean coastal erosion projections by 2100 (and vice-versa), because the Arctic-mean wave exposure increases more than the thawing temperature exposure along the coast, with respect to their historical values (Fig. S1a).

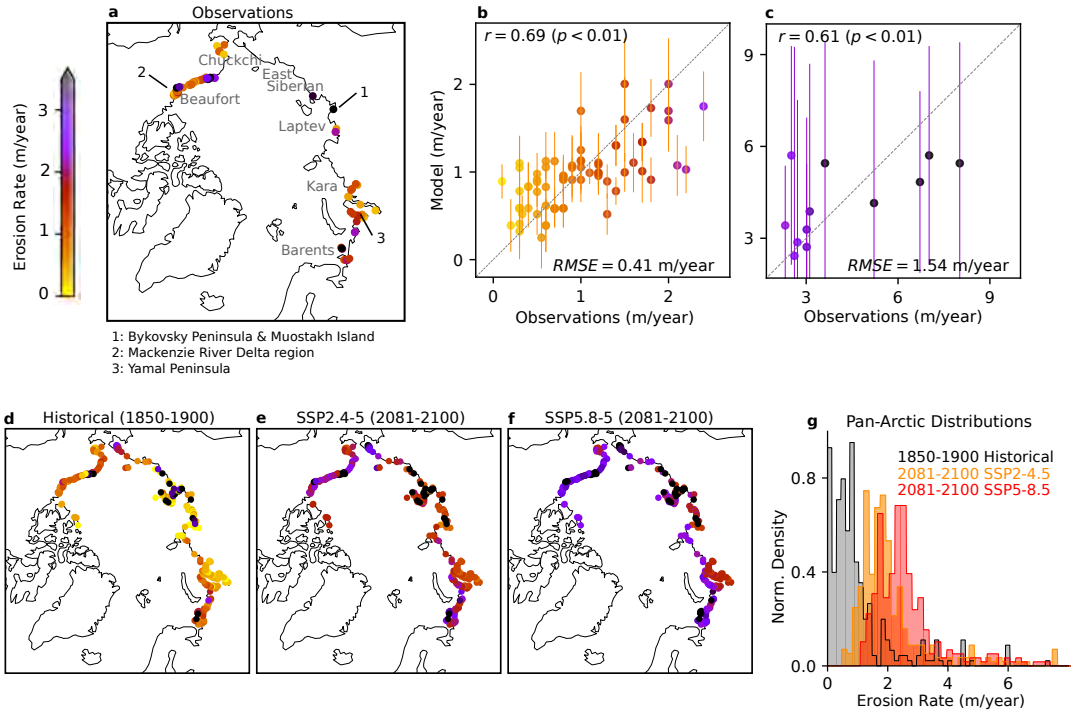

Figure B.2: **Observed and modelled erosion rate spatial variability. a)** Observed long-term coastal erosion mean rates from the ACD database (Lantuit et al., 2012) used in this study (*see Methods*). Modelled against observed erosion rates in **(b)** non-extreme and **(c)** extreme erosion segments. Observed values are denoted by colored circles on the maps and on the scatter plots. Uncertainties represent 2σ confidence intervals from the distribution of regression coefficients. Modelled historical-mean (1850-1900) (**d**) and end-of-the-century (2081-2100) erosion rates according to the SSP2-4.5 (**e**) and SSP5-8.5 (**f**) scenarios. The histograms in **g** display the historical and projected erosion time-means from the maps in d, e and f. Distributions shift and spread over time.

B.3 SPATIAL VARIABILITY OF EROSION

The thermal and mechanical drivers of erosion explain about 36-47% of its observed spatial variability in multiple linear regression models. On one hand, wave exposure, combined with ground-ice content, best explains the spatial variability of erosion in most of the coastal segments ($r = 0.69 \pm 0.12$, mean $\pm 2\sigma$, Fig. B.2b), where erosion is not extremely high ($\sim 90^{\text{th}}$ percentile, <2.5 m/year). The local wave exposure information indeed integrates several important sources of erosion variability. Not only does wave exposure promote cliff abrasion and subsequent sediment transport, but it is also proportional to open-water season (OWS) duration, which has been suggested to be the first-order driver of coastal erosion rate variability (Overeem et al., 2011; Nielsen et al., 2020). In addition, sea-ice melt, and thus increasing OWS duration, responds to increasing surface air temperature, which also drives permafrost thaw and thus erosion by thermo-denudation. On the other hand, spatial differences among segments of extremely high long-term erosion rates are best characterized by thawing temperature exposure combined with ground-ice content ($r = 0.61 \pm 0.42$, Fig. B.2c). This suggests that thermo-denudation plays a more important role in driving coastal erosion rates at extreme-erosion segments, than

at non-extreme ones. Among both extreme and non-extreme erosion segments, ground ice adds explanatory power, as it increases the susceptibility of permafrost to thaw and hence erosion. Our results are in accordance with previous work, which reported weak spatial correlations between ground-ice content and erosion rates (Lantuit et al., 2012). Strong temporal correlations between erosion and thawing temperature exposure have also been reported for Muostakh Island – Laptev Sea (Günther et al., 2015), where erosion rates are often in the range between 10 and 20 m/year (Günther et al., 2015; Grigoriev, 2019). We further combine the temporal evolution of the Arctic-mean erosion with its spatial distribution to make projections of erosion rates at the coastal segment resolution (Fig. B.2d-f).

The geographical distribution of low and high-erosion segments does not change substantially from observations over time in our projections, which is partially a consequence of our model design, as explained by the three following reasons. First, we assume that the spatial model coefficients, empirically determined, remain unchanged throughout our simulations. Second, ground-ice content, an explanatory variable in our regression model, is also assumed constant over time. Third, our regression model accounts for only a fraction of the spatial variability in erosion, and may thus underestimate larger spatial changes to occur over time. Moreover, and independent from model design, local anomalies of the dynamical variables (i.e. local wave and thawing temperature exposure) are smaller in magnitude than their Arctic-mean increase. Therefore, our modelled changes in the spatial variability of erosion are small in comparison to its Arctic-mean increase. Nonetheless, our modelled spatial spread of erosion increases with time (Fig. B.2g). The 5^{th}-95^{th} percentile range of erosion rate distributions increases from 3.6 (0-3.6) m/year in the historical period to 3.9 (0.9-4.8) and 4.2 (1.4-5.7) m/year in the SSP2-4.5 and SSP5-8.5 scenarios, respectively. Temporally resolved erosion rate observations are rare, often sparse in time, and only available at a relatively small number of locations (Jones B. M., 2020). Only with such observations, temporally resolved and at the pan-Arctic scale, would empirical models be able to better constrain the temporal evolution of spatial variability of coastal erosion.

B.4 Spatial variability of organic carbon losses

The pan-Arctic OC loss from coastal erosion increases from 6.9 (1.5-12.3) TgC year-1 during the historical period to between 13.1 (6.4-19.7) TgC year-1 and 17.2 (9.0-25.4) TgC year-1 by the end of the century in the SSP2.4-5 and SSP5-8.5 scenarios, respectively (Fig. B.3). For the present-day climate (i.e. the period for which erosion observations are available), we estimate a pan-Arctic OC loss from coastal erosion of 8.5 (3.3-13.7) TgC year-1. Both our simulated present-climate mean and uncertainty range are comparable with previous estimates from observations (Lantuit et al., 2012; Wegner et al., 2015). Our projections suggest a pan-Arctic OC flux increase by a factor of between 1.5 and 2.0 with respect to the present-day climate, or by a factor of between 1.9 and 2.5 by 2100 with respect to the historical period.

The Laptev and East Siberian Seas (LESS, Fig.B.2a) together account for about three quarters of the pan-Arctic OC losses in our simulations, in accordance with observations-based estimates (Wegner et al., 2015). This also holds truth for future scenarios. The reason for the relatively high OC fluxes from the LESS coast is

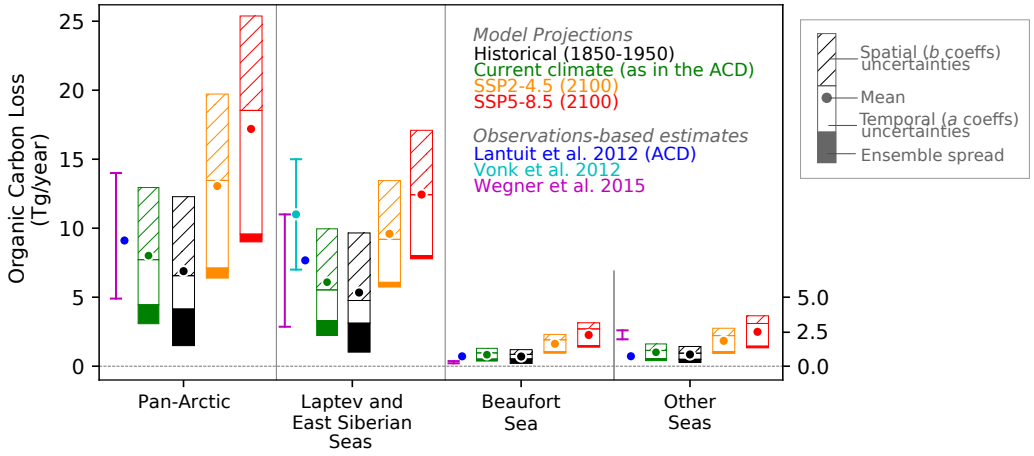

Figure B.3: **Projected organic carbon loss.** Changes in organic carbon released annually by coastal erosion according to observations-based estimates and in our model simulations for the historical period (1850-1950), current climate (according to observations from the ACD (Lantuit et al., 2012)) and at the end of the 21st century (2081-2100) in the two future scenarios. The height of bars represent the total uncertainty of our projections, which we disentangle between ensemble spread, spatial and temporal erosion model components. Most of the uncertainties originate from the empirical estimates of the erosion model parameters (76-97%) and the smallest fraction to the ensemble spread (3-24%).

twofold. First, the region comprises coastal segments of extremely rapid erosion, often between 10 and 20 m/year (Günther et al., 2015; Grigoriev, 2019). Second, the LESS coast is dominated by Yedoma ice-complex deposits, where ground-ice concentration reaches more than 80% of soil volume (Günther et al., 2015; Fuchs et al., 2018), and organic-carbon content is extremely high, reaching about 5% of weight (Lantuit et al., 2012). From the LESS, we simulate a present-climate OC flux of 6.5 (2.4-10.6) TgC year-1 , comparable to the 2.9-11.0 TgC year-1 range estimated by Wegner et al. (2015) (Wegner et al., 2015), and comprising the ACD value of 7.7 TgC year-1 . In an extensive campaign over the LESS continental shelf, Vonk et al. (2012)(Vonk et al., 2012) determined that about 20 TgC year-1 are buried in the LESS sediment, which would originate from a combination of coastal and seafloor erosion. Accounting for degradation before burial and assuming an equal contribution from coastal and subsea erosion, about 11 (7-15) TgC year-1 would be released by coastal erosion alone. The LESS estimate of Vonk et al. (2012) (Vonk et al., 2012) is 43-57% larger than other observations-based estimates (Wegner et al., 2015) and about 69% larger than our present-climate modelled value. These differences are likely due to extensive and high-resolution sampling, allowing for more accurate upscaling (Vonk et al., 2012). However, the uncertainties associated with the contribution between coastal and subsea erosion comprehend our modelled range (their Table S6 (Vonk et al., 2012)). Therefore, an underestimation from our side is not conclusive. From the LESS coast, we project an increase in OC fluxes from 5.3 (1.0-9.6) TgC year-1 in the historical period to 9.6 (5.7-13.4) TgC year-1 in the SSP2-4.5 and 12.4 (7.8-17.1) TgC year-1 in the SSP5-8.5 scenarios by 2100, which translates to an increase by a factor of between 1.8 and 2.3.

The Beaufort Sea coast accounts for about half of the remaining fraction of pan-Arctic OC flux, releasing 0.9 (0.4-1.4) TgC year-1 during the present climate in our simulations, in agreement with the 0.7 TgC year-1 estimates from the ACD (Lantuit et al., 2012), however larger than previous estimates of 0.2-0.4 TgC year-1 (Wegner et al., 2015) (Fig. B.3). Hotspots of extreme erosion are also observed in the Beaufort Sea coast. Extensive field work has been recently carried out, especially in the Yukon coast region, showing increasing erosion rates and suggesting that the associated OC fluxes could have been previously underestimated (Ramage et al., 2017; Couture et al., 2018; Irrgang et al., 2018; Tanski et al., 2019; Grotheer et al., 2020). We project an OC flux increase from the Beaufort Sea coast from 0.7 (0.2-1.2) TgC year-1 in the historical period to between 1.6 (0.9-2.3) TgC year-1 and 2.3 (1.4-3.1) TgC year-1 by 2100 in the SSP2-4.5 and SSP5-8.5 scenarios, respectively, translating to an increase by a factor of between 2.3 and 3.3. The remaining marginal Arctic Seas contribute with yearly OC fluxes at absolute amounts similar to those from Beaufort Sea in our projections, accounting for about 12-14% of the pan-Arctic totals.

Coastal erosion is estimated to sustain about one fifth of the total Arctic marine primary production at present-climate conditions (Terhaar et al., 2021). Therefore, the projected additional OC loss could have a substantial impact on the Arctic marine biogeochemistry. However, the fate of the organic carbon released by Arctic coastal erosion is currently under active debate. Field work has shown that between about 13% and 65% of the OC released into the ocean by coastal erosion could settle in the marine sediment (Hilton et al., 2015; Couture et al., 2018; Grotheer et al., 2020), slowing down remineralization. In the sediment, organic matter degradation would then take place at millennial time scales (Bröder et al., 2018). However, in the shallow nearshore zone, resuspension driven by waves and storm activity increases the residence time of OC in the water column, and allows for more effective remineralization (Jong et al., 2020). Moreover, partial degradation of the eroded material takes place before it enters the ocean, releasing greenhouse gases directly to the atmosphere (Vonk et al., 2012; Tanski et al., 2019; Tanski et al., 2021). The OC degradation time scale thus also depends on its transit time onshore (Tanski et al., 2021). It is therefore challenging to determine short-term impacts from the projected additional OC fluxes from coastal erosion, as large uncertainties still remain regarding pathways of OC degradation.

We partition the uncertainty sources in our projections between three sources: ensemble spread, temporal, and spatial erosion model components (see Methods). Our erosion model contributes the most to the uncertainties in our simulations: from about 76% of the total uncertainty range in the historical period and up to 97% by the end of the century in SSP5-8.5. The ensemble spread is responsible for the remaining 24% of the total uncertainty during the historical period, and for only 3% to 6% of the total range at the end of the future scenarios. The spatial component of the erosion model accounts for about half of the total range of uncertainties, on average, without significant changes in proportion over time. The fraction of uncertainties stemming from the temporal model component increases from about 33% of the total range in the historical period to about 55% by the end of the century in SSP5-8.5 due to the increasing magnitude of the erosion drivers. The distribution of sources of uncertainties in our projections is qualitatively similar between the pan-Arctic and the regional totals.

The sensitivity of Arctic coastal erosion to climate change increases over time in our simulations, and is tightly related with the Arctic amplification (AA) (Serreze et al., 2009) after its onset. Arctic coastal erosion increases more rapidly in response to increasing global mean surface air temperature (SAT) in the future scenarios than it does in the historical period. Before the mid 1970s, neither global nor Arctic-mean SAT decadal trends are consistently significantly positive yet (Fig. B.4a). During this period, the correlation between the Arctic-mean erosion rate and the Arctic-mean SAT is weak ($r = 0.26 \pm 0.29$, mean $\pm 2\sigma$ range, Fig. B.4b). However, after the 1970s, correlations between erosion and Arctic SAT increase substantially (SSP2-4.5: $r = 0.68 \pm 0.18$, SSP5-8.5: $r = 0.93 \pm 0.06$, 2081-2100 means), driven by the concurrent increasing trends. This turning point is also marked by the AA onset, when the Arctic SAT starts increasing at a faster pace than the global SAT, i.e. the AA factor is consistently larger than 1 (Fig. B.4c). Therefore, the sensitivity of erosion to global SAT reflects the sensitivity of Arctic SAT to global SAT – quantified as the AA factor – after the AA onset, given the strong correspondence between erosion and the Arctic SAT at that time (Fig. B.4d). The sharp increase of erosion sensitivity and the AA factor to their maximum values in the early 2000s is a signature from the so-called "hiatus" in global warming (Kosaka and Xie, 2013). Global mean SAT stalls between the late 1990s and the early 2010s, while the erosion drivers continue to increase (Fig. S1b,c). Sensitivity values level off in the second half of the 21st Century, when global mean SAT trends decelerate. End-of-century sensitivities are lowest in the SSP2-4.5 scenario, when Arctic SAT trends decrease sharply to reach the also consistently decreasing global SAT trends, and the AA factor approaches one. In order to avoid the effect of the warming hiatus, we quantify erosion sensitivity considering the historical period until before the AA onset, and during the last 50 years in the scenario simulations.

The sensitivity of the Arctic-mean erosion rate to global mean SAT increases significantly from 0.18±0.31 m year-1 oC-1 on average during the historical period until 1975, to at least double (between 0.40±0.16 and 0.48±0.21 m year-1 oC-1) during the second half of the 21st Century following the SSP2-4.5 and SSP5-8.5 scenarios, respectively. This translates to an increase in the sensitivity of OC losses to climate warming from 1.4 TgC year-1 oC-1 in the historical period before until 1975, on average, to between 2.3 and 2.8 TgC year-1 oC-1 following the SSP2-4.5 and SSP5-8.5 scenarios, respectively.

The sensitivity parameters are useful tools to assess the state of Arctic coastal erosion increase and the associated OC fluxes at intermediate states or policy-based targets of global warming. It must be noted, however, that the sensitivity parameters usually assume linear relationships between the forcing and outcome variables (Friedlingstein et al., 2006). Similarly, in our erosion model, we assume that the linear combination of thermal and mechanical drivers of erosion provides us with first-order large-scale information on the time evolution of Arctic coastal erosion, associated with a range of uncertainties and scenarios of proportionality factors. Non-linear effects could emerge, for example, from earlier onsets of the storm season overlapping with longer-lasting positive temperatures into fall. We do not consider sea-level change in our projections. Adding sea-level change as a temporal driver of

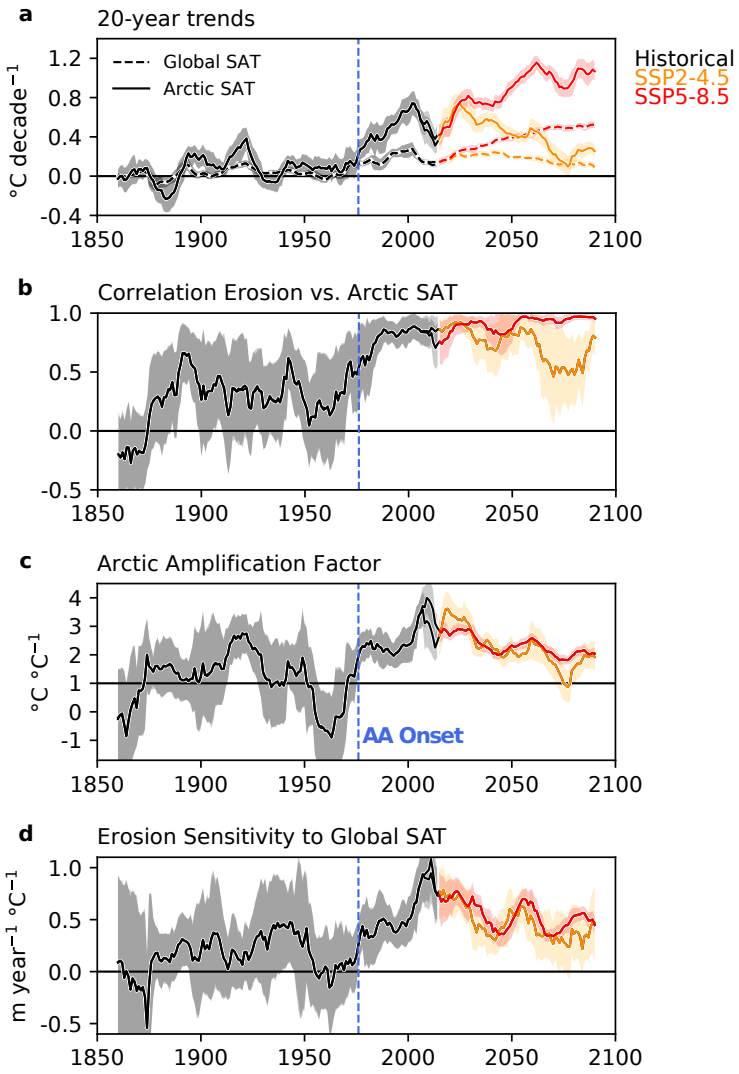

Figure B.4: **Sensitivity to climate change. a**: 20-year running trends of global and Arctic mean surface air temperature (SAT). **b**: Correlations between Arctic-mean erosion rates and Arctic mean SAT. **c**: The Arctic Amplification (AA) factor, expressed as regression coefficients of Arctic SAT changes on global SAT. The AA onset is defined when the AA factor is larger than 1. **d**: Sensitivity of Arctic-mean erosion rates to climate, expressed regression coefficients on global SAT. Running-window lengths are 20 years in all plots. Different window lengths show qualitatively similar results (not shown). The AA onset (dashed blue line) takes place in 1976, when the Arctic SAT increases at a faster pace than the global mean SAT, i.e. the AA factor is larger then 1. After the the 1970s, the AA factor is consistently significantly larger than 1, except for late 21st-century in the SSP2-4.5 scenario, when global and Arctic mean SATs deaccelerated and 20-year trends are momentarily similar.

erosion would increase future erosion and the sensitivity parameters, if it increases proportionally faster than our thermal and mechanical drivers with respect to the historical period. We do not directly consider episodic water level changes due to storms, which are relevant for coastal abrasion and sediment transport. However, by using a global dynamical wave model, and integrating yearly wave exposure at the coastal-segment level, we do incorporate the effect of storms in our mechanical driver of erosion. Our erosion model, relatively simple in comparison with higher-resolution process-based strategies (Hoque and Pollard, 2009; Ravens et al., 2012; Barnhart et al., 2014b; Thomas et al., 2020; Frederick et al., 2021; Rolph et al., 2021), does not intended to represent all processes, often of fine spatial scale (order of meters or less), associated with the erosion of the Arctic coast. Here, we empirically parameterize the role of the the main, first-order drivers of Arctic coastal erosion at larger-scales, compatible with the resolution and mechanisms represented in ESMs (order of tens or hundreds of kilometers). With our approach, we are able to make pan-Arctic projections of coastal erosion, its associated OC fluxes, and estimate their sensitivities to warming from their relationship with projected climate change.

B.6 CONCLUSIONS

We present a semi-empirical model for coastal erosion to make 21st-century pan-Arctic projections of erosion rates and associated organic carbon (OC) losses. Our model accounts for temporal and spatial variability of erosion, combining wave and thawing temperature exposure with ground-ice content as explanatory variables. With our approach, we are able to provide estimates of magnitude, timing and sensitivity of Arctic coastal erosion increase to climate change. The Arctic-mean erosion rate increases by a factor of between 2.2 and 2.9 from the historical period (1850-1900) to the end of the 21st Century following the SSP2-4.5 and the SSP5-8.5 scenarios, respectively. The associated pan-Arctic OC flux increases by a factor of 1.9-2.5 at the same time, reaching up to 17.2 (9.0-25.4, two standard-deviation range) TgC year-1 in the SSP5-8.5 scenario. Our projections show that Arctic coastal erosion is very likely (at least 90% probability) to exceed its historical range of variability before end of the century, even in the intermediate-emission scenario. We estimate that the sensitivity of Arctic coastal erosion to climate also increases with time, following the Arctic amplification after its onset in the 1970s, due to the strong relationship between erosion and Arctic SAT at that time. During the second half of the century, one degree of global warming is associated with an increase of the Arctic-mean erosion by about 0.4-0.5 m/year and 2.3-2.8 TgC/year of associated OC carbon loss, equivalent to about 5-8% of the present-climate OC yearly flux from the Arctic rivers into the Ocean. Arctic coastal erosion will increase more rapidly in the future in response climate change, roughly doubling in rates by 2100, and likely reaching values unseen before in the past century. Our projections allow future work to investigate the impact of Arctic coastal erosion on the permafrost-climate feedback, and the future evolution of the Arctic Ocean's ecosystems and its role as a global carbon sink. Moreover, our results should also inform policy makers on coastal conservation and socioeconomic planning at the pan-Arctic level, focusing on the sustainable future of Arctic coastal communities.

Data

Arctic coastal observations.
We use the Arctic Coastal Dynamics (ACD) database (Lantuit et al., 2012) as our observational reference. The ACD compiles several sources of data and provides a list of variables for a total of 1314 coastal segments along the Arctic coast, including: long-term erosion mean rates, organic carbon concentration, soil bulk density, ground-ice fraction, mean elevation and length. From the 1314 segments, we take those classified as erosive and non-lithified, which excludes segments from the rocky coasts in Greenland and in the Canadian Archipelago and other segments that present stable or aggrading dynamics. We also select segments containing excess ice, which excludes all the non-erosive segments from Svalbard, for example. We this work with a subset of 306 coastal segments in our analysis.

Reanalysis
We take 2-meter air temperature and significant wave heights from ERA20C reanalysis (Poli et al., 2016) as empirical variables in our coastal erosion model. Data are taken in the same periods for which the erosion rates are provided in the ACD. The temperature and wave data have $\sim 1.12^{o}$ (atmosphere) and 1.5^{o} (waves) horizontal resolution. We assign the closest land grid cell in ERA20C from its atmospheric grid to ACD segments, and two rows of adjacent cells from the ocean grid.

Ocean wave simulations
We use the wave model WAM (The WAMDI Group, 1988) to generate a 10-member ensemble of global waves for historical, SSP2-4.5 and SSP5-8.5 scenarios, forced by the MPI-ESM ensemble. In our setup, WAM has 1^{o} grid resolution and is forced with daily sea-ice concentration (threshold of 15% to define open-water), 6-hourly 10-meter winds, and a realistic ETOPO2-based bathymetry as boundary conditions.

Semi-empirical Arctic coastal erosion model

We present a simplified model for Arctic coastal erosion, compatible with the scales of Earth system models. Our model considers the dominant physical thermal and mechanical drivers of erosion, also referred to as thermal-abrasion (TA) and thermal-denudation (TD) (Aré, 1988). The model is constrained to only simulate erosion at the presence of ground ice and at the absence of coastal sea ice. We use an empirical approach to quantify the relationship between the physical drivers, constraints and the erosion rates, by comparing the observations from the ACD with ERA20C reanalysis. The empirically estimated parameters are then applied to all coastal segments, which provides us with erosion rates in the pan-Arctic scale. Our model has yearly time resolution, and the spatial resolution follows the definitions of the ACD coastal segments.

The total erosion E(t,x) [m year^{-1}], defined in every year t and coastal segment $x(lat, lon)$, is given as a combination of a temporal and a spatial component.

$$E(x,t) = \overline{E}(t) + \Delta E(x,t) \tag{B.1}$$

The temporal component represents the temporal evolution of the Arctic-mean erosion $\overline{E}(t)$ [m year^{-1}]. The spatial component $\Delta E(x,t)$ [m year^{-1}] represents local departures from the Arctic mean at every year and coastal segment, providing spatially distributed values of erosion. Hereafter, we use "Arctic mean", denoted by the overline, to refer to means along the Arctic coast. All data associated with ACD coastal segments are weighted by segment lengths in the computation of means.

The temporal component
The temporal component of our model is a linear combination of Arctic means of the thermal and mechanical drivers of erosion.

$$\overline{E}(t) = a_{TD}\,\overline{T}(t) + a_{TA}\,\overline{H}(t) \tag{B.2}$$

The thermal driver of erosion is represented by Arctic-mean yearly-accumulated daily-mean positive 2-meter air temperatures $\overline{T}$(t) [^{o}C day year^{-1}], also commonly known as positive degree-days or thawing-degree days. The mechanical driver of erosion is represented by Arctic-mean yearly-accumulated daily significant wave heights $\overline{H}$(t) [m day year^{-1}].

We empirically estimate the linear coefficients a_{TA} [m m^{-1} day^{-1} year] and a_{TD} [^{o}C m^{-1} day^{-1} year] by scaling the Arctic-mean physical drivers, from ERA20C reanalysis, with the observed coastal erosion rates from the ACD. This is done for the reference time t_{obs}, during which observations are available.

$$a_{TA} = q\frac{\overline{E}_{obs}}{\overline{H}(t_{obs})} \tag{B.3}$$

$$a_{TD} = (1-q)\frac{\overline{E}_{obs}}{\overline{T}(t_{obs})} \tag{B.4}$$

We assume that the thermal and mechanical drivers $a_{TD}\overline{T}(t)$ and $a_{TA}\overline{H}(t)$ contribute in equal proportions to the Arctic-mean erosion during the reference time. We do that by setting the proportionality factor q to 0.5. We test the sensitivity of our results to this assumption by making scenarios with $q = 0.1$ and $q = 0.9$ (see Table S1 and Fig. S1a in the supplementary material).

The spatial component
The spatial component of our erosion model calculates local erosion anomalies with respect to the Arctic-mean temporal evolution, and consists of two multiple linear regression (MLR) models. We split the coastal segments in two groups by classifying them between *extreme* and *non-extreme* with respect to erosion, using 2.5 m/year as a threshold ($\sim 90th$ percentile). We do not find a distinct separation between extreme and non-extreme segments in terms of geographical location (Fig. B.2a),

neither in terms of coastal morphology. Both groups show similar distributions of ground-ice content, mean cliff height, bathymetric profile, bulk density, as well as mean thermal and mechanical forcings derived from thawing temperature and ocean waves, for example (not shown). We test a comprehensive number of combinations of dynamical and geomorphological parameters as explanatory variables in MLR models, simultaneously maximizing goodness-of-fit and penalizing model complexity (Table S3). We fit MLR models using the usual Ordinary Least Square (OLS) method. The goodness-of-fit of models is assessed with the proportion of explained variance and root-mean squared error (RMSE). Since increasing the number of combined explanatory variables necessarily increases the model fit and may lead to overfitting, we penalize model complexity by assessing the changes in the Akaike Information Criterion (ΔAIC) in parallel. The best performing combination of covariates is the one which maximizes correlation (or proportion of explained variance) and minimizes RMSE and ΔAIC (Fig. S2). We train the spatial component of our erosion model only on those segments classified as "high quality" with respect to erosion data. We include medium-quality segments to train the model for the high-erosion case to increase our sample size and thus also statistical robustness. We validate each combination of regression coefficients with unseen data by performing a leave-one-out cross validation test. We use a Bootstrap approach with 10 thousand sampling iterations to obtain distributions of model coefficient estimates, and thus their associated uncertainties.

Three variables compose the best performing combinations: a) daily-mean thawing temperature exposure, expressed as the yearly-accumulated daily positive temperature divided by the number of positive-temperature days per year T_{day} [°C year^{-1}], b) daily-mean wave exposure, expressed as the yearly-accumulated daily significant wave heights divided by the number of open-water days per year H_{day} [m year^{-1}], and c) ground-ice content θ [% of soil volume]. On one hand, combining ground-ice content with daily-mean wave exposure (θ+H_{day}) explains about 47% of the observed spatial variance among non-extreme (2.5 m/year threshold) erosion segments ($r = 0.69$, 9-95$^{\text{th}}$-percentile range: $r = 0.60 - 0.78$, Fig. B.2b, Fig. S3a). On the other hand, combining ground-ice content with the daily-mean thawing temperature exposure (θ+T_{day}) explains about 36% of the variance among extreme-erosion segments ($r = 0.61$, 9-95$^{\text{th}}$-percentile range: $r = 0.31 - 0.94$, Fig. B.2c, Fig. S3a). The linear regression coefficients b obtained with the selected variable combinations are statistically significant ($p < 0.01$).

$$\Delta E(x,t) = \begin{cases} b_\theta \Delta\theta(x) + b_H \Delta H_{day}(x,t) & \text{if } E_{obs}(x) < 2.5 \text{ m year}^{-1} \\ b'_\theta \Delta\theta(x) + b_T \Delta T_{day}(x,t) & \text{otherwise} \end{cases} \tag{B.5}$$

Swapping the combinations and groups, that is, using θ+H_{day} for the extreme and θ+T_{day} for the non-extreme erosion segments, yields overall poorer fits (Fig. S3a,b) and less robust estimation of regression coefficients (Fig. S3c-e). We also test the sensitivity of these results to the choice of the threshold to define extreme erosion. Allowing for an overlap between the extreme and non-extreme segments by lowering the threshold to 2.0 m/year, for example, increases the robustness of the T_{day} regression coefficient estimate for the extreme group (Fig. S3d) by increasing

the number of data points, and yields a similar fit to that of the higher threshold (θ+T_{day} in Fig. S3a,b) and also similar ground-ice coefficients (θ+T_{day} in Fig. 3Sc).

Finally, the total erosion is constrained to the open-water period, and set to zero whenever and wherever sea-ice concentration (SIC) is above 15% at the coast. Combining the temporal (Eq. B.2) and spatial (Eq. B.5) components into our total erosion model (Eq. B.1), conditioned by open-water and the extreme-erosion threshold, our model assumes the complete form:

$$E(x,t) = \begin{cases} a_{TD}\,\overline{T}(t) + a_{TA}\,\overline{H}(t) + \begin{cases} b_\theta \Delta\theta(x) + b_H \Delta H_{day}(x,t) & \text{if } E_{obs}(x) < 2.5 \text{ m/year} \\ b'_\theta \Delta\theta(x) + b_T \Delta T_{day}(x,t) & \text{if } E_{obs}(x) \geq 2.5 \end{cases} & \text{if } SIC\,(x) < 15\% \\ 0 & \text{if } SIC\,(x) \geq 15\% \end{cases} \tag{B.6}$$

Bias correction

Before forcing the erosion model with MPI-ESM data, we adjust the historical and scenario simulatins for climate biases. The bias is removed between ERA20C data (used to estimate our model parameters) and MPI-ESM ensemble means at the coastal segments and reference periods from observations. The modelled distributions are shifted and scaled, so that their means and spread fit those of ERA20C at the reference time.

Organic carbon fluxes

We translate linear erosion rates into volumetric erosion rates E_{vol} [m^3 $year^{-1}$], sediment fluxes S [Kg $year^{-1}$], and carbon fluxes C_{flux} [Kg $year^{-1}$], considering the mean geometry and ground properties of each coastal segment.

$$\begin{aligned} E_{vol}(x,t) &= E(x,t)\; L(x)\; h(x) \\ S(x,t) &= E_{vol}(x,t)\; (1-\theta(x))\; \rho(x) \\ C_{flux}(x,t) &= S(x,t)\; C_{conc.}(x) \end{aligned} \tag{B.7}$$

where L and h are the segments' mean length and elevation [m], θ is the ground-ice content [% volume], ρ is the soil bulk density [Kg/m^3], and $C_{conc.}$ is the organic carbon concentration [% weight]. We integrate over the coastal segments:

$$\overline{C}_{flux}(t) = \sum_x C_{flux}(x,t) \tag{B.8}$$

to obtain the total Arctic flux.

Sensitivity to climate change

We estimate the sensitivity of the organic carbon release by Arctic coastal erosion to climate change following the approach of Friedlingstein et al. (2006) (Friedlingstein

et al., 2006); however, with a simplified set of tools. In their work, Friedlingstein et al. compare pairs of "coupled" and "uncoupled" simulations, where the increasing atmospheric CO_2 concentration either affects climate, or is neutral in terms of radiative effect. This pairwise comparison is necessary because the land-atmosphere and ocean-atmosphere carbon fluxes respond to changes in both climate and atmospheric CO_2 concentrations. Therefore, the difference between their coupled and uncoupled simulations provide the isolated effect of the CO_2-induced changes in climate on carbon fluxes from the effect of the changing atmospheric CO_2 concentration. In our case, changes in atmospheric CO_2 alone do not induce any Arctic coastal erosion response, if not by its radiative effect. An uncoupled simulation, where CO_2 does not induce a change in climate, would not yield any change in the organic carbon released by Arctic coastal erosion. Therefore, we can estimate the sensitivity of the organic carbon release by Arctic coastal erosion to climate γ [TgC year^{-1} ^{o}C^{-1}] by comparing changes in global mean surface temperature and the resulting changes in carbon fluxes from erosion.

Probability and onset of emergence from the historical range

We define the yearly probability density distribution of a modelled variable ψ as the normal distribution $N(t)$ at year t. The mean of $N(t)$ is the ensemble mean and its standard deviation is the ensemble standard deviation (plus the standard deviation of the distribution of erosion model uncertainties in specific situations, made clear in the text). Similarly, the historical range of a modelled variable ψ is the normal distribution fitted to its average over the period 1850-1950 N_{hist}. We calculate the area of distributions $A_{hist} = \int N_{hist} d\psi$ and $A(t) = \int N(t) d\psi$ to determine their overlap $A_{hist} \cap A(t)$. We define the probability of emergence from the historical range $P(t)$, i.e. the probability that $N(t)$ be different from N_{hist}, as the fraction of $A(t)$ that emerges from A_{hist}:

$$P(t) = \frac{A(t) - A_{hist} \cap A(t)}{A(t)} \times 100 \ [\%] \tag{B.9}$$

We define the onset of emergence as the year when the ensemble mean is larger than $\mu + 2\sigma$ from historical range N_{hist}.

Estimation of uncertainties

All ranges of uncertainties, except when clearly stated otherwise, are calculated with a Bootstrap method, which suits cases where the number of data is relatively small. From any vector $\mathbf{X}$ of arbitrary length, a large number (i.e. 10 thousand) of vectors $\mathbf{X}^i$ ($i = 1, 2, \cdots$ 10k) is generated by sampling with replacement from $\mathbf{X}$. The uncertainty of any statistics of $\mathbf{X}$ is estimated from the distribution of i realizations of the statistics obtained from $\mathbf{X}^i$.

DATA AVAILABILITY

The MPI-ESM CMIP6 simulations are publicly available from the Earth System Grid Federation's (ESGF) website: https://esgf-node.llnl.gov/search/cmip6/. The Arctic Coastal Dynamics (ACD) data (Lantuit et al., 2012) are publicly available on PANGAEA: https://doi.pangaea.de/10.1594/PANGAEA.919573. ERA20C reanalysis (Poli et al., 2016) data are publicly available from ECMWF's website: https://www.ecmwf.int/en/forecasts/datasets. Relevant model output, including wave heights, coastal erosion rates, and organic carbon flux projections, will be made available on the World Data Center for Climate (WDCC)/German Climate Computing Center (DKRZ) before publication: https://www.dkrz.de/up/systems/wdcc.

CODE AVAILABILITY

The scripts used to analyze the data are available from the corresponding author upon request.

AUTHORS' CONTRIBUTIONS

D.M.N., M.D., J.B. and V.B. conceived and designed the study. D.M.N., P.P., M.D., J.B. and V.B. designed the erosion model. D.M.N. and M.D. performed the Ocean wave simulations. All authors analyzed and discussed the results. D.M.N. wrote the paper with contributions from all co-authors.

COMPETING INTERESTS

The authors declare no competing interests.

ACKNOWLEDGEMENTS

D.M.N., M.D., P.O., T.I. and V.B. are funded by European Union's Horizon 2020 research and innovation programme under grant agreement number 773421 - project "Nunataryuk". D.M.N., P.P., A.B. T.I., J.B. and V.B. are funded by the Deutsche Forschungsgemeinschaft (DFG, German Research Foundation) under Germany's Excellence Strategy – EXC 2037 'CLICCS - Climate, Climatic Change, and Society' – Project Number: 390683824, contribution to the Center for Earth System Research and Sustainability (CEN) of Universität Hamburg. The authors thank Lars Kutzbach, Sebastian Brune and the Climate Modelling group at Universität Hamburg for the constructive discussions during the development of this work.

q	Historical m/year	SSP2-4.5 m/year (% increase)	SSP5-8.5 m/year (% increase)
0.1	0.86±0.42	1.64±0.50 (91±58)	2.11±0.61 (145±71)
0.5	0.89±0.45	1.99±0.66 (124±74)	2.62±0.84 (193±94)
0.9	0.93±0.48	2.36±0.79 (154±86)	3.12±1.03 (236±111)

Table B.1: Arctic-mean erosion rate projections in the historical period (1850-1950) and by the end of the 21st Century (2081-2100) in three scenarios of proportionality factors between $\overline{H}$ and $\overline{T}$ to compose $\overline{E}$ for the observational period. A factor of $q = 0.1$ represents a 10% contribution from $\overline{H}$ and a 90% contribution from $\overline{T}$, for example. Values are ensemble mean ± two standard deviations from the distribution of uncertainties, obtained with a bootstrap method for the estimation of the coastal erosion temporal component coefficients, plus the ensemble spread.

	Sediment (x10^2 Tg/year)			Organic Carbon (Tg/year)		
	Historical	SSP2-4.5	SSP5-8.5	Historical	SSP2-4.5	SSP5-8. 5
Pan-Arctic	2.78±1.38	6.69±1.85	9.43±2.32	6.89±2.70	13.05±3.33	17.19±4.09
Laptev	0.99±0.67	2.60±0.86	3.80±1.06	3.50±1.45	5.94±1.72	7.66±2.08
East Siberian	0.54±0.28	1.38±0.35	1.93±0.44	1.84±0.71	3.65±0.81	4.78±0.99
Beaufort	0.25±0.09	0.62±0.13	0.88±0.17	0.70±0.25	1.62±0.34	2.26±0.44
Chukchi	0.31±0.10	0.53±0.12	0.66±0.14	0.39±0.12	0.73±0.16	0.95±0.20
Kara	0.38±0.15	0.99±0.26	1.40±0.35	0.26±0.11	0.75±0.21	1.08±0.28
Barents	0.31±0.10	0.58±0.14	0.75±0.17	0.19±0.06	0.36±0.08	0.47±0.10

Table B.2: Annual sediment and organic carbon fluxes from Arctic coastal erosion. Uncertainties represent one standard deviation from the distribution of erosion model coefficients and ensemble spread.

Step No.	Variables
0	θ
1	OWS
2	T_{day}
3	T
4	H_{day}
5	H
6	θ + OWS
7	θ + T_{day}
8	θ + T
9	θ + H_{day}
10	θ + H
11	OWS + T_{day}
12	OWS + T
13	OWS + H_{day}
14	OWS + H
15	T_{day} + H_{day}
16	T_{day} + H
17	T + H_{day}
18	T + H
19	θ + OWS + T_{day}
20	θ + OWS + T
21	θ + OWS + H_{day}
22	θ + OWS + H
23	θ + T_{day} + H_{day}
24	θ + T_{day} + H
25	θ + T + H_{day}
26	θ + T + H
27	OWS + T_{day} + H_{day}
28	OWS + T_{day} + H
29	OWS + T + H_{day}
30	OWS + T + H
31	θ + OWS + T_{day} + H_{day}
32	θ + OWS + T_{day} + H
33	θ + OWS + T + H_{day}
34	θ + OWS + T + H

Table B.3: Combinations of explanatory variables tested in multiple linear regression models to explain the observed spatial variability of erosion. Performance metrics are displayed in Fig. B.6. A list of symbols is presented in Table B.4.

Symbol	Description	Unit
E	Erosion rate	m year^{-1}
H	Yearly-accumulated daily significant wave heights	m day year^{-1}
T	Yearly-accumulated daily positive degrees	^{o}C day year^{-1}
H_{day}	H divided by the number of open-water days per year	m year^{-1}
T_{day}	T divided by the number of positive-degree days per year	^{o}C year^{-1}
OWS	Open-water season duration	day
SIC	Sea-ice concentration	% area
θ	Ground-ice content	% volume
a_{TA}	Empirical temporal coefficient for Arctic-mean thermo-abrasion	m m^{-1} day^{-1}
a_{TD}	Empirical temporal coefficient for Arctic-mean thermo-denudation	^{o}C m^{-1} day^{-1}
b_{θ}	Spatial regression coefficient for ground ice (non-extreme segments)	m % year^{-1}
b'_{θ}	Spatial regression coefficient for ground ice (extreme segments)	m % year^{-1}
b_T	Spatial regression coefficient for T_{day}	m ^{o}C^{-1}
b_H	Spatial regression coefficient for H_{day}	m m^{-1}
C_{conc}	Soil organic-carbon concentration	% weight
C_{flux}	Soil organic-carbon flux	Tg year^{-1}
ρ	Soil bulk density	kg m^{-3}
L	Coastal segment length	m
h	Coastal segment mean height	m
$\overline{(\,)}$	Spatial Arctic mean, weighted by coastal segment length	
$\Delta(\,)$	Spatial anomalies with respect to Arctic mean	
x	Spatial dimension	ACD coastal segment
t	Temporal dimension	year

Table B.4: List of symbols.

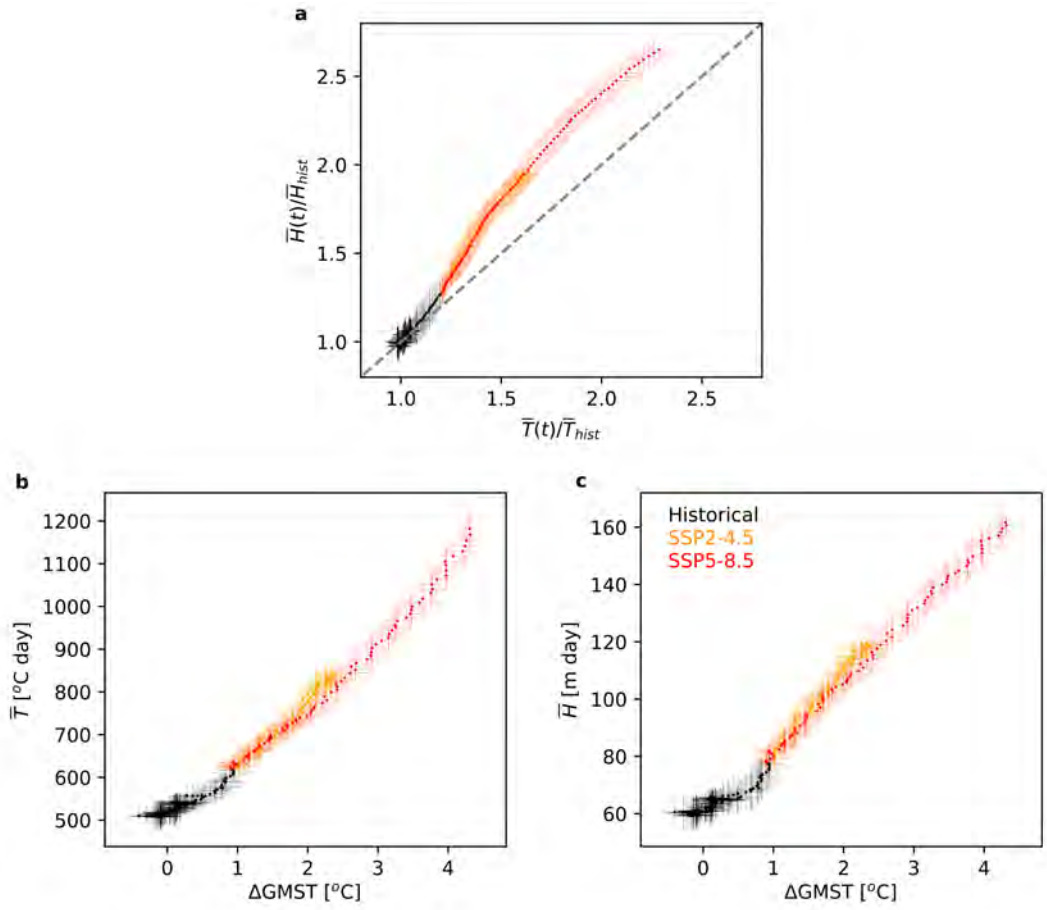

Figure B.5: **a)** Arctic-mean mechanical driver of erosion $\overline{H}$ [m day year^{-1}] normalized by its historical value (1850-1950), as a function of the Arctic-mean thermal driver of erosion $\overline{T}$ [^{o}C day year^{-1}] also normalized by its historical value. $\overline{H}$ increases proportionally more than $\overline{T}$. The mechanical driver increases more than the thermal driver in the 21st century with respect to historical values. By 2100, $\overline{H}$ and $\overline{T}$ increases 2.65 and 2.29 (1.63 and 1.96) times their respective historical values in the SSP5.8-5 (SSP2.4-5) scenario. By 2100, the mechanical and thermal drivers increase 2.65 and 2.29 (1.63 and 1.96) times their respective historical values in the SSP5.8-5 (SSP2.4-5) scenario. The erosion drivers $\overline{T}$ in **b**, and $\overline{H}$ in **c**, as a function of global mean surface temperature changes ΔGMST. Dots are the ensmble mean and lines depict 2 standard deviations of the ensemble spread. The erosion drivers, especially $\overline{H}$, increase sharply in the transition between the historical and future scenarios, at ΔGMST$\simeq$ 1, as a consequence of the apparent hiatus in global warming.

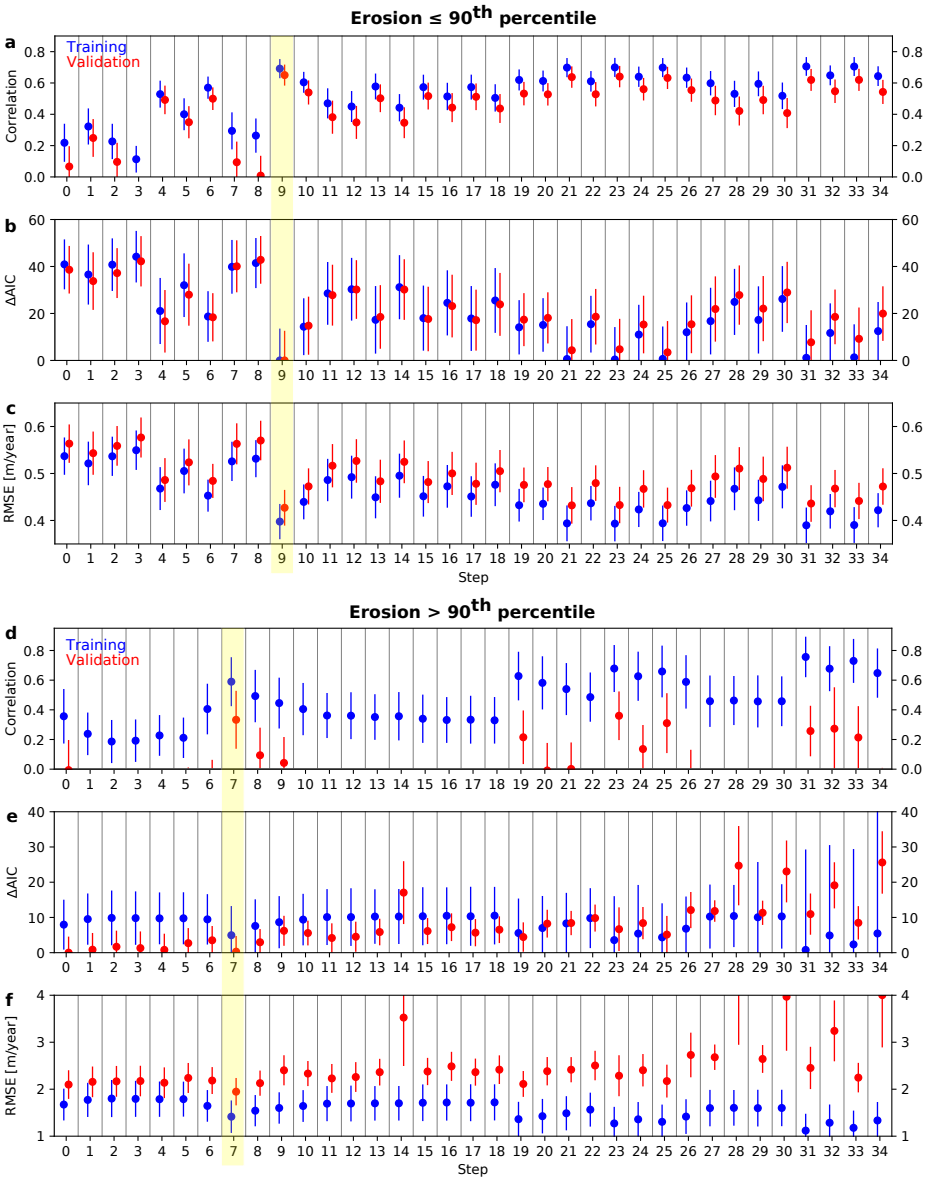

Figure B.6: Goodness-of-fit metrics for each variable combination (step) tested in multiple linear regression models to explain the spatial variability of observed erosion rates. Shown are the correlation coefficients (a, c), Akaike's Information Criterion differences (ΔAIC) (b, e) and root mean square errors (RMSE) (c, f) for the non-extreme (top) and extreme (bottom) erosion segments. Blue and red markers represent training and leave-one-out cross validation results. Vertical bars represent two standard deviations of distributions calculated with a Bootstrapping method. The best performing steps, highlighted in yellow, are selected with trade-off between high correlation and low ΔAIC and RMSE. The steps are described in Table B.3.

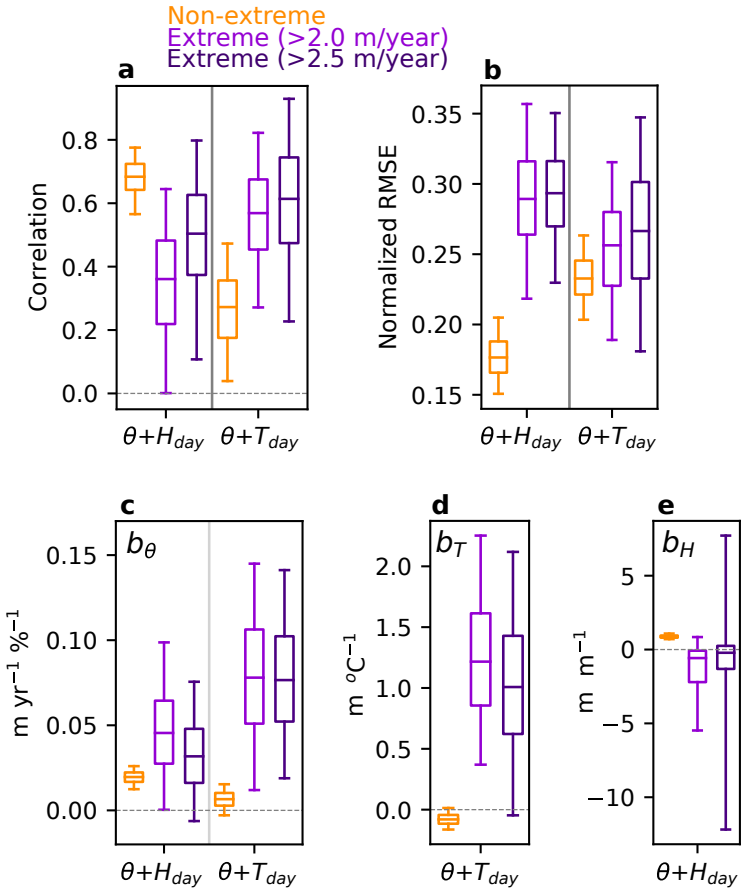

Figure B.7: Spatial erosion model component parameters for the non-extreme erosion group and for two different extreme-erosion groups, differing on the threshold. Correlation **a** and normalized root-mean squared error (RMSE) **b** between modelled and observed erosion rates. Multiple linear regression coefficients for combinations θ+H_{day} and θ+T_{day}, for the extreme and non-extreme coastal segments. Regression coefficients for **c**: ground-ice content θ, **d**: daily mean positive-degree sum T_{day}, and **e** daily mean wave heights H_{day}. Horizontal lines represent the median, bnxes represent the 25-75% percentile range, and whiskers the 9-95% percentile range. All parameter distributions are obtained with a 10-thousand sampling Bootstrap method.

BIBLIOGRAPHY

Anderson, L. G., S. Jutterström, S. Hjalmarsson, I. Wåhlström, and I. P. Semiletov (2009). "Out-gassing of CO2 from Siberian Shelf seas by terrestrial organic matter decomposition". *Geophysical Research Letters* 36.20. DOI: https://doi.org/10.1029/2009GL040046.

Aré, F. E. (1988). *Thermal abrasion of sea coasts*. Vol. 12. 1-2, pp. 1–157. DOI: 10.1080/10889378809377343.

AWI, Alfred-Wegener-Institut Helmholtz-Zentrum für Polar- und Meeresforschung (2020). *Research Station "Samoylov Island": A base for Russian-German permafrost research in siberia*. URL: https://www.awi.de/en/expedition/stations/island-samoylov.html.

Baldwin, Mark P. and Timothy J. Dunkerton (1999). "Propagation of the Arctic Oscillation from the stratosphere to the troposphere". *Journal of Geophysical Research: Atmospheres* 104.D24, pp. 30937–30946. DOI: https://doi.org/10.1029/1999JD900445.

Baranskaya, Alisa, Anna Novikova, Natalya Shabanova, Nataliya Belova, Stepan Maznev, Stanislav Ogorodov, and Benjamin M. Jones (2021). "The Role of Thermal Denudation in Erosion of Ice-Rich Permafrost Coasts in an Enclosed Bay (Gulf of Kruzenstern, Western Yamal, Russia)". *Frontiers in Earth Science* 8, p. 659. DOI: 10.3389/feart.2020.566227.

Barnhart, K. R., I. Overeem, and R. S. Anderson (2014a). "The effect of changing sea ice on the physical vulnerability of Arctic coasts". *Cryosphere* 8.5, pp. 1777–1799. DOI: 10.5194/tc-8-1777-2014.

Barnhart, Katherine R., Robert S. Anderson, Irina Overeem, Cameron Wobus, Gary D. Clow, and Frank E. Urban (2014b). "Modeling erosion of ice-rich permafrost bluffs along the Alaskan Beaufort Sea coast". *Journal of Geophysical Research: Earth Surface* 119.5, pp. 1155–1179. DOI: 10.1002/2013JF002845.

Barnhart, Katherine R., Christopher R. Miller, Irina Overeem, and Jennifer E. Kay (2016). "Mapping the future expansion of Arctic open water". *Nature Climate Change* 6.3, pp. 280–285. DOI: 10.1038/nclimate2848.

Barrell, Joseph (1912). "Criteria for the recognition of ancient delta deposits". *Bulletin of the Geological Society of America* 23.1, pp. 377–446. DOI: https://doi.org/10.1130/GSAB-23-377.

Bartsch, Annett, Sarah Ley, Ingmar Nitze, Georg Pointner, and Gonçalo Vieira (2020). "Feasibility Study for the Application of Synthetic Aperture Radar for Coastal Erosion Rate Quantification Across the Arctic". *Frontiers in Environmental Science* 8, p. 143. DOI: 10.3389/fenvs.2020.00143.

Bates, N. R. and J. T. Mathis (2009). "The Arctic Ocean marine carbon cycle: evaluation of air-sea CO_2 exchanges, ocean acidification impacts and potential feedbacks". *Biogeosciences* 6.11, pp. 2433–2459. DOI: 10.5194/bg-6-2433-2009.

Belova, Nataliya, Natalia Shabanova, Stanislav Ogorodov, Alisa Baranskaya, Anna Novikova, and Daria Aleksyutina (2018). "Coastal Erosion at Kharasavey Gas Condensate Field, Western Yamal Peninsula". SPE Russian Petroleum Technology Conference. DOI: 10.2118/191727-18RPTC-MS.

Biskaborn, Boris K. et al. (2019). "Permafrost is warming at a global scale". *Nat. Commun.* 10.1, p. 264. DOI: 10.1038/s41467-018-08240-4.

Brady, Michael B. and Robin Leichenko (2020). "The impacts of coastal erosion on Alaska's North Slope communities: a co-production assessment of land use damages and risks". *Polar Geography* 43.4, pp. 259–279. DOI: 10.1080/1088937X.2020.1755907.

Bristol, Emily M., Craig T. Connolly, Thomas D. Lorenson, Bruce M. Richmond, Anastasia G. Ilgen, R. Charles Choens, Diana L. Bull, Mikhail Kanevskiy, Go Iwahana, Benjamin M. Jones, and James W. McClelland (2021). "Geochemistry of Coastal Permafrost and Erosion-Driven Organic Matter Fluxes to the Beaufort Sea Near Drew Point, Alaska". *Frontiers in Earth Science* 8, p. 639. DOI: 10.3389/feart.2020.598933.

Bröder, Lisa, Tommaso Tesi, August Andersson, Igor Semiletov, and Örjan Gustafsson (2018). "Bounding cross-shelf transport time and degradation in Siberian-Arctic land-ocean carbon transfer". *Nature communications* 9.1, pp. 1–8. DOI: https://doi.org/10.1038/s41467-018-03192-1.

Brune, Sebastian and Johanna Baehr (2020). "Preserving the coupled atmosphere–ocean feedback in initializations of decadal climate predictions". *WIREs Climate Change* 11.3, e637. DOI: https://doi.org/10.1002/wcc.637.

Budyko, Mikhail Ivanovich (1969). "The effect of solar radiation variations on the climate of the Earth". *Tellus* 21.5, pp. 611–619. DOI: https://doi.org/10.1111/j.2153-3490.1969.tb00466.x.

Budyko, Mikhail Ivanovich (1972). "The future climate". *Eos, Transactions American Geophysical Union* 53.10, pp. 868–874. DOI: https://doi.org/10.1029/EO053i010p00868.

Bull, Diana L, Emily M. Bristol, Eloise Brown, Robert Charles Choens, Craig T. Connolly, Christopher Flanary, Jennifer M Frederick, Benjamin M. Jones, Craig A. Jones, Melissa Ward Jones, James W. McClelland, Alejandro Mota, and Irina Kalashnikova Tezaur (2020). *Arctic Coastal Erosion: Modeling and Experimentation*. Tech. rep. SAND2020-10223. Sandia National Laboratories. DOI: https://doi.org/10.2172/1670531.

Burke, E. J., Y. Zhang, and G. Krinner (2020). "Evaluating permafrost physics in the Coupled Model Intercomparison Project 6 (CMIP6) models and their sensitivity to climate change". *The Cryosphere* 14.9, pp. 3155–3174. DOI: 10.5194/tc-14-3155-2020.

Cai, Lei, Vladimir A. Alexeev, John E. Walsh, and Uma S. Bhatt (2018). "Patterns, impacts, and future projections of summer variability in the arctic from CMIP5 models". *Journal of Climate* 31.24, pp. 9815–9833. DOI: 10.1175/JCLI-D-18-0119.1.

Cai, Ziyi, Qinglong You, Fangying Wu, Hans W Chen, Deliang Chen, and Judah Cohen (2021). "Arctic warming revealed by multiple CMIP6 models: evaluation of historical simulations and quantification of future projection uncertainties". *Journal of Climate* 34.12, pp. 4871–4892. DOI: https://doi.org/10.1175/JCLI-D-20-0791.1.

Casas-Prat, Mercè and Xiaolan L. Wang (2020a). "Projections of Extreme Ocean Waves in the Arctic and Potential Implications for Coastal Inundation and Erosion". *Journal of Geophysical Research: Oceans* 125.8, e2019JC015745. DOI: https://doi.org/10.1029/2019JC015745.

Casas-Prat, Mercè and Xiaolan L. Wang (2020b). "Sea Ice Retreat Contributes to Projected Increases in Extreme Arctic Ocean Surface Waves". *Geophysical Research Letters* 47.15, e2020GL088100. DOI: https://doi.org/10.1029/2020GL088100.

Castruccio, Frederic S., Yohan Ruprich-Robert, Stephen G. Yeager, Gokhan Danabasoglu, Rym Msadek, and Thomas L. Delworth (Mar. 2019). "Modulation of Arctic Sea ice loss by atmospheric teleconnections from Atlantic multidecadal variability". *Journal of Climate* 32.5, pp. 1419–1441. DOI: 10.1175/JCLI-D-18-0307.1.

Cohen, J, James A Screen, Jason C Furtado, Mathew Barlow, David Whittleston, Dim Coumou, Jennifer Francis, Klaus Dethloff, Dara Entekhabi, James Overland, and Justin Jones (2014). "Recent Arctic amplification and extreme mid-latitude weather". *Nature Geoscience* 7.9, pp. 627–637. DOI: 10.1038/ngeo2234.

Colony, R. and A. S. Thorndike (1984). "An estimate of the mean field of Arctic sea ice motion". *Journal of Geophysical Research: Oceans* 89.C6, pp. 10623–10629. DOI: https://doi.org/10.1029/JC089iC06p10623.

Comiso, Josefino C., Walter N. Meier, and Robert Gersten (2017). "Variability and trends in the Arctic Sea ice cover: Results from different techniques". *Journal of Geophysical Research: Oceans* 122.8, pp. 6883–6900. DOI: https://doi.org/10.1002/2017JC012768.

Couture, Nicole J, Anna Irrgang, Wayne Pollard, Hugues Lantuit, and Michael Fritz (2018). "Coastal Erosion of Permafrost Soils Along the Yukon Coastal Plain and Fluxes of Organic Carbon to the Canadian Beaufort Sea". *Journal of Geophysical Research: Biogeosciences* 123.2, pp. 406–422. DOI: 10.1002/2017JG004166.

Cowell, Peter J., Marcel J. F. Stive, Alan W. Niedoroda, Huib J. de Vriend, Donald J. P. Swift, George M. Kaminsky, and Michele Capobianco (2003). "The Coastal-Tract (Part 1): A Conceptual Approach to Aggregated Modeling of Low-Order Coastal Change". *Journal of Coastal Research* 19.4, pp. 812–827. DOI: https://www.jstor.org/stable/4299222.

Crawford, Alex, Julienne Stroeve, Abigail Smith, and Alexandra Jahn (2021). "Arctic open-water periods are projected to lengthen dramatically by 2100". *Communications Earth & Environment* 2.1, pp. 1–10. DOI: https://doi.org/10.1038/s43247-021-00183-x.

Cunliffe, Andrew, George Tanski, Boris Radosavljevic, William Palmer, Torsten Sachs, Hugues Lantuit, Jeffrey Kerby, and Isla Myers-Smith (2019). "Rapid retreat of permafrost coastline observed with aerial drone photogrammetry". *Cryosphere* 13.5, pp. 1513–1528. DOI: 10.5194/tc-13-1513-2019.

Davy, Richard and Stephen Outten (2020). "The Arctic surface climate in CMIP6: status and developments since CMIP5". *Journal of Climate* 33.18, pp. 8047–8068. DOI: https://doi.org/10.1175/JCLI-D-19-0990.1.

Dease, Peter W. and Thomas Simpson (1838). *An Account of the Recent Arctic Discoveries by Messrs. Dease and T. Simpson*. Vol. 8. Wiley on behalf of The Royal Geographical Society (with the Institute of British Geographers), pp. 213–225. URL: https://www.jstor.org/stable/1797798.

Dee, D. P. et al. (2011). "The ERA-Interim reanalysis: Configuration and performance of the data assimilation system". *Quarterly Journal of the Royal Meteorological Society* 137.656, pp. 553–597. DOI: 10.1002/qj.828.

Deser, Clara, John E. Walsh, and Michael S. Timlin (2000). "Arctic Sea Ice Variability in the Context of Recent Atmospheric Circulation Trends". *Journal of Climate* 13.3, pp. 617–633. DOI: 10.1175/1520-0442(2000)013<0617:ASIVIT>2.0.CO;2.

Ding, Qinghua, Axel Schweiger, Michelle L'Heureux, David S. Battisti, Stephen Po-Chedley, Nathaniel C. Johnson, Eduardo Blanchard-Wrigglesworth, Kirstin Harnos, Qin Zhang, Ryan Eastman, and Eric J. Steig (2017). "Influence of high-latitude atmospheric circulation changes on summertime Arctic sea ice". *Nature Climate Change* 7.4, pp. 289–295. DOI: 10.1038/nclimate3241.

Dobrynin, M., J. Murawsky, and S. Yang (2012). "Evolution of the global wind wave climate in CMIP5 experiments". *Geophysical Research Letters* 39.18. DOI: 10.1029/2012GL052843.

Dobrynin, Mikhail, Daniela I. V. Domeisen, Wolfgang A. Müller, Louisa Bell, Sebastian Brune, Felix Bunzel, André Düsterhus, Kristina Fröhlich, Holger Pohlmann, and Johanna Baehr (2018). "Improved Teleconnection-Based Dynamical Seasonal Predictions of Boreal Winter". *Geophysical Research Letters* 45.8, pp. 3605–3614. DOI: https://doi.org/10.1002/2018GL077209.

Dobrynin, Mikhail, Jens Murawski, Johanna Baehr, and Tatiana Ilyina (2015). "Detection and Attribution of Climate Change Signal in Ocean Wind Waves". *Journal of Climate* 28.4, pp. 1578–1591. DOI: 10.1175/JCLI-D-13-00664.1.

Docquier, D. and T. Koenigk (2021). "Observation-based selection of climate models projects Arctic ice-free summers around 2035". *Nature Communications Earth and Environment* 2.144. DOI: https://doi.org/10.1038/s43247-021-00214-7.

Edwards, Martin, Gregory Beaugrand, Pierre Helaouët, Jürgen Alheit, and Stephen Coombs (2013). "Marine ecosystem response to the Atlantic Multidecadal Oscillation". *PloS one* 8.2, e57212. DOI: https://doi.org/10.1371/journal.pone.0057212.

Emanuel, Kerry (2020). "The Relevance of Theory for Contemporary Research in Atmospheres, Oceans, and Climate". *AGU Advances* 1.2, e2019AV000129. DOI: https://doi.org/10.1029/2019AV000129.

Enfield, David B., Alberto M. Mestas-Nuñez, and Paul J. Trimble (2001). "The Atlantic Multidecadal Oscillation and its relation to rainfall and river flows in the continental U.S." *Geophysical Research Letters* 28.10, pp. 2077–2080. DOI: https://doi.org/10.1029/2000GL012745.

Esteves, Luciana S. (2018). "Erosion of Coastal Systems". In: *Encyclopedia of Coastal Science*. Ed. by Charles W. Finkl and Christopher Makowski. Cham: Springer International Publishing, pp. 1–12. DOI: 10.1007/978-3-319-48657-4_402-1.

Farquharson, Louise M, DH Mann, DK Swanson, BM Jones, RM Buzard, and JW Jordan (2018). "Temporal and spatial variability in coastline response to declining sea-ice in northwest Alaska". *Marine Geology* 404, pp. 71–83. DOI: https://doi.org/10.1016/j.margeo.2018.07.007.

Fofonova, V., A. Androsov, S. Danilov, M. Janout, E. Sofina, and K. Wiltshire (2014). "Semidiurnal tides in the Laptev Sea Shelf zone in the summer season". *Continental Shelf Research* 73, pp. 119–132. DOI: https://doi.org/10.1016/j.csr.2013.11.010.

Frederick, Jennifer, Alejandro Mota, Irina Tezaur, and Diana Bull (2021). "A thermo-mechanical terrestrial model of Arctic coastal erosion". *Journal of Computational*

and Applied Mathematics, p. 113533. DOI: https://doi.org/10.1016/j.cam.2021.113533.

Friedlingstein, P. et al. (2020). "Global Carbon Budget 2020". *Earth System Science Data* 12.4, pp. 3269–3340. DOI: 10.5194/essd-12-3269-2020.

Friedlingstein, Pierre, Peter Cox, Richard Betts, Laurent Bopp, Werner von Bloh, Victor Brovkin, Patricia Cadule, Scott Doney, Michael Eby, Inez Fung, et al. (2006). "Climate–carbon cycle feedback analysis: results from the C4MIP model intercomparison". *Journal of climate* 19.14, pp. 3337–3353. DOI: https://doi.org/10.1175/JCLI3800.1.

Fritz, Michael, Jorien E. Vonk, and Hugues Lantuit (2017). "Collapsing Arctic coastlines". *Nature Climate Change* 7.1, pp. 6–7. DOI: 10.1038/nclimate3188.

Fuchs, M., G. Grosse, J. Strauss, F. Günther, M. Grigoriev, G. M. Maximov, and G. Hugelius (2018). "Carbon and nitrogen pools in thermokarst-affected permafrost landscapes in Arctic Siberia". *Biogeosciences* 15.3, pp. 953–971. DOI: 10.5194/bg-15-953-2018.

Fuchs, Matthias, Josefine Lenz, Suzanne Jock, Ingmar Nitze, Benjamin M. Jones, Jens Strauss, Frank Günther, and Guido Grosse (2019). "Organic Carbon and Nitrogen Stocks Along a Thermokarst Lake Sequence in Arctic Alaska". *Journal of Geophysical Research: Biogeosciences* 124.5, pp. 1230–1247. DOI: https://doi.org/10.1029/2018JG004591.

Fuchs, Matthias, Ingmar Nitze, Jens Strauss, Frank Günther, Sebastian Wetterich, Alexander Kizyakov, Michael Fritz, Thomas Opel, Mikhail N. Grigoriev, Georgii T. Maksimov, and Guido Grosse (2020). "Rapid Fluvio-Thermal Erosion of a Yedoma Permafrost Cliff in the Lena River Delta". *Frontiers in Earth Science* 8, p. 336. DOI: 10.3389/feart.2020.00336. URL: https://www.frontiersin.org/article/10.3389/feart.2020.00336.

GAO, U.S. General Accounting Office (2003). *Alaska Native Villages: Most Are Affected by Flooding and Erosion, but Few Qualify for Federal Assistance*. Tech. rep. URL: https://www.gao.gov/products/gao-04-142.

GAO, U.S. General Accounting Office (2009). *Alaska Native Villages: Limited Progress Has Been Made on Relocating Villages Threatened by Flooding and Erosion*. Tech. rep. URL: https://www.gao.gov/products/gao-09-551.

Gibbs, A.E. and B.M. Richmond (2006). *Oblique aerial photography of the Arctic coast of Alaska, Nulavik to Demarcation Point*. Vol. 436. U.S. Geological Survey Data Series, p. 6. URL: https://pubs.usgs.gov/ds/436/.

Gong, Hainan, Lin Wang, Wen Chen, Xiaolong Chen, and Debashis Nath (2016). "Biases of the wintertime Arctic Oscillation in CMIP5 models". *Environmental Research Letters* 12.1, p. 014001. DOI: 10.1088/1748-9326/12/1/014001.

Goode, Erica and Josh Haner (2016). "A Wrenching Choice for Alaska Towns in the Path of Climate Change". *The New York Times*. URL: https://www.nytimes.com/interactive/2016/11/29/science/alaska-global-warming.html (visited on 06/18/2021).

Grigoriev, MN (2019). "Coastal retreat rates at the Laptev Sea key monitoring sites". *PANGAEA*. DOI: https://doi.org/10.1594/PANGAEA.905519.

Grotheer, H., V. Meyer, T. Riedel, G. Pfalz, L. Mathieu, J. Hefter, T. Gentz, H. Lantuit, G. Mollenhauer, and M. Fritz (2020). "Burial and Origin of Permafrost-Derived

Carbon in the Nearshore Zone of the Southern Canadian Beaufort Sea". *Geophysical Research Letters* 47.3, e2019GL085897.

Günther, F., P P Overduin, A V Sandakov, G Grosse, and M N Grigoriev (2013). "Short- and long-term thermo-erosion of ice-rich permafrost coasts in the Laptev Sea region". *Biogeosciences* 10.6, pp. 4297–4318. DOI: 10.5194/bg-10-4297-2013.

Günther, F, P P Overduin, I A Yakshina, T Opel, A V Baranskaya, and M N Grigoriev (2015). "Observing Muostakh disappear: Permafrost thaw subsidence and erosion of a ground-ice-rich Island in response to arctic summer warming and sea ice reduction". *Cryosphere* 9.1, pp. 151–178. DOI: 10.5194/tc-9-151-2015.

Hayes, Tryck Nyman and URS Corporation (2006). *Relocation Planning Project - Master Plan - Kivalina, Alaska*. Tech. rep. DACW85-03-D-0006-0003. URL: https://www.gao.gov/products/gao-09-551.

Henry, William and Joseph Banks (1803). "III. Experiments on the quantity of gases absorbed by water, at different temperatures, and under different pressures". *Philosophical Transactions of the Royal Society of London* 93, pp. 29–274. DOI: 10.1098/rstl.1803.0004.

Hequette, Arnaud and Peter W. Barnes (1990). "Coastal retreat and shoreface profile variations in the Canadian Beaufort Sea". *Marine Geology* 91.1, pp. 113–132. ISSN: 0025-3227. DOI: https://doi.org/10.1016/0025-3227(90)90136-8.

Hilton, Robert G, Valier Galy, Jérôme Gaillardet, Mathieu Dellinger, Charlotte Bryant, Matt O'Regan, Darren R Gröcke, Helen Coxall, Julien Bouchez, and Damien Calmels (2015). "Erosion of organic carbon in the Arctic as a geological carbon dioxide sink". *Nature* 524.7563, pp. 84–87. DOI: https://doi.org/10.1038/nature14653.

Holloway, Greg and Andrey Proshutinsky (2007). "Role of tides in Arctic ocean/ice climate". *Journal of Geophysical Research: Oceans* 112.C4. DOI: https://doi.org/10.1029/2006JC003643.

Hoque, Md. Azharul and Wayne H. Pollard (2009). "Arctic coastal retreat through block failure". *Canadian Geotechnical Journal* 46.10, pp. 1103–1115. DOI: 10.1139/T09-058.

Hošeková, Lucia, Mika P. Malila, W. Erick Rogers, Lettie A. Roach, Emily Eidam, Luc Rainville, Nirnimesh Kumar, and Jim Thomson (2020). "Attenuation of Ocean Surface Waves in Pancake and Frazil Sea Ice Along the Coast of the Chukchi Sea". *Journal of Geophysical Research: Oceans* 125.12, e2020JC016746. DOI: https://doi.org/10.1029/2020JC016746.

Hugelius, G. et al. (2013). "A new data set for estimating organic carbon storage to 3 m depth in soils of the northern circumpolar permafrost region". *Earth System Science Data* 5.2, pp. 393–402. DOI: https://doi.org/10.5194/essd-5-393-2013.

Huissteden, Jan van (2020). *Thawing Permafrost. Thawing Permafrost*. Springer Nature Switzerland AG 2020. DOI: https://doi.org/10.1007/978-3-030-31379-1.

Humborg, Christoph, Marc C. Geibel, Leif G. Anderson, Göran Björk, Carl-Magnus Mörth, Marcus Sundbom, Brett F. Thornton, Barbara Deutsch, Erik Gustafsson, Bo Gustafsson, Jörgen Ek, and Igor Semiletov (2017). "Sea-air exchange patterns along the central and outer East Siberian Arctic Shelf as inferred from continuous CO2, stable isotope, and bulk chemistry measurements". *Global Biogeochemical Cycles* 31.7, pp. 1173–1191. DOI: https://doi.org/10.1002/2017GB005656.

Ilyina, Tatiana, Katharina D. Six, Joachim Segschneider, Ernst Maier-Reimer, Hongmei Li, and Ismael Núñez-Riboni (2013). "Global ocean biogeochemistry model HAMOCC: Model architecture and performance as component of the MPI-Earth system model in different CMIP5 experimental realizations". *Journal of Advances in Modeling Earth Systems* 5.2, pp. 287–315. DOI: https://doi.org/10.1029/2012MS000178.

IPCC (2013). *Summary for policymakers*. Tech. rep. Cambridge, UK: Cambridge. URL: https://www.ipcc.ch/site/assets/uploads/2018/02/WG1AR5_SPM_FINAL.pdf.

Irrgang, Anna M., Hugues Lantuit, Gavin K. Manson, Frank Günther, Guido Grosse, and Pier Paul Overduin (2018). "Variability in Rates of Coastal Change Along the Yukon Coast, 1951 to 2015". *Journal of Geophysical Research: Earth Surface* 123.4, pp. 779–800. DOI: 10.1002/2017JF004326.

Itkin, Polona and Thomas Krumpen (2017). "Winter sea ice export from the Laptev Sea preconditions the local summer sea ice cover and fast ice decay". *Cryosphere* 11.5, pp. 2383–2391. DOI: 10.5194/tc-11-2383-2017.

Jensen, A. (2020). "Critical information for the study of ecodynamics and socio-natural systems: Rescuing endangered heritage and data from Arctic Alaskan Coastal sites". *Quaternary International* 549, pp. 227–238. DOI: https://doi.org/10.1016/j.quaint.2019.05.001.

Jin-Qing, Zuo, Li Wei-Jing, and Ren Hong-Li (2013). "Representation of the Arctic Oscillation in the CMIP5 Models". *Advances in Climate Change Research* 4.4, pp. 242–249. DOI: https://doi.org/10.3724/SP.J.1248.2013.242.

Jones B. M. Irrgang A. M., Farquharson A. M. et al. (2020). "Coastal Permafrost Erosion". In: *Arctic Report Card 2020*. Ed. by Frey K. E. et al. DOI: https://doi.org/10.25923/e47w-dw52.

Jones, B M, C D Arp, M T Jorgenson, K M Hinkel, J A Schmutz, and P L Flint (2009). "Increase in the rate and uniformity of coastline erosion in Arctic Alaska". *Geophysical Research Letters* 36.3. DOI: 10.1029/2008GL036205.

Jones, Benjamin M., Kenneth M. Hinkel, Christopher D. Arp, and Wendy R. Eisner (2008). "Modern Erosion Rates and Loss of Coastal Features and Sites, Beaufort Sea Coastline, Alaska". *Arctic* 61.4, pp. 361–372. DOI: https://doi.org/10.14430/ARCTIC44.

Jones, Benjamin M. et al. (2018). "A decade of remotely sensed observations highlight complex processes linked to coastal permafrost bluff erosion in the Arctic". *Environ. Res. Lett.* 13.11, p. 115001. DOI: 10.1088/1748-9326/aae471.

Jong, Dirk, Lisa Bröder, George Tanski, Michael Fritz, Hugues Lantuit, Tommaso Tesi, Negar Haghipour, Timothy I. Eglinton, and Jorien E. Vonk (2020). "Nearshore Zone Dynamics Determine Pathway of Organic Carbon From Eroding Permafrost Coasts". *Geophysical Research Letters* 47.15, e2020GL088561. DOI: https://doi.org/10.1029/2020GL088561.

Jongejans, L. L., J. Strauss, J. Lenz, F. Peterse, K. Mangelsdorf, M. Fuchs, and G. Grosse (2018). "Organic matter characteristics in yedoma and thermokarst deposits on Baldwin Peninsula, west Alaska". *Biogeosciences* 15.20, pp. 6033–6048. DOI: 10.5194/bg-15-6033-2018.

Kaleschke, L., C. Lüpkes, T. Vihma, J. Haarpaintner, A. Bochert, J. Hartmann, and G. Heygster (2001). "SSM/I Sea Ice Remote Sensing for Mesoscale Ocean-Atmosphere

Interaction Analysis". *Canadian Journal of Remote Sensing* 27.5, pp. 526–537. DOI: 10.1080/07038992.2001.10854892.

Kerr, Richard A (2000). "A North Atlantic climate pacemaker for the centuries". *Science* 288.5473, pp. 1984–1985. DOI: 10.1126/science.288.5473.1984.

Klein, Konstantin P, Hugues Lantuit, Birgit Heim, Frank Fell, David Doxaran, and Anna M Irrgang (2019). "Long-term high-resolution sediment and sea surface temperature spatial patterns in Arctic nearshore waters retrieved using 30-year landsat archive imagery". *Remote Sensing* 11.23, p. 2791. DOI: https://doi.org/10.3390/rs11232791.

Kleinen, Thomas and Victor Brovkin (2018). "Pathway-dependent fate of permafrost region carbon". *Environmental Research Letters* 13.9, p. 094001. DOI: https://doi.org/10.1088/1748-9326/aad824.

Knight, Jeff R., Chris K. Folland, and Adam A. Scaife (2006). "Climate impacts of the Atlantic Multidecadal Oscillation". *Geophysical Research Letters* 33.17. DOI: https://doi.org/10.1029/2006GL026242.

Kobayashi, N., J. C. Vidrine, R. B. Nairn, and S. M. Soloman (1999). "Erosion of Frozen Cliffs Due to Storm Surge on Beaufort Sea Coast". *Journal of Coastal Research* 15.2, pp. 332–344. URL: http://www.jstor.org/stable/4298946.

Kobayashi, Nobuhisa (1985). "Formation of thermoerosional niches into frozen bluffs due to storm surges on the Beaufort Sea coast". *Journal of Geophysical Research: Oceans* 90.C6, pp. 11983–11988. DOI: https://doi.org/10.1029/JC090iC06p11983.

Kosaka, Yu and Shang-Ping Xie (2013). "Recent global-warming hiatus tied to equatorial Pacific surface cooling". *Nature* 501.7467, pp. 403–407. DOI: https://doi.org/10.1038/nature12534.

Koul, Vimal, Camilla Sguotti, Marius Årthun, Sebastian Brune, André Düsterhus, Bjarte Bogstad, Geir Ottersen, Johanna Baehr, and Corinna Schrum (2021). "Skilful prediction of cod stocks in the North and Barents Sea a decade in advance". DOI: https://doi.org/10.1038/s43247-021-00207-6.

Koven, Charles D, William J Riley, and Alex Stern (2013). "Analysis of permafrost thermal dynamics and response to climate change in the CMIP5 Earth System Models". *Journal of Climate* 26.6, pp. 1877–1900. DOI: https://doi.org/10.1175/JCLI-D-12-00228.1.

Kriest, I. and A. Oschlies (2008). "On the treatment of particulate organic matter sinking in large-scale models of marine biogeochemical cycles". *Biogeosciences* 5.1, pp. 55–72. DOI: 10.5194/bg-5-55-2008.

Krumpen, T, M Janout, K I Hodges, R Gerdes, F Girard-Ardhuin, J A Hölemann, and S Willmes (2013). "Variability and trends in Laptev Sea ice outflow between 1992-2011". *Cryosphere* 7.1, pp. 349–363. DOI: 10.5194/tc-7-349-2013.

Lacroix, F., T. Ilyina, and J. Hartmann (2020). "Oceanic CO_2 outgassing and biological production hotspots induced by pre-industrial river loads of nutrients and carbon in a global modeling approach". *Biogeosciences* 17.1, pp. 55–88. DOI: 10.5194/bg-17-55-2020.

Landrum, Laura and Marika M Holland (2020). "Extremes become routine in an emerging new Arctic". *Nature Climate Change*, pp. 1–8. DOI: https://doi.org/10.1038/s41558-020-0892-z.

Lantuit, H. and W.H. Pollard (2008). "Fifty years of coastal erosion and retrogressive thaw slump activity on Herschel Island, southern Beaufort Sea, Yukon Territory,

Canada". *Geomorphology* 95.1, pp. 84–102. DOI: https://doi.org/10.1016/j.geomorph.2006.07.040.

Lantuit, Hugues (2008). "The modification of arctic permafrost coastlines". doctoralthesis. Potsdam, Germany: Universität Potsdam. URL: http://opus.kobv.de/ubp/volltexte/2008/1973/.

Lantuit, Hugues, David Atkinson, Pier Paul Overduin, Mikhail Grigoriev, Volker Rachold, Guido Grosse, and Hans Wolfgang Hubberten (2011). "Coastal erosion dynamics on the permafrost-dominated Bykovsky Peninsula, north Siberia, 1951-2006". *Polar Research* 30.SUPPL.1. DOI: 10.3402/polar.v30i0.7341.

Lantuit, Hugues et al. (2012). "The Arctic Coastal Dynamics Database: A New Classification Scheme and Statistics on Arctic Permafrost Coastlines". *Estuaries and Coasts* 35.2, pp. 383–400. DOI: 10.1007/s12237-010-9362-6.

Lantz, Trevor C. and Steven V. Kokelj (2008). "Increasing rates of retrogressive thaw slump activity in the Mackenzie Delta region, N.W.T., Canada". *Geophysical Research Letters* 35.6. DOI: https://doi.org/10.1029/2007GL032433.

Larsen, Joan Nymand, Peter Schweitzer, Khaled Abass, Natalia Doloisio, Susanna Gartler, Thomas Ingeman-Nielsen, Jón Haukur Ingimundarson, Leneisja Jungsberg, Alexandra Meyer, Arja Rautio, et al. (2021). "Thawing permafrost in arctic coastal communities: A framework for studying risks from climate change". *Sustainability* 13.5, p. 2651. DOI: https://doi.org/10.3390/su13052651.

Laruelle, Goulven G., Ronny Lauerwald, Benjamin Pfeil, and Pierre Regnier (2014). "Regionalized global budget of the CO2 exchange at the air-water interface in continental shelf seas". *Global Biogeochemical Cycles* 28.11, pp. 1199–1214. DOI: https://doi.org/10.1002/2014GB004832.

Lavelle, J. W., H. O. Mofjeld, and E. T. Baker (1984). "An in situ erosion rate for a fine-grained marine sediment". *Journal of Geophysical Research: Oceans* 89.C4, pp. 6543–6552. DOI: https://doi.org/10.1029/JC089iC04p06543.

Leffingwell, Ernest de Koven (1908). "Flaxman Island, a Glacial Remnant". *The Journal of Geology* 16.1, pp. 55–63. URL: https://www.jstor.org/stable/30063850.

Leffingwell, Ernest de Koven (1919). *The Canning River region, northern Alaska*. United States Geological Survey, p. 251. URL: https://doi.org/10.3133/pp109.

Lim, Michael, Dustin Whalen, Paul J. Mann, Paul Fraser, Heather Bay Berry, Charlotte Irish, Kendyce Cockney, and John Woodward (2020). "Effective Monitoring of Permafrost Coast Erosion: Wide-scale Storm Impacts on Outer Islands in the Mackenzie Delta Area". *Frontiers in Earth Science* 8, p. 454. DOI: 10.3389/feart.2020.561322.

Madrigal-González, Jaime, Juan A Ballesteros-Cánovas, Asier Herrero, Paloma Ruiz-Benito, Markus Stoffel, Manuel E Lucas-Borja, Enrique Andivia, Cesar Sancho-Garcıa, and Miguel A Zavala (2017). "Forest productivity in southwestern Europe is controlled by coupled North Atlantic and Atlantic Multidecadal Oscillations". *Nature communications* 8.1, pp. 1–8. DOI: https://doi.org/10.1038/s41467-017-02319-0.

Manizza, M., M. J. Follows, S. Dutkiewicz, D. Menemenlis, J. W. McClelland, C. N. Hill, B. J. Peterson, and R. M. Key (2011). "A model of the Arctic Ocean carbon cycle". *Journal of Geophysical Research: Oceans* 116.C12. DOI: https://doi.org/10.1029/2011JC006998.

Manizza, Manfredi, Dimitris Menemenlis, Hong Zhang, and Charles E. Miller (2019). "Modeling the Recent Changes in the Arctic Ocean CO2 Sink (2006–2013)". *Global Biogeochemical Cycles* 33.3, pp. 420–438. DOI: https://doi.org/10.1029/2018GB006070.

Mann, Michael E, Byron A Steinman, Daniel J Brouillette, and Sonya K Miller (2021). "Multidecadal climate oscillations during the past millennium driven by volcanic forcing". *Science* 371.6533, pp. 1014–1019. DOI: https://doi.org/10.1126/science.abc5810.

Mann, Michael E, Byron A Steinman, and Sonya K Miller (2020). "Absence of internal multidecadal and interdecadal oscillations in climate model simulations". *Nature communications* 11.1, pp. 1–9. DOI: https://doi.org/10.1038/s41467-019-13823-w.

Martin, John H, George A Knauer, David M Karl, and William W Broenkow (1987). "VERTEX: carbon cycling in the northeast Pacific". *Deep Sea Research Part A. Oceanographic Research Papers* 34.2, pp. 267–285.

Mauritsen, Thorsten et al. (2019). "Developments in the MPI-M Earth System Model version 1.2 (MPI-ESM1.2) and Its Response to Increasing CO2". *Journal of Advances in Modeling Earth Systems* 11.4, pp. 998–1038. DOI: https://doi.org/10.1029/2018MS001400.

McGuire, A. David et al. (2018). "Dependence of the evolution of carbon dynamics in the northern permafrost region on the trajectory of climate change". *Proceedings of the National Academy of Sciences* 115.15, pp. 3882–3887. DOI: 10.1073/pnas.1719903115.

Milfont, Taciano L, Laurel Evans, Chris G Sibley, Jan Ries, and Andrew Cunningham (2014). "Proximity to coast is linked to climate change belief". *PLoS One* 9.7, e103180. DOI: https://doi.org/10.1371/journal.pone.0103180.

Mooney, Chris (2015). "The remote Alaskan village that needs to be relocated due to climate change". *The Washington Post*. URL: https://www.washingtonpost.com/news/energy-environment/wp/2015/02/24/the-remote-alaskan-village-that-needs-to-be-relocated-due-to-climate-change/ (visited on 06/18/2021).

Nicholls, Robert J and Anny Cazenave (2010). "Sea-level rise and its impact on coastal zones". *science* 328.5985, pp. 1517–1520. DOI: 10.1126/science.1185782.

Nicu, I., L. Rubensdotter, K. Stalsberg, and Erich Nau (2021). "Coastal Erosion of Arctic Cultural Heritage in Danger: A Case Study from Svalbard, Norway". *Water* 13, p. 784. DOI: https://doi.org/10.3390/w13060784.

Nielsen, David Marcolino, Mikhail Dobrynin, Johanna Baehr, Sergey Razumov, and Mikhail Grigoriev (2020). "Coastal erosion variability at the southern Laptev Sea linked to winter sea ice and the Arctic Oscillation". *Geophysical Research Letters* 47.5, e2019GL086876. DOI: 10.1029/2019GL086876.

Nielsen, David Marcolino, Patrick Pieper, Armineh Barkhordarian, Paul Overduin, Victor Brovkin, Tatiana Ilyina, Johanna Baehr, and Mikhail Dobrynin (2021). "Projected increase of Arctic coastal erosion and its sensitivity to warming in the 21st Century". *Under review*. Preprint available at Research Square. DOI: 10.21203/rs.3.rs-634673/v1.

North, G. R., T. L. Bell, and R. F. Cahalan (1982). "Sampling Errors in the Estimation of Empirical Orthogonal Functions". *Monthly Weather Review* 110.7, pp. 669–706. DOI: https://doi.org/10.1175/1520-0493(1982)110<0699:SEITEO>2.0.CO;2.

Notz, Dirk and SIMIP Community (2020). "Arctic Sea Ice in CMIP6". *Geophysical Research Letters* 47.10. DOI: https://doi.org/10.1029/2019GL086749.

Notz, Dirk and Julienne Stroeve (2016). "Observed Arctic sea-ice loss directly follows anthropogenic CO2 emission". *Science* 354.6313, pp. 747–750. DOI: 10.1126/science.aag2345.

O'Neill, B. C., C. Tebaldi, D. P. van Vuuren, V. Eyring, P. Friedlingstein, G. Hurtt, R. Knutti, E. Kriegler, J.-F. Lamarque, J. Lowe, G. A. Meehl, R. Moss, K. Riahi, and B. M. Sanderson (2016). "The Scenario Model Intercomparison Project (ScenarioMIP) for CMIP6". *Geoscientific Model Development* 9.9, pp. 3461–3482. DOI: 10.5194/gmd-9-3461-2016.

Oertel, George F. (2005). "Coasts, Coastlines, Shores, and Shorelines". In: *Encyclopedia of Coastal Science*. Ed. by Maurice L. Schwartz. Dordrecht: Springer Netherlands, pp. 323–327. DOI: 10.1007/1-4020-3880-1_94.

Ogi, Masayo, Ignatius G. Rigor, Miles G. McPhee, and John M. Wallace (2008). "Summer retreat of Arctic sea ice: Role of summer winds". *Geophysical Research Letters* 35.24, p. L24701. DOI: 10.1029/2008GL035672.

Ogi, Masayo, Søren Rysgaard, and David G Barber (2016). "Importance of combined winter and summer Arctic Oscillation (AO) on September sea ice extent". *Environmental Research Letters* 11.3, p. 034019. DOI: 10.1088/1748-9326/11/3/034019.

Ogi, Masayo, Koji Yamazaki, and Yoshihiro Tachibana (2004). "The summertime annular mode in the Northern Hemisphere and its linkage to the winter mode". *Journal of Geophysical Research* 109.D20, p. D20114. DOI: 10.1029/2004JD004514.

Ogorodov, Stanislav, Daria Aleksyutina, Alisa Baranskaya, Nataliya Shabanova, and Olga Shilova (2020). "Coastal Erosion of the Russian Arctic: An Overview". *Journal of Coastal Research* 95.sp1, pp. 599–604. DOI: 10.2112/SI95-117.1.

Otterå, Odd Helge, Mats Bentsen, Helge Drange, and Lingling Suo (2010). "External forcing as a metronome for Atlantic multidecadal variability". *Nature Geoscience* 3.10, pp. 688–694. DOI: https://doi.org/10.1038/ngeo955.

Overduin, P. P., M. C. Strzelecki, M. N. Grigoriev, N. Couture, H. Lantuit, D. St-Hilaire-Gravel, F. Günther, and S. Wetterich (2014). "Coastal changes in the Arctic". *Geological Society, London, Special Publications* 388.1, pp. 103–129. DOI: 10.1144/SP388.13.

Overduin, P. P., S. Wetterich, F. Günther, M. N. Grigoriev, G. Grosse, L. Schirrmeister, H.-W. Hubberten, and A. Makarov (2016). "Coastal dynamics and submarine permafrost in shallow water of the central Laptev Sea, East Siberia". *The Cryosphere* 10.4, pp. 1449–1462. DOI: 10.5194/tc-10-1449-2016.

Overeem, Irina, Robert S Anderson, Cameron W Wobus, Gary D Clow, Frank E Urban, and Nora Matell (2011). "Sea ice loss enhances wave action at the Arctic coast". *Geophysical Research Letters* 38.17, p. 17503. DOI: 10.1029/2011GL048681.

Palmer, T. N. (2016). "A personal perspective on modelling the climate system". *Proceedings of the Royal Society A: Mathematical, Physical and Engineering Sciences* 472.2188, p. 20150772. DOI: 10.1098/rspa.2015.0772.

Pavlidis, Yu. A., I. O. Leont'ev, S. L. Nikiforov, F. Rahold, M. N. Grigor'ev, S. R. Razumov, and A. A. Vasil'ev (2007). "General forecast of the evolution of the coastal zone of the Eurasian Arctic seas in the 21st century". *Oceanology* 47.1, pp. 116–126. DOI: 10.1134/s0001437007010146.

Perovich, Donald K., Bonnie Light, Hajo Eicken, Kathleen F. Jones, Kay Runciman, and Son V. Nghiem (2007). "Increasing solar heating of the Arctic Ocean and adjacent seas, 1979–2005: Attribution and role in the ice-albedo feedback". *Geophysical Research Letters* 34.19. DOI: https://doi.org/10.1029/2007GL031480.

Pihl, Erik, Eva Alfredsson, Magnus Bengtsson, Kathryn J Bowen, Vanesa Castan Broto, Kuei Tien Chou, Helen Cleugh, Kristie Ebi, Clea M Edwards, Eleanor Fisher, and et al. (2021). "10 New Insights in Climate Science 2020 - a Horizon Scan". *Global Sustainability* 4, pp. 1–65. DOI: 10.1017/sus.2021.2.

Pohlmann, Holger, Frank Sienz, and Mojib Latif (2006). "Influence of the multidecadal Atlantic meridional overturning circulation variability on European climate". *Journal of climate* 19.23, pp. 6062–6067.

Poli, Paul, Hans Hersbach, Dick P Dee, Paul Berrisford, Adrian J Simmons, Frédéric Vitart, Patrick Laloyaux, David G.H. Tan, Carole Peubey, Jean Noël Thépaut, Yannick Trémolet, Elías V Hólm, Massimo Bonavita, Lars Isaksen, and Michael Fisher (2016). "ERA-20C: An atmospheric reanalysis of the twentieth century". *Journal of Climate* 29.11, pp. 4083–4097. DOI: 10.1175/JCLI-D-15-0556.1.

Ramage, Justine L., Anna M. Irrgang, Ulrike Herzschuh, Anne Morgenstern, Nicole Couture, and Hugues Lantuit (2017). "Terrain controls on the occurrence of coastal retrogressive thaw slumps along the Yukon Coast, Canada". *Journal of Geophysical Research: Earth Surface* 122.9, pp. 1619–1634. DOI: https://doi.org/10.1002/2017JF004231.

Ravens, Thomas M., Benjamin M. Jones, Jinlin Zhang, Christopher D. Arp, and Joel A. Schmutz (2012). "Process-Based Coastal Erosion Modeling for Drew Point, North Slope, Alaska". *Journal of Waterway, Port, Coastal, and Ocean Engineering* 138.2, pp. 122–130. DOI: 10.1061/(asce)ww.1943-5460.0000106.

Redfield, Alfred Clarence (1934). *On the proportions of organic derivatives in sea water and their relation to the composition of plankton*. Vol. 1. University Press of Liverpool Liverpool.

Rigor, Ignatius G, John M Wallace, and Roger L Colony (2002). "Response of sea ice to the Arctic Oscillation". *Journal of Climate* 15.18, pp. 2648–2663. DOI: https://doi.org/10.1175/1520-0442(2002)015<2648:ROSITT>2.0.CO;2.

Rivero-Calle, Sara, Anand Gnanadesikan, Carlos E Del Castillo, William M Balch, and Seth D Guikema (2015). "Multidecadal increase in North Atlantic coccolithophores and the potential role of rising CO2". *Science* 350.6267, pp. 1533–1537. DOI: 10.1126/science.aaa8026.

Rolph, R., P. P. Overduin, T. Ravens, H. Lantuit, and M. Langer (2021). "ArcticBeach v1.0: A physics-based parameterization of pan-Arctic coastline erosion". *Geoscientific Model Development Discussions* 2021, pp. 1–26. DOI: 10.5194/gmd-2021-28.

Rossi, Marcello (2019). "Surrendering to the sea by choice". *Nature Climate Change* 9, pp. 904–905. DOI: https://doi.org/10.1038/s41558-019-0655-x.

Russell-Head, D. S. (1980). "The Melting of Free-Drifting Icebergs". *Annals of Glaciology* 1, pp. 119–122. DOI: 10.3189/S0260305500017092.

Sakakibara, Chie (2008). ""Our home is drowning": Iñupiat storitelling and climate change in Point Hope, Alaska". *Geographical Review* 98.4, pp. 456–475. DOI: https://doi.org/10.1111/j.1931-0846.2008.tb00312.x.

Sakur, Stephen (2013). "The Alaskan village set to disappear under water in a decade". *BBC News*. URL: https://www.bbc.com/news/magazine-23346370 (visited on 06/26/2021).

Sánchez-García, Laura, Vanja Alling, Svetlana Pugach, Jorien Vonk, Bart van Dongen, Christoph Humborg, Oleg Dudarev, Igor Semiletov, and Örjan Gustafsson (2011). "Inventories and behavior of particulate organic carbon in the Laptev and East Siberian seas". *Global Biogeochemical Cycles* 25.2. DOI: https://doi.org/10.1029/2010GB003862.

Schaefer, Kevin, Hugues Lantuit, Vladimir E. Romanovsky, Edward A.G. Schuur, and Ronald Witt (2014). "The impact of the permafrost carbon feedback on global climate". *Environmental Research Letters* 9.8. DOI: 10.1088/1748-9326/9/8/085003.

Schirojan, Danial E. (2021). "Predictability of coastal erosion in the Laptev Sea using the Max Planck Institute Earth System Model". Bachelor's thesis in Geophysics/Oceanography. Hamburg, Germany: Universität Hamburg.

Schirrmeister, L., V. Kunitsky, G. Grosse, S. Wetterich, H. Meyer, G. Schwamborn, O. Babiy, A. Derevyagin, and C. Siegert (2011). "Sedimentary characteristics and origin of the Late Pleistocene Ice Complex on north-east Siberian Arctic coastal lowlands and islands – A review". *Quaternary International* 241.1, pp. 3–25. DOI: https://doi.org/10.1016/j.quaint.2010.04.004.

Schuur, Edward A. G., Jason G. Vogel, Kathryn G. Crummer, Hanna Lee, James O. Sickman, and T. E. Osterkamp (2009). "The effect of permafrost thaw on old carbon release and net carbon exchange from tundra". *Nature* 459.7246, pp. 556–559. DOI: 10.1038/nature08031.

Schuur, Edward AG, A David McGuire, C Schädel, Guido Grosse, JW Harden, Daniel J Hayes, Gustaf Hugelius, Charles D Koven, Peter Kuhry, David M Lawrence, et al. (2015). "Climate change and the permafrost carbon feedback". *Nature* 520.7546, pp. 171–179. DOI: https://doi.org/10.1038/nature14338.

Schwalm, Christopher R., Spencer Glendon, and Philip B. Duffy (2020). "RCP8.5 tracks cumulative CO_2 emissions". *Proceedings of the National Academy of Sciences* 117.33, pp. 19656–19657. DOI: 10.1073/pnas.2007117117.

Serreze, M. C., A. P. Barrett, J. C. Stroeve, D. N. Kindig, and M. M. Holland (Feb. 2009). "The emergence of surface-based Arctic amplification". *The Cryosphere* 3.1, pp. 11–19. DOI: 10.5194/tc-3-11-2009.

Sharples, Jonathan, Jack J. Middelburg, Katja Fennel, and Timothy D. Jickells (2017). "What proportion of riverine nutrients reaches the open ocean?" *Global Biogeochemical Cycles* 31.1, pp. 39–58. DOI: https://doi.org/10.1002/2016GB005483.

Shu, Qi, Qiang Wang, Zhenya Song, Fangli Qiao, Jiechen Zhao, Min Chu, and Xinfang Li (2020). "Assessment of Sea Ice Extent in CMIP6 With Comparison to Observations and CMIP5". *Geophysical Research Letters* 47.9, e2020GL087965. DOI: https://doi.org/10.1029/2020GL087965.

Steinman, Byron A, Michael E Mann, and Sonya K Miller (2015). "Atlantic and Pacific multidecadal oscillations and Northern Hemisphere temperatures". *Science* 347.6225, pp. 988–991. DOI: 10.1126/science.1257856.

Stevens, Bjorn, Masaki Satoh, Ludovic Auger, Joachim Biercamp, Christopher S Bretherton, Xi Chen, Peter Düben, Falko Judt, Marat Khairoutdinov, Daniel Klocke, et al. (2019). "DYAMOND: the DYnamics of the Atmospheric general circulation

Modeled On Non-hydrostatic Domains". *Progress in Earth and Planetary Science* 6.1, pp. 1–17. DOI: https://doi.org/10.1186/s40645-019-0304-z.

Strauss, Jens, Lutz Schirrmeister, Guido Grosse, Sebastian Wetterich, Mathias Ulrich, Ulrike Herzschuh, and Hans-Wolfgang Hubberten (2013). "The deep permafrost carbon pool of the Yedoma region in Siberia and Alaska". *Geophysical Research Letters* 40.23, pp. 6165–6170. DOI: https://doi.org/10.1002/2013GL058088.

Stroeve, Julienne and Dirk Notz (2018). "Changing state of Arctic sea ice across all seasons". *Environmental Research Letters* 13.10, p. 103001. DOI: 10.1088/1748-9326/aade56.

Takahashi, Taro, Wallace S. Broecker, and Sara Langer (1985). "Redfield ratio based on chemical data from isopycnal surfaces". *Journal of Geophysical Research: Oceans* 90.C4, pp. 6907–6924. DOI: https://doi.org/10.1029/JC090iC04p06907.

Tanski, G, D Wagner, C Knoblauch, M Fritz, T Sachs, and H Lantuit (2019). "Rapid CO_2 release from eroding permafrost in seawater". *Geophysical Research Letters*, pp. 1–17. DOI: 10.1029/2019GL084303.

Tanski, George, Lisa Bröder, Dirk Wagner, Christian Knoblauch, Hugues Lantuit, Christian Beer, Torsten Sachs, Michael Fritz, Tommaso Tesi, Boris P. Koch, Negar Haghipour, Timothy I. Eglinton, Jens Strauss, and Jorien E. Vonk (2021). "Permafrost Carbon and CO2 Pathways Differ at Contrasting Coastal Erosion Sites in the Canadian Arctic". *Frontiers in Earth Science* 9, p. 207. DOI: 10.3389/feart.2021.630493.

Tanski, George, Nicole Couture, Hugues Lantuit, Antje Eulenburg, and Michael Fritz (2016). "Eroding permafrost coasts release low amounts of dissolved organic carbon (DOC) from ground ice into the nearshore zone of the Arctic Ocean". *Global Biogeochemical Cycles* 30.7, pp. 1054–1068. DOI: https://doi.org/10.1002/2015GB005337.

Tarnocai, C., J. G. Canadell, E. A. G. Schuur, P. Kuhry, G. Mazhitova, and S. Zimov (2009). "Soil organic carbon pools in the northern circumpolar permafrost region". *Global Biogeochemical Cycles* 23.2. DOI: https://doi.org/10.1029/2008GB003327.

Terhaar, J., J. C. Orr, C. Ethé, P. Regnier, and L. Bopp (2019). "Simulated Arctic Ocean Response to Doubling of Riverine Carbon and Nutrient Delivery". *Global Biogeochemical Cycles* 33.8, pp. 1048–1070. DOI: https://doi.org/10.1029/2019GB006200.

Terhaar, Jens, Ronny Lauerwald, Pierre Regnier, Nicolas Gruber, and Laurent Bopp (2021). "Around one third of current Arctic Ocean primary production sustained by rivers and coastal erosion". *Nature Communications* 12.169. DOI: https://doi.org/10.1038/s41467-020-20470-z.

The WAMDI Group (1988). "The WAM Model—A Third Generation Ocean Wave Prediction Model". *Journal of Physical Oceanography* 18.12, pp. 1775–1810.

Thomas, Matthew A., Alejandro Mota, Benjamin M. Jones, R. Charles Choens, Jennifer M. Frederick, and Diana L. Bull (2020). "Geometric and Material Variability Influences Stress States Relevant to Coastal Permafrost Bluff Failure". *Frontiers in Earth Science* 8, p. 143. DOI: 10.3389/feart.2020.00143.

Thompson, Andrea (2017). "Alaska's Coast Is Vanishing, 1 Storm at a Time". *Scientific American*. URL: https://www.scientificamerican.com/article/alaskas-coast-is-vanishing-1-storm-at-a-time/ (visited on 06/26/2021).

Thompson, David W. J. and John M. Wallace (2001). "Regional Climate Impacts of the Northern Hemisphere Annular Mode". *Science* 293.5527, pp. 85–89. DOI: 10.1126/science.1058958.

Thompson, David W.J. and John M Wallace (2000). "Annular Modes in the Extratropical Circulation. Part I: Month-to-Month Variability*". *Journal of Climate* 13.5, pp. 1000–1016. DOI: https://doi.org/10.1175/1520-0442(2000)013<1000:AMITEC>2.0.CO;2.

Thompson, David W.J. and John M. Wallace (1998). "The Arctic oscillation signature in the wintertime geopotential height and temperature fields". *Geophysical Research Letters* 25.9, pp. 1297–1300. DOI: 10.1029/98GL00950.

Ting, Mingfang, Yochanan Kushnir, Richard Seager, and Cuihua Li (2011). "Robust features of Atlantic multi-decadal variability and its climate impacts". *Geophysical Research Letters* 38.17. DOI: https://doi.org/10.1029/2011GL048712.

Turetsky, Merritt R, Benjamin W Abbott, Miriam C Jones, Katey Walter Anthony, David Olefeldt, Edward AG Schuur, Guido Grosse, Peter Kuhry, Gustaf Hugelius, Charles Koven, et al. (2020). "Carbon release through abrupt permafrost thaw". *Nature Geoscience* 13.2, pp. 138–143. DOI: https://doi.org/10.1038/s41561-019-0526-0.

Turetsky, Merritt R, Benjamin W Abbott, Miriam C Jones, Katey Walter Anthony, David Olefeldt, Edward AG Schuur, Charles Koven, A David McGuire, Guido Grosse, Peter Kuhry, et al. (2019). "Permafrost collapse is accelerating carbon release". DOI: https://doi.org/10.1038/d41586-019-01313-4.

Vancoppenolle, Martin, Laurent Bopp, Gurvan Madec, John Dunne, Tatiana Ilyina, Paul R Halloran, and Nadja Steiner (2013). "Future Arctic Ocean primary productivity from CMIP5 simulations: Uncertain outcome, but consistent mechanisms". *Global Biogeochemical Cycles* 27.3, pp. 605–619. DOI: https://doi.org/10.1002/gbc.20055.

Vonk, J E, L. Sanchez-Garca, B E Van Dongen, V Alling, D Kosmach, A Charkin, I P Semiletov, O V Dudarev, N Shakhova, P Roos, T I Eglinton, A Andersson, and A. Gustafsson (2012). "Activation of old carbon by erosion of coastal and subsea permafrost in Arctic Siberia". *Nature* 489.7414, pp. 137–140. DOI: 10.1038/nature11392.

Vonk, Jorien E., Paul J. Mann, Sergey Davydov, Anna Davydova, Robert G. M. Spencer, John Schade, William V. Sobczak, Nikita Zimov, Sergei Zimov, Ekaterina Bulygina, Timothy I. Eglinton, and Robert M. Holmes (2013). "High biolability of ancient permafrost carbon upon thaw". *Geophysical Research Letters* 40.11, pp. 2689–2693. DOI: https://doi.org/10.1002/grl.50348.

Vonk, Jorien E., Igor P. Semiletov, Oleg V. Dudarev, Timothy I. Eglinton, August Andersson, Natalia Shakhova, Alexander Charkin, Birgit Heim, and Orjan Gustafsson (2014). "Preferential burial of permafrost-derived organic carbon in Siberian-Arctic shelf waters". *Journal of Geophysical Research: Oceans* 119.12, pp. 8410–8421. DOI: 10.1002/2014JC010261.

Wadhams, Peter, Vernon A. Squire, Dougal J. Goodman, Andrew M. Cowan, and Stuart C. Moore (1988). "The attenuation rates of ocean waves in the marginal ice zone". *Journal of Geophysical Research: Oceans* 93.C6, pp. 6799–6818. DOI: https://doi.org/10.1029/JC093iC06p06799.

Wåhlström, Iréne, Anders Omstedt, Göran Björk, and Leif G. Anderson (2013). "Modeling the CO2 dynamics in the Laptev Sea, Arctic Ocean: Part II. Sensitivity of fluxes to changes in the forcing". *Journal of Marine Systems* 111-112, pp. 1–10. ISSN: 0924-7963. DOI: https://doi.org/10.1016/j.jmarsys.2012.09.001.

Walker, Richard Arlin (2021). "Native communities confront painful choice: move away, or succumb to rising waters?" *The Guardian*. URL: https://www.theguardian.com/environment/2021/apr/12/native-communities-quileute-tribal-school (visited on 06/18/2021).

Wang, Jia and Moto Ikeda (2000). "Arctic oscillation and Arctic Sea-Ice oscillation". *Geophysical Research Letters* 27.9, pp. 1287–1290. DOI: 10.1029/1999GL002389.

Wegner, C., D. Bauch, J. A. Hölemann, M. A. Janout, B. Heim, A. Novikhin, H. Kassens, and L. Timokhov (2013). "Interannual variability of surface and bottom sediment transport on the Laptev Sea shelf during summer". *Biogeosciences* 10.2, pp. 1117–1129. DOI: 10.5194/bg-10-1117-2013.

Wegner, Carolyn, Katrina E. Bennett, Anne de Vernal, Matthias Forwick, Michael Fritz, Maija Heikkilä, Magdalena Łacka, Hugues Lantuit, Michał Laska, Mateusz Moskalik, Matt O'Regan, Joanna Pawłowska, Agnieszka Promińska, Volker Rachold, Jorien E. Vonk, and Kirstin Werner (2015). "Variability in transport of terrigenous material on the shelves and the deep Arctic Ocean during the Holocene". *Polar Research* 34.1. DOI: 10.3402/polar.v34.24964.

Wernli, Heini and Lukas Papritz (2018). "Role of polar anticyclones and mid-latitude cyclones for Arctic summertime sea-ice melting". *Nature Geoscience* 11.2, pp. 108–113. DOI: 10.1038/s41561-017-0041-0.

Wetterich, S., A. Kizyakov, M. Fritz, J. Wolter, G. Mollenhauer, H. Meyer, M. Fuchs, A. Aksenov, H. Matthes, L. Schirrmeister, and T. Opel (2020). "The cryostratigraphy of the Yedoma cliff of Sobo-Sise Island (Lena delta) reveals permafrost dynamics in the central Laptev Sea coastal region during the last 52 kyr". *The Cryosphere* 14.12, pp. 4525–4551. DOI: 10.5194/tc-14-4525-2020.

Wheeling, K. (2019). "Where does the carbon go when permafrost coasts erode?" *EOS* 100. DOI: https://doi.org/10.1029/2019EO136377.

White, Frank M, Malcolm L Spaulding, and L Gominho (1980). *Theoretical Estimates of the Various Mechanisms Involved in Iceberg Deterioration in the Open Ocean Environment*. Tech. rep. Rhode Island University Kingston.

Woosley, Ryan J. and Frank J. Millero (2020). "Freshening of the western Arctic negates anthropogenic carbon uptake potential". *Limnology and Oceanography* 65.8, pp. 1834–1846. DOI: https://doi.org/10.1002/lno.11421.

Yasunaka, S., E. Siswanto, A. Olsen, M. Hoppema, E. Watanabe, A. Fransson, M. Chierici, A. Murata, S. K. Lauvset, R. Wanninkhof, T. Takahashi, N. Kosugi, A. M. Omar, S. van Heuven, and J. T. Mathis (2018). "Arctic Ocean CO_2 uptake: an improved multiyear estimate of the air–sea CO_2 flux incorporating chlorophyll *a* concentrations". *Biogeosciences* 15.6, pp. 1643–1661. DOI: 10.5194/bg-15-1643-2018.

Zenkovich, VP (1962). *Osnovy ucheniia o razvitii morskikh beregov (Fundamentals of the Theory of Sea Coast Evolution)*. Izd-vo Akademii nauk SSSR.

Zhang, Rong (2015). "Mechanisms for low-frequency variability of summer Arctic sea ice extent". *Proceedings of the National Academy of Sciences* 112.15, pp. 4570–4575. DOI: 10.1073/pnas.1422296112.

Zhang, Rong and Thomas L. Delworth (2006). "Impact of Atlantic multidecadal oscillations on India/Sahel rainfall and Atlantic hurricanes". *Geophysical Research Letters* 33.17. DOI: https://doi.org/10.1029/2006GL026267.

Zhang, Rong and Thomas L. Delworth (2007). "Impact of the Atlantic Multidecadal Oscillation on North Pacific climate variability". *Geophysical Research Letters* 34.23. DOI: https://doi.org/10.1029/2007GL031601.

Zhang, Xiangdong, Moto Ikeda, and John E Walsh (2003). "Arctic sea ice and freshwater changes driven by the atmospheric leading mode in a coupled sea ice–ocean model". *Journal of Climate* 16.13, pp. 2159–2177. DOI: https://doi.org/10.1175/2758.1.

VERSICHERUNG AN EIDES STATT

Hiermit erkläre ich an Eides statt, dass ich die vorliegende Dissertationsschrift selbst verfasst und keine anderen als die angegebenen Quellen und Hilfsmittel benutzt habe.

DECLARATION OF OATH

I hereby declare upon oath that I have written the present dissertation independently and have not used further resources and aids than those stated.

Hamburg, August 2021

David Marcolino Nielsen

Hinweis / Reference

Die gesamten Veröffentlichungen in der Publikationsreihe des MPI-M
„Berichte zur Erdsystemforschung / Reports on Earth System Science“,
ISSN 1614-1199

sind über die Internetseiten des Max-Planck-Instituts für Meteorologie erhältlich:
http://www.mpimet.mpg.de/wissenschaft/publikationen.html

All the publications in the series of the MPI -M
„Berichte zur Erdsystemforschung / Reports on Earth System Science“,
ISSN 1614-1199

are available on the website of the Max Planck Institute for Meteorology:
http://www.mpimet.mpg.de/wissenschaft/publikationen.html